THESIS

HYDROLOGIC AND HYDRAULIC RESPONSE TO WILDFIRES IN THE UPPER CACHE

LA POUDRE WATERSHED USING A SWAT AND HEC-RAS MODEL CASCADE

Submitted by

Aaron Havel

Department of Civil and Environmental Engineering

In partial fulfillment of the requirements

For the Degree of Master of Science

Colorado State University

Fort Collins, Colorado

Fall 2015

Master's Committee:

    Advisor: Mazdak Arabi

    Daniel Baker
    Ellen Wohl

ABSTRACT

HYDROLOGIC AND HYDRAULIC RESPONSE TO WILDFIRES IN THE UPPER CACHE

LA POUDRE WATERSHED USING A SWAT AND HEC-RAS MODEL CASCADE

The enhanced possibility of catastrophic wildfires in the western USA and other regions around the world has increased the need to evaluate the effects of wildfire on the hydrology of watersheds and the hydraulic behavior of rivers. Understanding the effects of wildfires is vital in water-resources management and for public safety especially in regions where communities depend on surface water supply. Similarly, areas adjacent to river systems may be at risk of increased flooding due to wildfires in their upstream watersheds. Effects of wildfires on hydrologic fluxes in watersheds and rivers have been extensively studied; but, characterization of responses to wildfires is difficult due to the spatial variability of post-wildfire conditions. At the watershed scale, hydrologic responses comprise a network of complex nonlinear interactions. Hence, comprehensive watershed models serve as a useful tool to understand these relationships. Watershed models commonly lack the ability to represent channel geometry and channel process with sufficient spatial frequency. Thus, a hydrologic and hydraulic model cascade provides a bridge between the nonlinear interactions of the uplands and the river responses at the channel scale.

The overall goal of this study is to examine the spatial variability of the effects of the 2012 High Park and Hewlett wildfires that occurred within the headwaters of the Cache la Poudre River located in northern Colorado, USA. Two commonly used models were calibrated and used in combination. First, the Soil and Water Assessment Tool (SWAT) was used to

evaluate the hydrologic responses of the upper Cache la Poudre watershed to the wildfire events. Subsequently, the results from the SWAT model were used as inputs for the hydraulic model Hydrologic Engineering Center River Analysis System (HEC-RAS) to simulate channel hydraulics along 42.5 km of the upper Cache la Poudre River. The baseline SWAT model was established to simulate the hydrology of the study area between the years 2000 and 2014. This model accounts for wildfires by modifying land use/land cover inputs and corresponding parameters during simulations. Daily streamflow data were used for model calibration and testing. Using the calibrated baseline model, no-wildfire and wildfire scenarios were created. The two scenarios were then compared for changes in average annual total runoff volume, water budgets, and full streamflow statistics at the watershed and sub-basin scales. Then a HEC-RAS model was developed to simulate the hydraulic responses of the stream network using streamflows for various floods extracted from the two SWAT scenarios. High resolution DEM data and surveyed water surface elevations are used for model calibration and testing, respectively. Channel hydraulic behavior including flood inundation area, streamflow velocities, and channel shear stress were compared for the two scenarios at the channel scale.

At the watershed scale, wildfire conditions have little effect on the hydrologic responses, but at the sub-basin scale a total runoff increase up to 75 percent between scenarios was found. Generally, wildfire affected water budgets showed more surface runoff versus subsurface runoff, suggesting a decrease in infiltration rates under post-wildfire conditions. Flow-duration curves developed using full streamflow statistics for burned sub-basins show that less frequent streamflows become greater in magnitude leading to ecosurplus values up to 0.279. Also, simulations revealed that there is a strong and significant ($R^2 > 0.8$ and $p < 0.001$) positive correlation between runoff increase and percentage of burned area upstream. Streamflow

increases were between 2 and 14 percent depending on the reach's proximity to the wildfire and the flood. Lastly, along the main stem only slight increases in flood area, average cross section velocity, and shear stress as a result of wildfire were observed in the simulations. The results have important implications on improving post-wildfire water resources management.

ACKNOWLEDGMENTS

TABLE OF CONTENTS

LIST OF TABLES

LIST OF FIGURES

CHAPTER. 1 INTRODUCTION

1.1   Background

In recent decades, the amount and severity of wildfires in the United States of America (USA) and elsewhere in the world is becoming an increasing concern. In part, this concern is driven by second-order effects including water quality, carbon storage, and ecosystem disturbance, but is mostly an artifact of the increase of populations in or near wildfire prone areas. These areas are susceptible to loss of life and catastrophic destruction from floods and debris flows as a result of runoff and erosion enhanced by post-wildfire conditions (Moody et al., 2013). Further, snow accumulation and runoff from mountainous regions is relied upon to meet economic, environmental, and recreation water demands throughout the world (Richer, 2009). Wildfires could alter the timing and magnitude of runoff along with other hydrologic fluxes. Thus, wildfire effects to these areas are of particular interest.

Understanding the response of watersheds to wildfires has been the subject of extensive research since the 1950s; however, large differences in results have hindered progress towards a comprehensive understanding of the subject. Characterization of complex responses to wildfires is difficult due to the spatial variability of post-wildfire conditions (Moody et al., 2013). Wildfires can substantially change land use/land cover (LULC) and vegetation within watersheds, which may subsequently result in altering hydrologic regimes including: (1) increased availability of rainfall for runoff by decreasing canopy interception; (2) increased base flow through the decrease of water normally lost through evapotranspiration; and (3) increased runoff velocities and reduced interception/storage through loss of ground cover, litter, duff, and debris (Moody and Martin, 2001). At the watershed scale, these alterations can cause increased

hillslope erosion and may significantly alter terrestrial habitat. These alterations may also increase channel flooding, decrease channel stability, fill the streambed with fine sediment, and modify temperature regimes (Ryan et al., 2011).

Mathematical modeling is a useful and well accepted approach for improving our understanding of complex watershed processes (Kiesel et al., 2013). For example, watershed models have been used for simulating streamflow in snow-dominated systems to identify important interactions and processes in mountainous watersheds (Sanadhya et al., 2014). Further, the Soil and Water Assessment Tool (SWAT) has been used to characterize and quantify the effects of land use change, climate change, and mitigation strategies on average annual runoff, evapotranspiration, streamflow, groundwater and other hydrologic responses (El-Khoury et al., 2015; Fan and Shibata, 2015). More specifically, numerous studies involving SWAT model development and calibration have been conducted to evaluate the hydrology in mountainous regions throughout the world, including this study watershed (Foy et al., 2009); the Little River watershed, Tennessee (Zhu and Li, 2011); two Himalayan drainages of Nepal (Neupane et al., 2015); and the Yingluoxia watershed of northwest China (Lu et al., 2015).

Simulation has been used for evaluating the response of a system to wildfire in several areas throughout the world (Batelis and Nalbantis, 2014; Goodrich et al., 2005; McLin et al., 2001). For example, Batelis and Nalbantis (2014) used simulation to predict potential impact from hypothetical wildfires in a Mediterranean basin. One of the challenges in using models is lack of components for representing LULC change. This is required for continuous simulation and is particularly important when assessing effects of wildfires. The land use change module within SWAT has been shown to be useful for evaluating hydrologic condition where land use has changed as the result of urbanization (Pai and Saraswat, 2001), but to the author's

knowledge, no studies have used a comprehensive hydrologic model with dynamic LULC updating to characterize hydrologic response to wildfires at the sub-basin and watershed scales in mountainous regions using long-term simulation scenario analysis. Thus, the second chapter of this thesis describes the use of SWAT for this purpose.

Comprehensive watershed models can be inadequate for investigating in-channel conditions due to their inability to represent channel geometry and channel process with sufficient spatial frequency. One-dimensional (1-D) hydraulic models like the widely-used Hydrologic Engineering Center River Analysis System (HEC-RAS) are needed for their capacity in simulating channel hydraulics at finer spatial resolutions. HEC-RAS may be applied to various scenarios ranging from small scale drainage systems to large river networks (Brunner, 2010a). The program is commonly used for floodway encroachment and velocity determination. Examples include: the Tana River in Kenya (Maingi and Marsh, 2002); the Atrato River in Colombia (Mosquera-Machado and Ahmad, 2007); the Cache and Stony Creeks in California (Spencer et al., 2013); and the Jokulsa a Fjollum river in Iceland (Alho et al., 2007). Also, the program has been successfully implemented in steep bedrock reaches such as the Ocoee River in Tennessee (Goode and Wohl, 2010).

HEC-RAS requires upstream boundary conditions to represent spatially varying streamflow. These boundary conditions may be provided by a watershed model if a spatial connection between models is established. Hydrologic and hydraulic model cascades have been previously implemented for various purposes (Javaheri and Babbar-Sebens, 2014; Kiesel et al., 2013). For example, Kiesel et al. (2013) demonstrated the use of a modeling cascade to investigating water and sediments fluxes at the watershed, channel, and reach scales in lowland. Their proposed approach included the application of three models: a hydrologic model, a 1-D

hydraulic model, and a two-dimensional hydraulic model. These models were used in series to show a comprehensive simulation of water and sediment fluxes (Kiesel et al., 2013). Another example includes the use of a model to compare peak flow, flood inundation maps, and velocity maps for the purpose of evaluating effects of restored wetlands on channel processes (Javaheri and Babbar-Sebens, 2014). Despite the widespread usage of HEC-RAS, only limited research involving the implementation of a modelling cascade to characterize response to wildfires could be found in the literature. McLin (2001) used HEC-RAS in combination with a watershed model to predict floodplain boundary changes following the Cerro Grande wildfire in New Mexico, USA. However, this study was limited to a small study reach and only examined the 100-year flood event. Thus, the third chapter of this thesis describes a modeling cascade approach that couples the results from a SWAT model with a HEC-RAS model to characterize channel hydraulic behavior response to wildfires at the channel scale in a major river downstream of wildfire activity.

1.2   Study Area

The Cache la Poudre (Poudre) Watershed, with an area of approximately 5,230 km^2 above its confluence with the South Platte River on the Great Plains, is situated mostly in northern Colorado, USA with a portion reaching into southern Wyoming, USA (Wohl, 2010). The Poudre River (Figure 1) is supplied by two major tributaries within its headwaters, the South and North Forks, the latter being the longer of the two joining the main-stem farther downstream. After streamflow retreats from the Poudre's headwaters in the Rocky Mountain Range the river passes through the cities of Fort Collins and Greeley. Eventually, the river joins the South Platte River and progresses downstream to the Platte River and then to the Missouri River. The Poudre

River, with its minimally-developed mountainous headwaters, is widely utilized as a drinking water source for several cities and communities located along its banks (Richer, 2009).

During May and June of 2012 the Hewlett and High Park wildfires burned approximately 384 km^2 of primarily forested landscape within the Poudre Watershed. The burned area includes numerous drainages tributary to the main-stem Poudre River. Local areas related to burn severity with the watershed, susceptible to erosion and flooding, was the result of widespread loss of vegetation and burned soils from the wildfires. Localized summertime thunderstorms immediately following the wildfire worsened the effects by washing sediment and debris into the river channel posing a threat to the safety of people and homes in the area (Oropeza and Heath, 2013). The affected area extends along the Poudre River from the mountain front upstream to several kilometers south of the community of Rustic, Colorado. Therefore, a study watershed outlet was defined near the mountain front at Colorado Division of Water Recourses' (CDWR) surface water gauge CLAFTCCO18 (formally USGS Gage 06752000) and the study reach was defined from the outlet upstream to the wildfire boundary (Figure 1). This outlet location is commonly referred to as the Mouth of Canyon.

The resulting study watershed is approximately 2,732 km^2 and the study reach is approximately 42.5 km in length. At higher elevations, streamflow is dominated by snowmelt runoff and at lower elevations rainfall runoff from summer convective storms greatly affect streamflow. The storms combined with the upstream snowmelt runoff, can produce high-magnitude, short-lived floods (Wohl, 2010). The resulting hydrograph is snowmelt dominated with a rise typically beginning in April and a recession lasting into August. Generally, peak streamflow occurs at the end of May or early June and base flow levels occur in September or October (Richer, 2009).
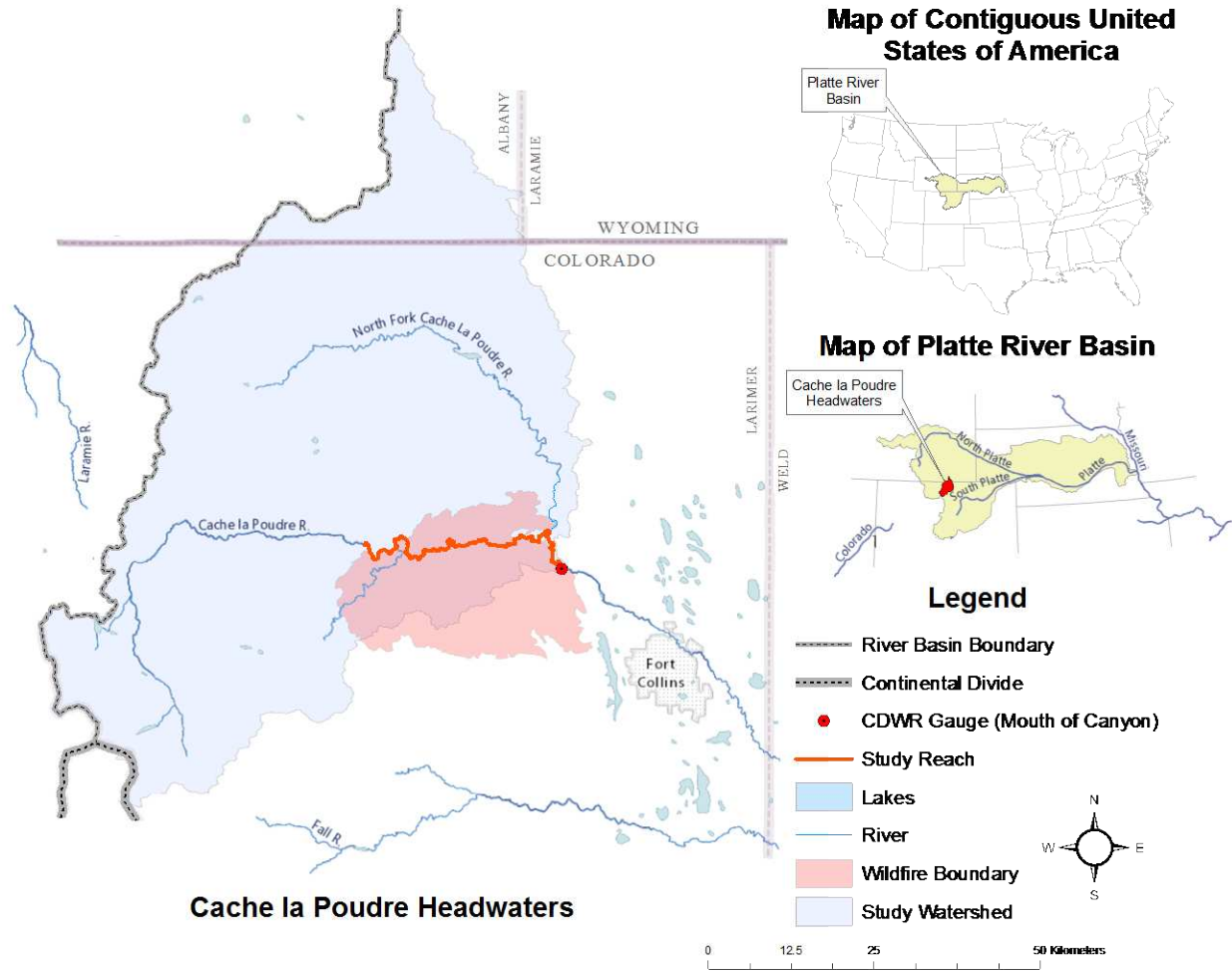
Figure 1. Study area map which includes the location of study watershed, study reach, CDWR surface water gauge, and hydrologic reference basemap for the study area (Esri, 2015a).

1.3   Model Framework

To achieve the main objectives of this work, the application of two models in a cascading fashion is proposed: a hydrologic model and then a hydraulic model. This approach, as given by Figure 2, was proposed to consider large scale effects on small scales. Maintaining a continuous spatial connection between the models allows simulation of water fluxes from the watershed to the channel scale for evaluating wildfire effects. SWAT was used for the first component of the modeling cascade (labeled "Hydrologic Model – Watershed Scale" in Figure 2). The SWAT model is used for simulating the effects of watershed characteristics, climate, and LULC changes (i.e., wildfires) on water fluxes and water balances within the study watershed. However,

6

SWAT's spatial representation through sub-basins is unfavorable for obtaining differentiated in-stream results along the study reach because each reach within the SWAT model can be many kilometers in length and the same result value is given for each reach (Kiesel et al., 2013). Thus, usage of a separate in-stream model for representing processes in the main channel is driven by the need for high (i.e., on the order of 10^1 m) resolution outputs that SWAT is not able to supply (e.g., velocity and streamflow depth distributions). This separate model is introduced under the second component of the modeling cascade where HEC-RAS is applied to the study reach (labeled "Hydraulic Model – Channel Scale" in Figure 2).
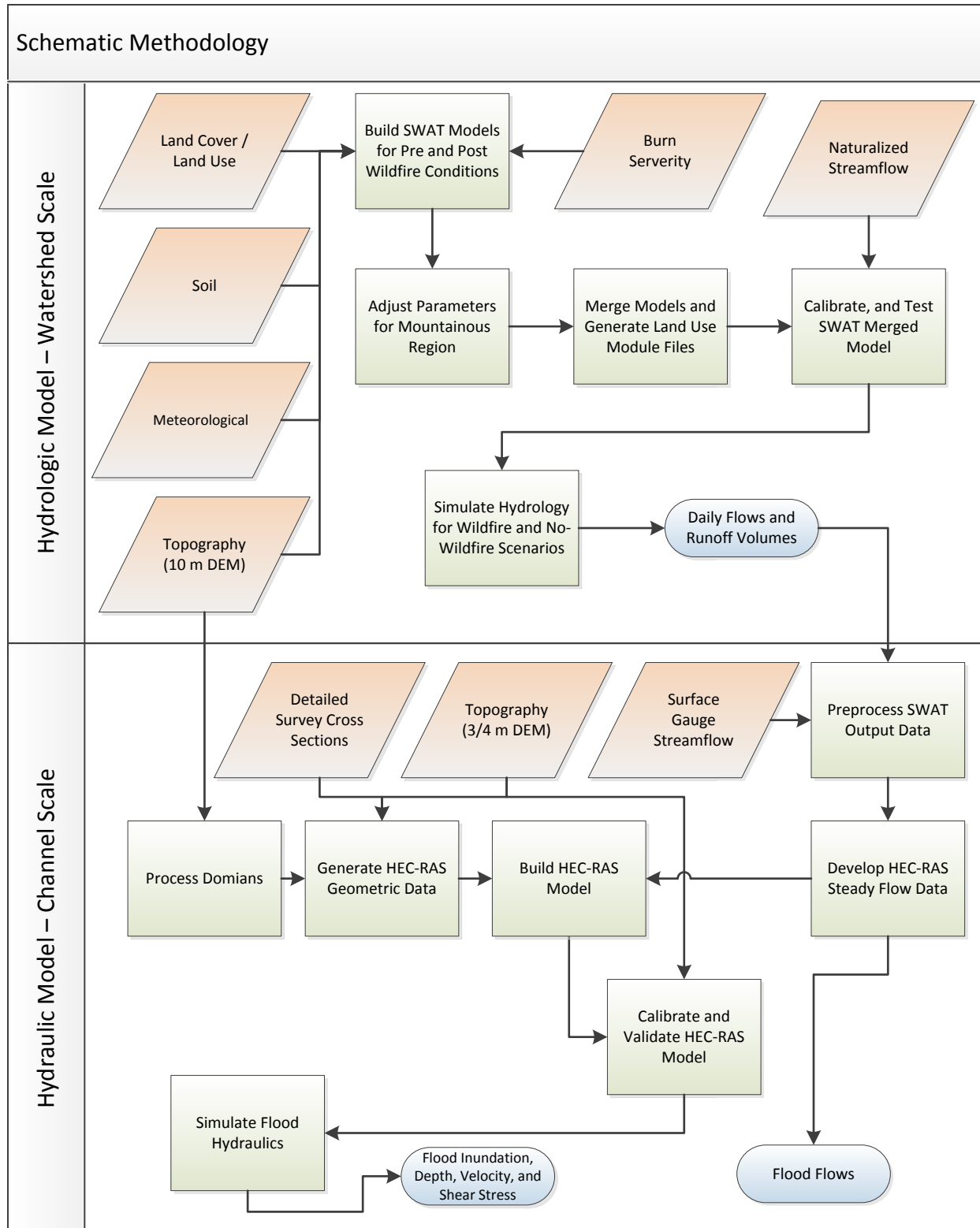
Figure 2. Schematic of the model framework used for this study.

CHAPTER. 2 CHARACTERIZING HYDROLOGIC RESPONSE TO WILDFIRES USING
THE SWAT MODEL

2.1 Introduction

Large watersheds are rarely subject to wildfire with a boundary that covers a significant portion of their area and as a result the effects of wildfire are practically indiscernible (Batelis and Nalbantis, 2014). Because of this, previous studies have been limited due to a lack of pre-fire data on burned watersheds (Canfield et al., 2005; Foltz et al., 2009; Mahat et al., 2015). Recent, significant wildfire activity in northern Colorado, USA has provided a unique opportunity for examining hydrologic response to wildfires, specifically in a mountainous region. This unique opportunity stems from the fact that a relatively significant proportion of a gaged mountainous watershed (approximately 14 percent from the Mouth of Canyon) has burned as the result of wildfire. The pre and post-wildfire streamflow data availability allows for the development, calibration, and testing of a hydrologic model that accounts for spatial variability in LULC to continuously simulate the hydrology from pre-wildfire conditions through post-wildfire conditions. Further, due to the magnitude of the wildfire activity, burn severity mapping is available. These mapping data allow for a land use change module to be implemented during calibration efforts, which adjusts hydrologic parameters impacted by wildfire seamlessly during simulation.

The primary goal for the research discussed in this chapter is to characterize hydrologic response to wildfires at the sub-basin and watershed scales in mountainous regions using long term simulation scenario analysis. To accomplish this goal, a mountainous system recently exposed to significant wildfire activity located in northern Colorado, USA was analyzed with a SWAT model. This analysis includes simulation of no-wildfire and wildfire scenarios over a 15

year (2000 to 2014) period. Specific objects of this study are to: (1) quantify changes in average annual total runoff volume and explore how these changes fluctuate with the percent of the area burned; (2) quantify changes in average annual hydrologic budgets; and (3) highlight potential implications of these changes using full streamflow statistics, all at both the sub-basin and watershed scales.

2.2   Methods

2.2.1   Hydrologic Model

This section is organized in the following manner:

- Section 2.2.1.1 – Describes the SWAT software in detail.

- Section 2.2.1.2 – Reviews the SWAT model data used for this study.

- Section 2.2.1.3 – Provides detailed information regarding the development of the initial SWAT models (one representing pre-wildfire conditions and one representing post-wildfire conditions).

- Section 2.2.1.4 – Describes the major modeling options selected for this study.

- Section 2.2.1.5 – Shows how the initial SWAT models were adjusted account for the mountainous terrain of the study watershed.

- Section 2.2.1.6 – Describes how the two SWAT models were merged together.

- Section 2.2.1.7 – Describes how the merged SWAT model was calibrated and tested.

- Section 2.2.1.8 – Describes the two scenarios proposed to represent average wildfire and no-wildfire conditions for analysis.

2.2.1.1   SWAT

The SWAT 2012 Revision 591 (U.S. Department of Agriculture Agricultural Research Service, 2012) developed by the United States Department of Agricultural (USDA) Agricultural Research Service (ARS) was used for this study. The SWAT model was developed in the early 1990s and is public domain software. SWAT initially incorporated features of several previously

developed ARS models and has since endured continued review and expansion of capabilities. The model was established for evaluation of large complex watersheds over long periods of time and accounts for differing soils, land use, and management conditions (Neitsch et al., 2011).

SWAT is a comprehensive hydrologic model that allows for numerous physical processes to be simulated in a watershed. These processes may be separated into two coarse divisions of the hydrologic cycle: the land phase and the routing phase. These divisions include important processes such as precipitation, surface runoff, evapotranspiration, groundwater flow, snowmelt, and flood routing. The model is physically based, meaning each hydrologic process is directly modeled by SWAT, as opposed to empirical, regression-based equations. Thus, specific information about weather, soil properties, topography, vegetation, and land management practices occurring in the watershed is required (most of which can be directly measured in the field). This deterministic approach allows the user to study the relative impact of alternative input data on particular variables of interest. SWAT is driven by a water balance equation which relates individual components of the hydrologic cycle. Additional details including specific equations associated with the water balance and the individual hydrologic processes may be found in the SWAT Theoretical Documentation, Version 2009 (Neitsch et al., 2011).

SWAT is a continuous time model which allows simulations to be performed at the watershed scale over a specified period of time (Neitsch et al., 2011). Compared to single-event models, continuous time models better represent watersheds where channel storage may be significant and/or where significant variability exists in land use (e.g., urbanization), soil types, and/or topography (Nicklow et al., 2006). Further, SWAT is considered a semi-distributed spatial model as it divides a watershed into sub-basins, which are further divided into hydrologic response units (HRUs). Sub-basins are spatially related to each other and may be defined with

unique climate and hydrologic properties. Each sub-basin is assigned a reach (i.e., main channel) which transfers loadings from the sub-basin to the other reaches within the watershed. Combined, the reaches create the channel network of the watershed. The HRUs are areas within each sub-basin that consist of unique combinations of LULC, soil, and terrain attributes. Each of the HRUs within a given sub-basin may be scattered, but are lumped together to create one HRU. Loadings from each HRU are calculated independently and then summed together to determine the total loadings from the sub-basin (i.e., it is assumed that there is no interaction between HRUs) (Neitsch et al., 2011).

The SWAT model uses Manning's equation to define the rate and velocity of streamflow. Both routing options within SWAT, variable storage and Muskingum, are distributed flow routing models, meaning variables may be determined as functions of space and time. Both of these methods are based on variations of the kinematic wave model. SWAT assumes a trapezoidal channel shape with 2:1 side slopes for streamflow routing calculations. The user may enter the width and depth of the channel when filled to the top of the banks. The user is also required to enter the channel length, which in many cases is quite long, depending on the stream initiation threshold and sub-basin outlet locations (Neitsch et al., 2011).

2.2.1.2   SWAT Model Data

The hydrologic modeling process was initiated by first collecting and preparing the necessary data, summarized in Table 1. Each spatial dataset was converted to North American 1983 Geographic Coordinate System and transformed to Universal Transverse Mercator Zone 13 North Projection using Esri's Geographic Information System mapping software, ArcMap 10.1 (ArcMap). When necessary, the spatial datasets were also clipped and merged to produce single, seamless spatial datasets.

Table 1. SWAT model input data.

Data type	Data used	Description
Terrain	Digital Elevation Model	National Elevation Dataset | 1/3 arc-second (~10 m)
Land Use / Land Cover	2011 Land Cover	National Land Cover Dataset | 30 m
Burn Severity	Thematic Burn Severity Delineation	Monitoring Trends in Burn Severity High Park Fire Assessment | 30 m
Soil	Soil Map Unit Delineation	Gridded Soil Survey Geographic Database for Colorado and Wyoming | 10 m
Meteorological	Precipitation and Temperature Measurements	Global Historical Climatology Network Database | Daily
Streamflow	Naturalized Streamflow Data	Northern Colorado Water Conservancy District | Daily
Model Parameters	SWAT Model Databases	Land Cover/Land Use, Soil, and Weather Parameters

Terrain

The 10 m resolution Digital Elevation Model (DEM), courtesy of the United States Geological Survey (USGS) National Elevation Dataset (Gesch, 2007; Gesch et al., 2002), was used to describe the topography within the watershed. The study watershed ranges in elevation from 4,138 m at the Continental Divide down to 1,493 m at the Mouth of Canyon. The distribution of elevation within the study watershed is displayed in APPENDIX A.

Land Use, Land Cover, and Burn Severity

The 30 m resolution National Land Cover Database (NLCD) 2011 Land Cover (Jin et al., 2013) dataset created through a project conducted by the Multi-Resolution Land Characteristics (MRLC) Consortium was used to describe the LULC distribution for the study watershed. NLCD 2011 Land Cover uses 16 classifications that are based primarily on an analysis of circa 2011 Landsat imagery (Jin et al., 2013). Distribution of the major types found within the study

watershed may be seen in APPENDIX A and a complete breakdown is shown in APPENDIX B. Generally the study watershed consists of forest (primary evergreen type) with considerably large portions covered by shrubland and herbaceous vegetation. Note the study watershed is relatively undeveloped, with less than 1 percent of the land surface developed for commercial, industrial, or residential purposes. Through comparison of earlier NLCD products, it is evident that LULC changes little between the years 2000, 2006, and 2011. Therefore, it was assumed appropriate to use NLCD 2011 Land Cover for the entire simulation period. A comprehensive LULC change analysis for the study watershed using NLCD 2000, 2006, and 2011 Land Cover is included in APPENDIX B.

Burned areas within the watershed were identified using the High Park Wildfire Assessment (Monitoring Trends in Burn Severity Project, 2014) conducted as a part of the Monitoring Trends in Burn Severity (MTBS) project directed by groups within the USGS and United States Forest Service. The MTBS project was introduced to consistently map burn severity and boundaries of wildfires across all lands of the USA from 1984 and beyond. The product of this assessment includes a Thematic Burn Severity Delineation which depicts severity as unburned to low, low, moderate, high, and increased greenness (i.e., increase post-wildfire vegetation response) (Finco et al., 2012). Through examining the wildfire boundary, it is evident that the High Park Wildfire Assessment includes the Hewlett wildfire which occurred just prior to the High Park wildfire. The burn severity distribution of the Hewlett and High Park wildfire within the study watershed may be seen in APPENDIX A. The distribution of the different burn severities within the wildfire boundary is relatively even.

The NLCD 2011 Land Cover spatial dataset was preprocessed to allow the High Park and Hewlett wildfires to be simulated by SWAT. The NLCD 2011 Land Cover was overlaid with the

Thematic Burn Severity Delineation. Then the NLCD 2011 Land Cover was reclassified to incorporate low, medium, and high burn severity distinctions. To simplify the analysis, the unburned to low, increased greenness, and non-processing areas were omitted and not incorporated into the simulated burn area. The reclassification was accomplished using tools within ArcMap. The preprocessing retained the pre-wildfire classification, but added a burn severity identifier. For example, portions of the NLCD 2011 Land Cover that consist of Evergreen Forest and overlap with a low burn area were reclassified to a newly created Evergreen Forest Low Burn classification.

The SWAT Model Database contains various model parameters for many LULC types and the SWAT LULC lookup table relates NLCD classifications to the LULC types found in the SWAT Model Database. The approach taken to seamlessly represent wildfire during the simulation period discussed in subsequent sections requires alteration to the SWAT Model Database and SWAT LULC lookup table. Thus, the original SWAT Model Database and original SWAT LULC lookup table, shown in APPENDIX B, were edited to create two separate databases and tables independently representing pre and post-wildfire conditions.

The new database and tables were created by including the new classifications. For the pre-wildfire database, the newly added LULC types consisted of attributes identical to the original classification, but with a new description and identification code. For example, a new LULC type was added to the database for pre-wildfire Evergreen Forest Low Burn with attributes identical to the Evergreen Forest LULC type. Thus, the SWAT model created using this database will represent pre-wildfire condition, but areas influenced by wildfire will be delineated from non-burned areas. For the post-wildfire database, the newly added LULC types included a new description and identification code similar to the pre-wildfire database; however,

for the post-wildfire case, attributes were altered from their original classifications. For all burn areas, LULC attributes in the database were changed to match those of the Range-Grasses LULC. This change was implemented to aid with appropriately representing loss of canopy in burned areas. Additionally, Curve Numbers (CNs) were adjusted to account for expected increases in runoff based on a methodology used in Higginson and Jarnecke (2007). This methodology entails adding 5, 10, and 15 to pre-wildfire CNs for low, moderate, and high burn areas, respectively. The original and edited SWAT LULC lookup tables as well as curve numbers for both pre and post-wildfire conditions may be found in APPENDIX B.

Soil

The Gridded Soil Survey Geographic (gSSURGO) database for Colorado and Wyoming (Soil Survey Staff, 2015a; Soil Survey Staff, 2015b), obtained from the USDA Natural Resources Conservation Service (NRCS), was used to represent the distribution of soil within the study watershed. This dataset contains soil mapping, which includes outlined areas called map units. These map units have unique properties, interpretations, and productivity which describe the soils. The study watershed contains 153 different map units. The SWAT SSURGO Soils database (U.S. Department of Agriculture Agricultural Research Service, 2012) was used to describe various model parameters for each gSSURGO map unit. One model parameter of particular interest is the Hydrologic Soil Group (HSG). The HSG is a classification established by the NRCS which is based on the runoff potential of a given soil. This classification consists of four groups: A, B, C, and D. Generally, soils designated as type A have the smallest runoff potential and soils designated as type D have the greatest. The distribution of soil as represented by HSG within the study watershed is shown in APPENDIX A. Generally, the study watershed

consists of D type soils, indicating the area has very low to moderate infiltration rates. This implies that the study watershed may have a high runoff potential.

Meteorological

Daily measurements of precipitation, maximum temperature, and minimum temperature for the study watershed were obtained from the Global Historical Climatology Network (GHCN) Daily dataset (Menne et al., 2012), which is maintained by the National Climatic Data Center (NCDC). The NCDC extensively quality assures GHCN daily data prior to data release. This is accomplished using a multi-tiered approach including a formatting check as well as a quality test looking for a variety of data problems (Menne et al., 2012). Based on this, no further quality control beside removal of flagged data was conducted. The stations were selected based on location, type of data provided, length of record, and completeness of record. A complete list of stations may be found in APPENDIX B. Mean annual precipitation ranges from 330 mm at the lower elevations to 1350 mm at the higher elevations and mean annual temperature ranges from approximately 9° C at the lower elevations to -5° C at the higher elevations (Richer, 2009).

SWAT uses the WXGEN weather generator model to simulate variables not measured at stations. In this case, these variables include solar radiation, relative humidity, and wind speed. The WXGEN weather generator model also fills in missing daily values of precipitation, maximum temperature, and minimum temperature. SWAT contains several weather databases that may be used to populate required parameters in order to use the WXGEN weather generator model. The weather database selected for this study contains information for 18,254 first order and second order National Weather Service Cooperative Observer Program climate stations. Details regarding implementation and use of the WXGEN weather generator model within

SWAT may be found in the SWAT Theoretical Documentation, Version 2009 (Neitsch et al., 2011).

Naturalized Streamflows

Precipitation within the study watershed is greatest during the winter months. Snow accumulates which generates the mountain snowpack that is then released during the spring and early summer months. In an effort to support economic, environmental, and recreational water demands downstream, manmade structures such as diversions, storage reservoirs, and irrigation canals are used to store and distribute the snowmelt runoff during times of the year when the demand of water exceeds its availability. Thus, the Poudre River streamflow regime is modified. One study of the Poudre watershed described several flow regime modifications including delayed hydrograph rise, decreased peak streamflows, and lower winter base flows (Richer, 2009). In an effort to ensure hydrologic processes are represented appropriately, naturalized streamflows were used for model calibration and testing. Naturalized streamflows remove the influence of afore mentioned features such as diversions and impoundments. Daily naturalized streamflows were collected from Northern Colorado Water Conservancy District (Northern Water) at the Mouth of Canyon (Northern Water, 2014).

2.2.1.3 Initial Model Development

Two models representing pre and post-wildfire conditions were developed and then later merged. Two sets of initial SWAT model input files for the study watershed were created using ArcSWAT version 2012.10_1.13 (U.S. Department of Agriculture Agricultural Research Service, 2014). ArcSWAT is an ArcMap extension that provides a graphical user interface for

creating a SWAT model. The interface was used to process the previously described model data

to generate initial SWAT input files. This process is summarized in Figure 3.
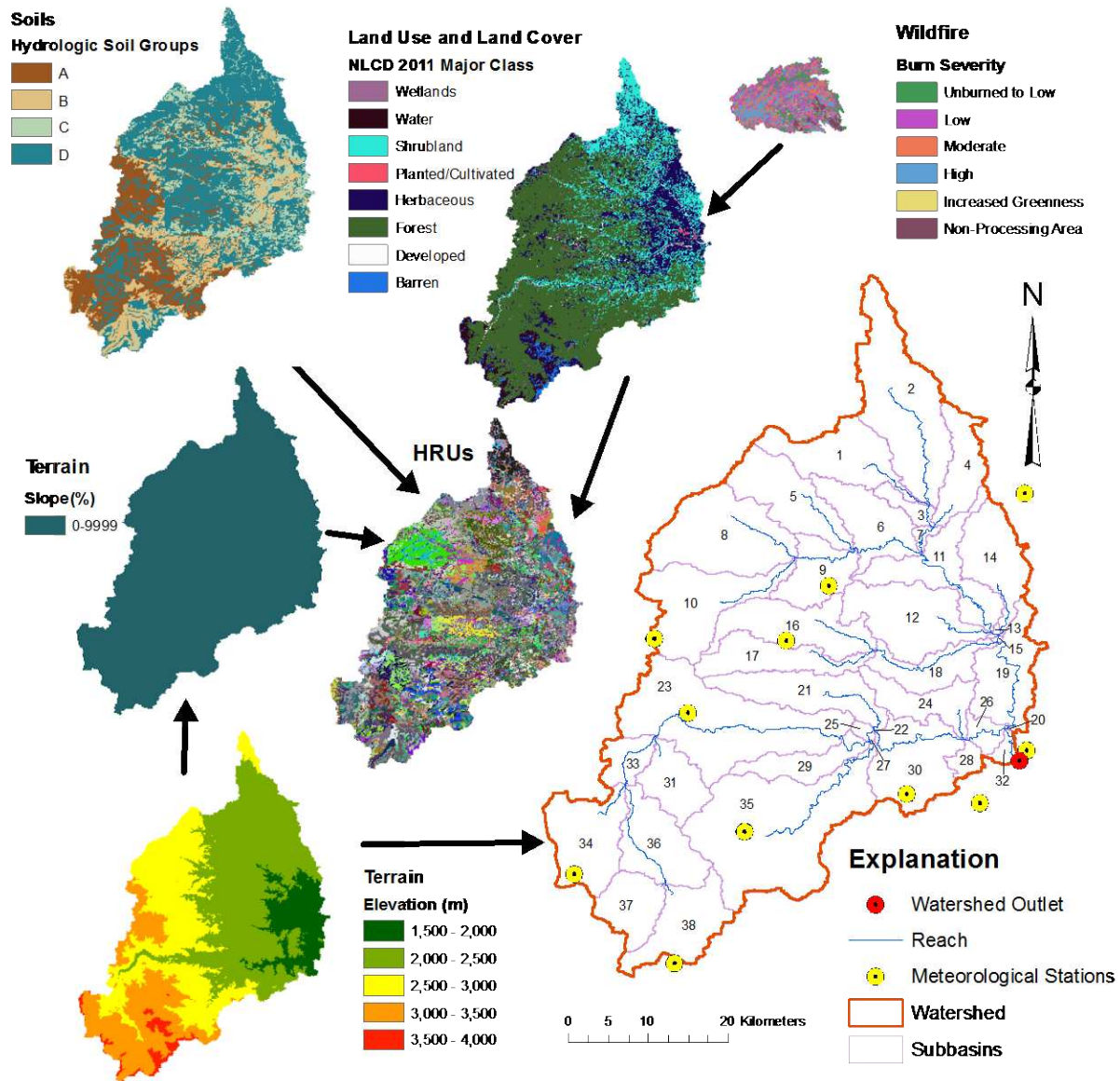
Figure 3. Initial SWAT model development summary. Note that for illustrative purposes the soils and LULC classifications shown are simplified versions of the actual classifications used to establish HRUs.

Delineation

The ArcSWAT Automatic Watershed Delineation tool was used to create a stream

network, define sub-basin outlet locations, delineate the watershed, and calculate the sub-basin

parameters. This tool uses Spatial Analyst functions within ArcMap to perform these tasks (Winchell et al., 2013). This process was initiated by first loading the 10 m DEM. Using the 10 m DEM, flow direction and accumulation for the study watershed were established. Next, a stream network was derived using a value of 5,000 hectares (the lower end of the range recommended by the tool for this watershed) as the stream initiation threshold. To avoid oversimplifying the stream network, a lower value for the stream initiation threshold was selected as it is expected to result in a more detailed stream network. During this process, outlets were automatically created at stream junctions. Also, additional outlets were manually placed at locations where a large tributary entered the study reach and the whole watershed outlet was defined at the Mouth of Canyon. Lastly, the watershed was delineated and the sub-basin parameters were calculated.

HRU Definition

The previously discussed LULC and soil data were loaded into ArcSWAT. The appropriate options to pair the input data with the SWAT database for model parameter extraction were selected. Next, using the previously loaded 10 m DEM, a slope classification layer was generated using a single slope class. A single slope class was selected to limit the total number of HRUs, which is expected to shorten computation time. With the appropriate datasets defined, ArcSWAT was then used to determine LULC/soil/slope combinations and distributions for each sub-basin. ArcSWAT overlays these layers and determines the unique combinations of all the LULC, soils, and slope classifications. These combinations are then used to determine the distribution of HRUs for the entire watershed. The multiple HRUs option was selected to create multiple HRUs with each sub-basin. This allows threshold levels (one each for land use, soil, and slope) to be applied, which aids in avoiding small HRUs that generally have little influence on

the model results. The LULC threshold eliminates minor LULCs in each sub-basin. For example, a 20 percent land use threshold indicates that all land uses that cover less than 20 percent of a sub-basin will be neglected, of which the area will be evenly reapportioned to all remaining land uses. The soil threshold eliminates minor soils within each remaining land use whose coverage is less than the value. Thus, a 10 percent threshold eliminates all soils which cover less than 10 percent of a given land use. In this case, since only one slope classification was used, no slope threshold was applied. The ArcSWAT Documentation (Winchell et al., 2013) indicates a LULC threshold of 20 percent and soil threshold of 10 percent are adequate for most applications. However, in an effort to avoid oversimplification, thresholds of 10 percent and 5 percent were applied to LULC and soils, respectively. The HRU definition criteria was further refined through applying threshold exemptions to combinations located within the wildfire boundary. This ensured the spatial distribution of the wildfire is not modified through the threshold elimination and reapportionment process.

2.2.1.4   Model Options

Options for both models are identical and were selected based on previous modeling studies using SWAT in mountainous regions (Foy et al., 2009; Lu et al., 2015; Neupane et al., 2015). A modified version of the commonly applied United States Soil Conservation Service (now the NRCS) CN procedure was adopted to simulate surface runoff in the watershed. This method with its simple structure contains only one undetermined parameter, which is the CN. The CN depends on the HSG, LULC, and hydrologic condition (Lu et al., 2015). Also, the Penman-Monteith method based on energy balance components was selected to estimate potential evapotranspiration. Lastly, channel routing was represented using the Muskingum River Routing Method. Other model options were left as default selections. Additional details

regarding all model options may be found in the SWAT Theoretical Documentation, Version 2009 (Neitsch et al., 2011).

2.2.1.5   Accounting for Mountainous Terrain

Elevation bands and curve number adjustments were incorporated into the two models as discussed below, as a result of the mountainous terrain within the study watershed.

Elevation Bands and Lapse Rates

The study watershed is located within the rainshadow of the Rocky Mountains and overall experiences a topographically-driven climate. Significate difference in elevation within the study watershed yields large variability in the quantity and type of precipitation. Thus, lapse rates as well as elevation band parameters were assigned to each sub-basin to account for orographic effects. The precipitation lapse rate (i.e., increase in mean annual precipitation with an increase in elevation) of 658.4 mm/km obtained from Foy (2009) was incorporated into the model. Additionally, the temperature lapse rate (i.e., decrease in mean annual temperature with an increase in elevation) of -5.5 ^{0}C/km reported by Foy (2009) was used.

SWAT is capable of integrating up to 10 elevation bands in each sub-basin. These bands were derived by topographically discretizing each sub-basin within the watershed. SWAT requires the input of the elevation at the center of each band and the fraction of sub-basin area within the elevation band. A code created by Dr. Mazdak Arabi with MathWorks Matlab (Matlab) software was used to generate these elevation band parameters. The code reads the Topography Report generated by AcrSWAT and takes the maximum elevation and subtracts the minimum elevation of each sub-basin and divides by ten, which creates ten equal-interval elevation bands. Next, the elevation at the center of each band and the fraction of sub-basin area

within the elevation band is calculated. Lastly, the code modifies the previously generated SWAT input files to contain these parameters. These parameters allow SWAT to use the elevation band equations described in the SWAT Theoretical Documentation, Version 2009 (Neitsch et al., 2011) to simulate orographic effects.

Curve Number Slope Adjustment

The curve numbers provided in the SWAT Model Database are appropriate for slopes up to 5 percent (Neitsch et al., 2011). The average slope was extracted from each HRU and plotted on a histogram, which may be found in APPENDIX A. This plot indicates many of the HRU slopes exceed 5 percent. A Matlab code developed by Ali Tasdighi at Colorado State University (CSU) was used to adjust curve numbers for different slopes at the HRU level. This code utilizes the following equation developed by Williams (1995) and is recommended for this purpose by the SWAT Theoretical Documentation, Version 2009 (Neitsch et al., 2011):

$$CN_{2s} = \frac{(CN_3 - CN_2)}{3} * [1 - 2 * e^{-13.86*S}] + CN_2$$

where CN_{2S} is the moisture condition II CN adjusted for slope, CN_3 is the moisture condition III CN for the default 5 percent slope, CN_2 is the moisture condition II CN for the default 5 percent slope, and S is the average fraction slope of the sub-basin. Note that upon simulation SWAT caps CN values at 98.

2.2.1.6 Merging the Models

The pre-wildfire and post-wildfire models described above have identical HRU distributions. Further, all of the HRUs outside of the burn area are the same. These two models were merged using a Matlab code written by Dr. Mazdak Arabi. This code was used to add the

23

burned HRUs from the post-wildfire model to the pre-wildfire model. For these burned HRUs, the code re-numbers and adjusts the HRU fractions to nearly zero (i.e., 0.000001). The HRU fraction is a HRU parameter that represents the fraction of sub-basin area represented by that HRU (Neitsch et al., 2011). Land use update files are also produced by the code. Land use update files tell SWAT to change the pre-wildfire HRU fractions to nearly zero and increase the post-wildfire HRU fractions to represent the burn area at the appropriate time during the simulation. In this case, the High Park and Hewlett wildfires occurred during May and June of 2012. Thus, for model calibration the land use update was initiated on July 1, 2012.

2.2.1.7 *Model Calibration and Testing*

The SWAT model was calibrated and tested for the daily naturalized streamflows at the Mouth of Canyon. Calibration, pre-wildfire testing, and post-wildfire testing periods were 2005-2014, 2000-2004, and 2014, respectively. These simulation periods were selected based on data availability. Initial calibration parameters were identified from previous modeling efforts for the study watershed published in Foy (2009). These parameters were supplemented with additional parameters identified from a previous study utilizing SWAT (Records, 2013). A total of 38 modal parameters were used for calibration. A SWAT auto-calibration tool developed by Mehdi Ahmadi at CSU was used to employ a global optimization algorithm named dynamically dimensioned search (DDS). DDS is designed to arrive at good solutions within a maximum number of user-defined function evaluations for use in model calibration with many parameters (Tolson and Shoemaker, 2007). This auto-calibration tool was used to generate 498 model runs. Each model run consisted of a unique combination of the 38 model calibration parameters. The tool works towards minimizing an objective function. In this case, we based this objective function on two primary error statistics, relative error (RE) and Nash-Sutcliffe efficiency

coefficient (E_{NS}). The error statistics are used to determine how accurately SWAT is representing hydrologic processes through comparison of observed and simulated streamflows at the Mouth of Canyon. These primary error statistics, along with supplemental error statistics, are displayed and described in APPENDIX C. Also, model calibration parameter starting values and ranges are displayed in APPENDIX B.

2.2.1.8   Scenario Analysis

With the SWAT model calibrated and tested, two scenario models were created. First, a no-wildfire scenario model was created. This was achieved by simply removing the land use update files, thus representing no wildfire activity throughout the entire simulation period. Second, a wildfire scenario model was created. This was achieved by adjusting the land use update files to reflect a wildfire occurring at the beginning of the simulation. Thus, wildfire is simulated throughout the entire simulation period. Note the simulation period for each scenario was between 2000 and 2014 (15 years).

2.2.2   Output Data Post-Processing

SWAT outputs were post-processed in Matlab. Simple summing functions were used to calculate total runoff volumes and water budgets throughout the study watershed. Full streamflow statistics were used to develop flow-duration curves for burned sub-basins. These represent the percentage of time that streamflow is likely to equal or exceed a given streamflow value for both scenarios. This was achieved using code developed by Parkyn (2010), which sorts, ranks, and plots the input streamflow data to generate flow-duration curves. Flow-duration curves are a widely accepted method for characterizing streamflow regime. They are commonly used for hydropower, water resource management, water quality management, habitat suitability, and flood control applications (Fan and Li, 2004). However, they have not been frequently used

in evaluating response to wildfire (Newtson, 2013). Next, the ecodeficit and ecosurplus metrics introduced by Vogel (2007) were computed for each flow-duration curve. These metrics provide a simplified representation of hydrologic impacts (Vogel et al., 2007). For this study, ecodeficit is defined as the ratio of the area below the no-wildfire scenario flow-duration curve and above the wildfire scenario flow-duration curve divided by the total area under the no-wildfire scenario flow-duration. Conversely, ecosurplus is defined as the ratio of the area above the no-wildfire scenario flow-duration curve and below the wildfire scenario flow-duration curve divided by the total area under the no-wildfire scenario flow-duration. Thus, these values represent the overall loss (ecodeficit) and gain (ecosurplus) in streamflow (Vogel et al., 2007) between scenarios.

2.3 Results and Discussion

2.3.1 SWAT Model Performance

The optimal parameter set found during the calibration effort generally yielded good results. The model performed best during the post-wildfire testing period, but still performed well during the calibration period and pre-wildfire testing period. Final values for the 38 calibration parameters are displayed in APPENDIX B. Model performance was evaluated based on primary statistical results (at both the daily and monthly timesteps) and visual inspection of the graphical results.

The best calibration achieved for the Mouth of Canyon naturalized streamflow at the daily timestep is E_{NS} of 0.82 and RE of 1.68. The testing E_{NS} values for the pre-wildfire and post-wildfire periods were 0.71 and 0.88, with RE values of -19.52 and 9.31, respectively. Model performance during the calibration and testing periods at a daily timestep was considered good if $E_{NS} \geq 0.75$ and was considered satisfactory for values of E_{NS} between 0.75 and 0.36 (Motovilov

et al., 1999). Also, upon reviewing available literature, these results are consistent with previous studies using SWAT at a daily timestep (Li et al., 2010; Zhu and Li, 2011). Table 2 presents a summary of the model performance at the daily timestep with supplementary error statistics displayed in APPENDIX B.

Table 2. Error statistics between observed and simulated daily streamflows for the calibration period as well as the testing periods. Performance ratings based on Motovilov (1999).

Simulation	Simulation period	Relative error	Nash-Sutcliffe efficiency	Performance rating
Pre-wildfire testing	2000-2004	-19.52	0.71	Satisfactory
Calibration	2005-2013	1.68	0.82	Good
Post-wildfire testing	2014	9.31	0.88	Good
All	2000-2014	-2.73	0.82	Good

Additional performance ratings were assigned to the calibration and testing periods for monthly simulations of streamflow. This evaluation was based on suggested ratings found in published literature for monthly timesteps, which include ratings of very good ($0.75 < E_{NS} \leq$ 1.00), good ($0.65 < E_{NS} \leq 0.75$), satisfactory ($0.5 < E_{NS} \leq 0.65$), and unsatisfactory ($E_{NS} \leq 0.5$) (Moriasi et al., 2007). All simulation periods earned a performance rating of very good at the monthly timestep. Further, monthly results are generally comparable to those from other SWAT modeling studies involving mountainous watersheds (Foy et al., 2009; Lu et al., 2015; Neupane et al., 2015). Table 2 presents a summary of the model performance at the monthly timestep and supplementary error statistics are displayed in APPENDIX B.

Generally, simulations yielded good visual agreement between observed and simulated daily streamflows and total runoff volume, as shown in Figure 4. A slight discrepancy between the observed and simulated total runoff volume exists for the no-wildfire testing period. This difference propagates through to the statistical results, most notably, the RE value of -19.52. A

negative relative error shows that the model overestimates runoff volume compared to observations. Based on visual examination of the hydrograph, the calibration period may be slightly "wetter" relative to the pre-wildfire testing period, which may be the cause of the noted discrepancy.

Table 3. Error statistics between observed and simulated monthly streamflows for the calibration period as well as the testing periods. Performance ratings based on Moriasi and Arnold (2007).

Simulation	Simulation period	Relative error	Nash-Sutcliffe efficiency	Performance rating
Pre-wildfire testing	2000-2004	-19.36	0.80	Very Good
Calibration	2005-2013	1.77	0.88	Very Good
Post-wildfire testing	2014	9.42	0.96	Very Good
All	2000-2014	-2.61	0.89	Very Good
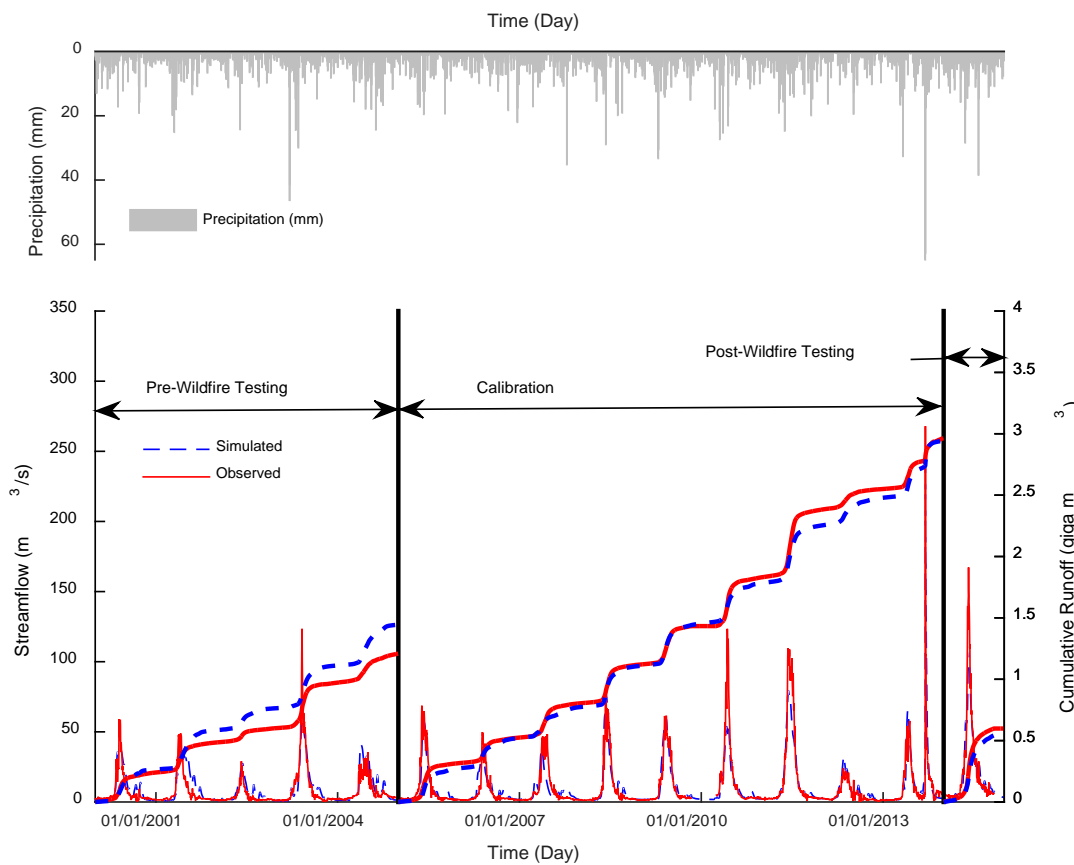
Figure 4. Total daily precipitation during simulation period (top). Observed versus simulated average daily streamflow shown by the thiner line and runoff volume shown by the thicker line (bottom) during simulation period.

Also, the simulated and observed flow-duration curves for the entire simulation period yielded good visual agreement, as shown in Figure 5. The simulated flow-duration curve generally follows the observed flow-duration curve with the exception of a slight deviation for less frequent flows. For the less frequent streamflows the model is underestimating streamflows. A deviation is expected as less frequent streamflows correspond to larger streamflows which are less predictable and less understood.
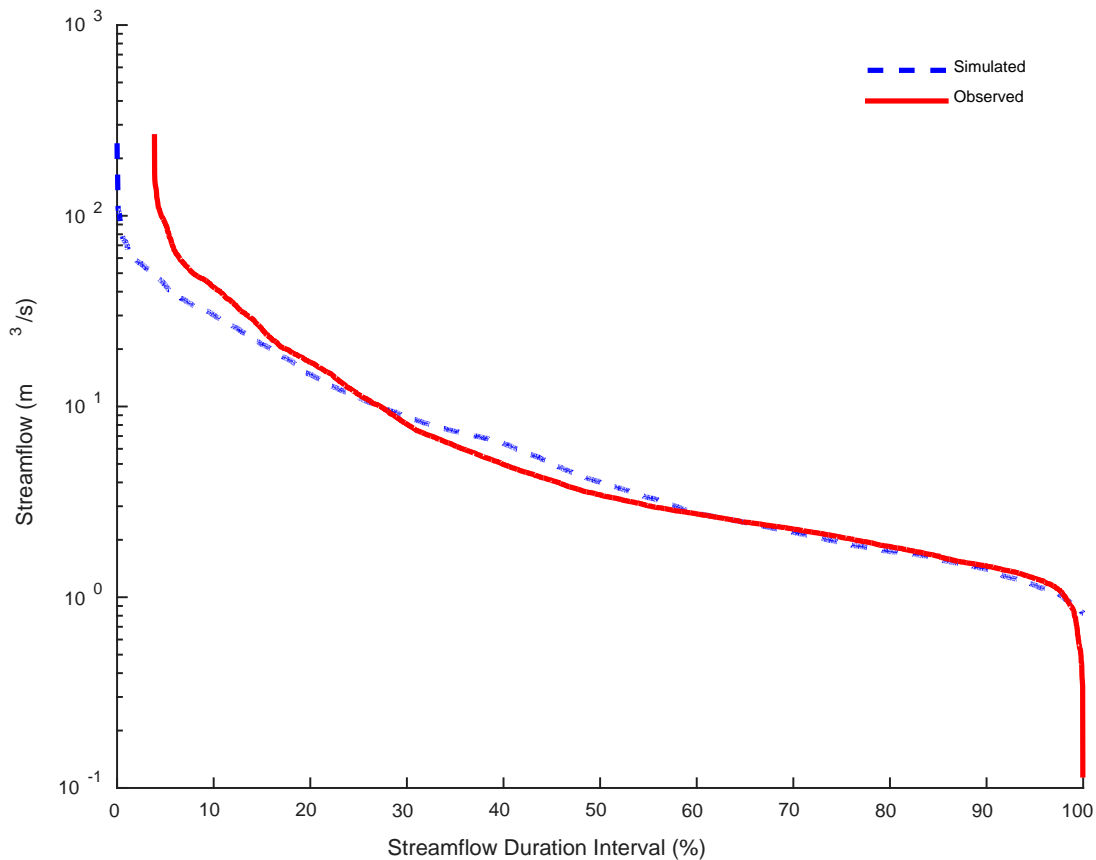
Figure 5. Flow-duration curve at the mouth of canyon for the entire simulation period.

Previous studies have used SWAT along with similar calibration techniques throughout this region for hydrologic analysis. However, use of the SWAT land use change module to investigate hydrologic response to wildfires has not been well documented. The performance results above indicate that the comprehensive methodology of using the SWAT land use change

29

module along with multi-variable parameter calibration was an effective technique to represent the hydrology of an area which has been exposed to wildfire.

2.3.2 *Wildfire Effects on Runoff Volume*

The daily simulation outputs from both the no-wildfire and wildfire scenarios were analyzed and compared in order to characterize an average hydrologic response to wildfire during the simulation period of 15 years (2000 to 2014). Total runoff values, represented as both depth and volume for each burned sub-basin as well as for the entire study watershed are shown in Table 4. Also, Figure 6 displays the burn severity distribution and average annual total runoff percent increase (based on the values presented in Table 4) for each burned sub-basin and for the entire study watershed. The average annual total runoff includes surface runoff, lateral flow, and base flow.

Table 4. Average annual total runoff volumes and depths for both the no-wildfire and fire scenarios, shown for the burned sub-basins as well as for the entire study watershed. Area is also include for reference.

Sub-basin	Area (km^2)	Average annual total runoff volume (mega m^3/yr)		Average annual total runoff depth (mm/yr)	
		No-wildfire	Wildfire	No-wildfire	Wildfire
19	89.56	1.82	2.10	20.4	23.4
24	56.53	0.74	1.01	13.1	17.9
25	5.41	0.14	0.14	25.4	25.7
26	17.39	0.61	0.98	35.0	56.4
28	14.64	0.33	0.58	22.8	39.8
29	47.15	1.59	1.67	33.7	35.3
30	106.95	4.16	6.81	38.9	63.7
32	10.86	0.30	0.49	27.4	45.4
35	269.11	38.91	41.70	144.6	154.9
Study Watershed	2,732	323.52	330.38	118.5	121.1
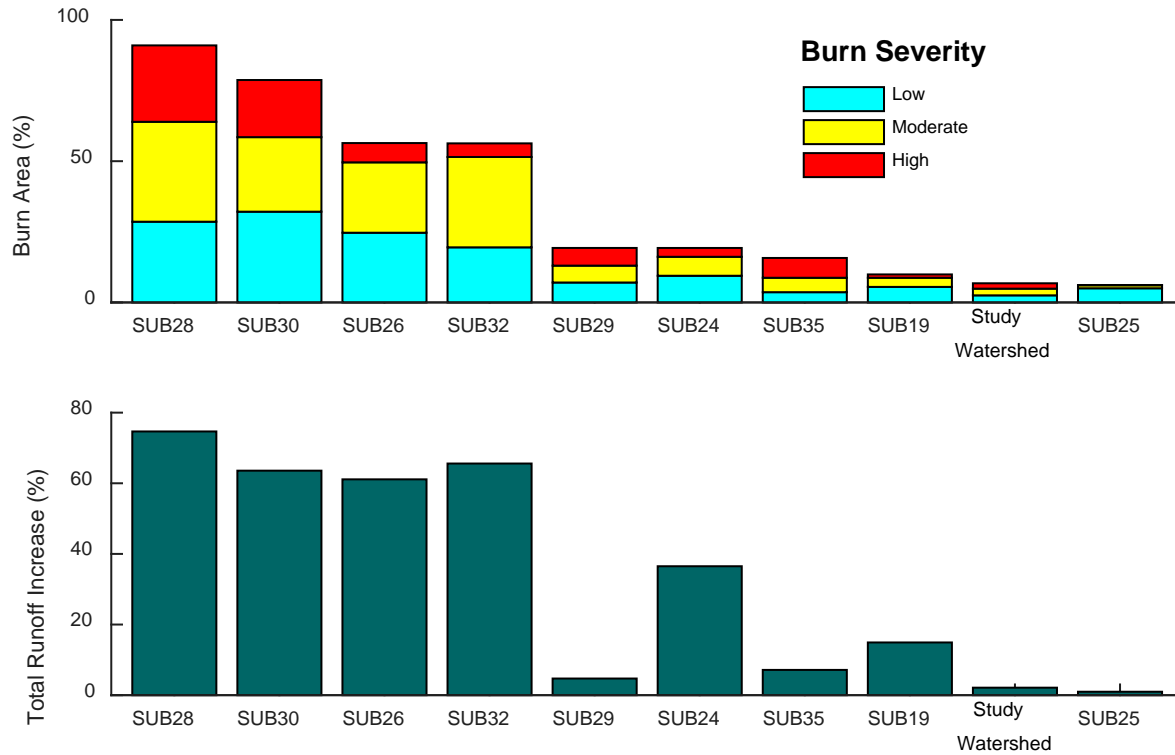
Figure 6. Burn severity distribution (top) and average annual total runoff percent increase between the no-wildfire and fire scenarios (bottom). Results are shown for the burned sub-basins as well as for the entire study watershed ("Study Watershed') arranged in descending order from left to right based on total percent burned area.

Figure 6 shows that in the case of sub-basins 28, 30, 26, and 32 more than 50 percent of the area experienced burning as a result of the High Park and Hewlett wildfires. Sub-basins 28 and 30 were the most severely burned with large high burn severity percentages. The remaining sub-basins had smaller burn area percentages.

The total runoff percent increase between scenarios was greatest on average for sub-basins 28, 30, 26, and 32. For these sub-basins, increases in runoff between the no-wildfire and wildfire scenarios ranged from approximately 66 to 75 percent. For the remaining sub-basins, as well as the entire study watershed, runoff percent increases are found to be considerably less. This is likely because those sub-basins were not as heavily burned. Nevertheless, the results indicate wildfire effects at larger scales are still substantial, but only in terms of the magnitude

31

rather than percent change of total runoff volume increase. Larger areas (i.e., sub-basin 35 and the entire study watershed) appear to experience much greater absolute increases in total runoff volume between scenarios, despite having smaller total burn area percentages. This is what we might expect given that each sub-basin is nested within the study watershed, resulting in a cumulative effect.

Many previous studies have documented total runoff increases under post-wildfire conditions (Benavides-Solorio and MacDonald, 2001; Inbar et al., 1998; Lavabre et al., 1993; Robichaud et al., 2000; Scott, 1993). For example, Lavabre et al. (1993) used a lumped conceptual hydrological model to evaluate a small Mediterranean basin which experienced a burn covering 85 percent of its surface area in 1990. They suggested a 30 percent increase in the annual runoff yield. Scott (1993) showed total streamflow volume increases of 15.3 and 9.4 percent in response to burning in two small mountainous catchments using a paired catchment method. The amount of total runoff volume increase following wildfire disturbance varies greatly between locations depending on wildfire intensity, proportion of the forest vegetation burned, climate, precipitation, geology, soils, watershed aspect, and tree species (Neary et al., 2003). Thus, it is not surprising that results vary. Also, comparison between studies is difficult because of changes in size of disturbance (i.e., wildfire) in relation to the size of the catchment (Robichaud et al., 2000). This emphasizes the need to examine increases based on percent burn area upstream.

Figure 6 is arranged in descending order of percent burned area from left to right. Generally, we see an increase in total runoff as percentage of total burn area increases. This observation is consistent with reports in the literature indicating total runoff volume increase following wildfire disturbance is in part a function of the proportion of the contributing area

burned (Neary et al., 2003; Robichaud et al., 2000). This relationship is further explored by applying linear regression to the data. Figure 7 shows a linear regression model fitted between the total runoff volume increase and total burned area percentage. Note that the entire study watershed results were not included in this regression. Also, sub-basin average slope was categorized as low (slope < 0.30), moderate ($0.30 \leq$ slope < 0.40), and steep (slope ≥ 0.40) for each sub-basin.
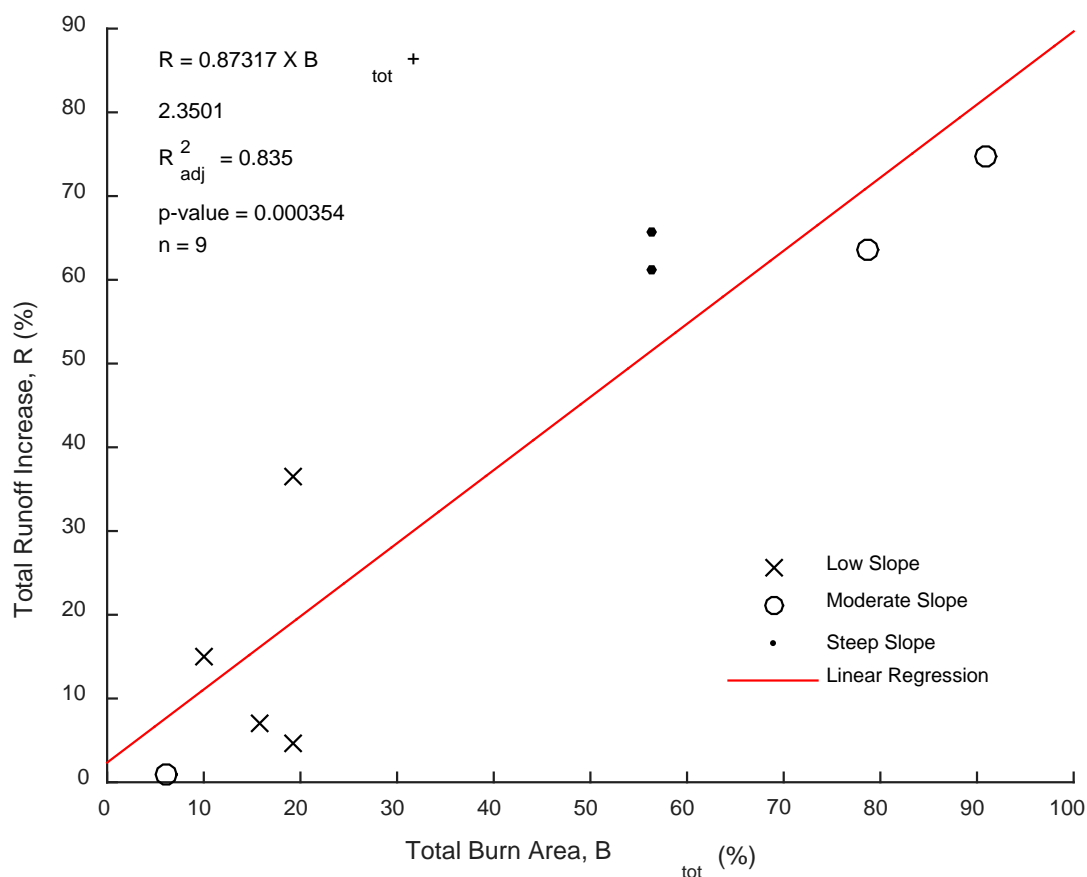
Figure 7. Linear regression model fitted between the total runoff volume increase and total burn area percentage. Catchment slope is categorized as low (slope < 0.30), moderate ($0.30 \leq$ slope < 0.40), and steep (slope ≥ 0.40) for each sub-basin.

An F-test was performed using Matlab to determine if this particular model fits the data well. The regression generally yields a good fit, with a p-value for the F-test < 0.001. No previous study documenting this relationship with linear regression could be found, but the

general trend is consistent with the literature. Thus, this study suggests it may be reasonable to use total burn area percentage as a predictor for an increase in total runoff volume with a linear regression model. Also, the figure indicates that generally for the High Park and Hewlett wildfires the sub-basins with moderate to steep slopes experienced wildfire in a larger percentage of their area relative to low slope sub-basins.

2.3.3 *Wildfire Effects on Hydrologic Budgets*

The daily simulation outputs from both no-wildfire and wildfire scenarios were further analyzed and compared in order to quantify changes in average annual hydrologic budgets as a result of wildfire during the simulation period of 15 years (2000 to 2014). Figure 8 shows hydrologic budgets for select sub-basins as well as the entire study watershed. These hydrologic budgets show the fate of average annual precipitation along with the fate of average annual total runoff. The fate of precipitation (rainfall and snowfall) is shown as evapotranspiration, total runoff, and other (deep aquifer contribution and soil water storage). Also, the major hydrologic processes for the fate of runoff were defined as surface and subsurface (lateral flow and base flow) runoff.
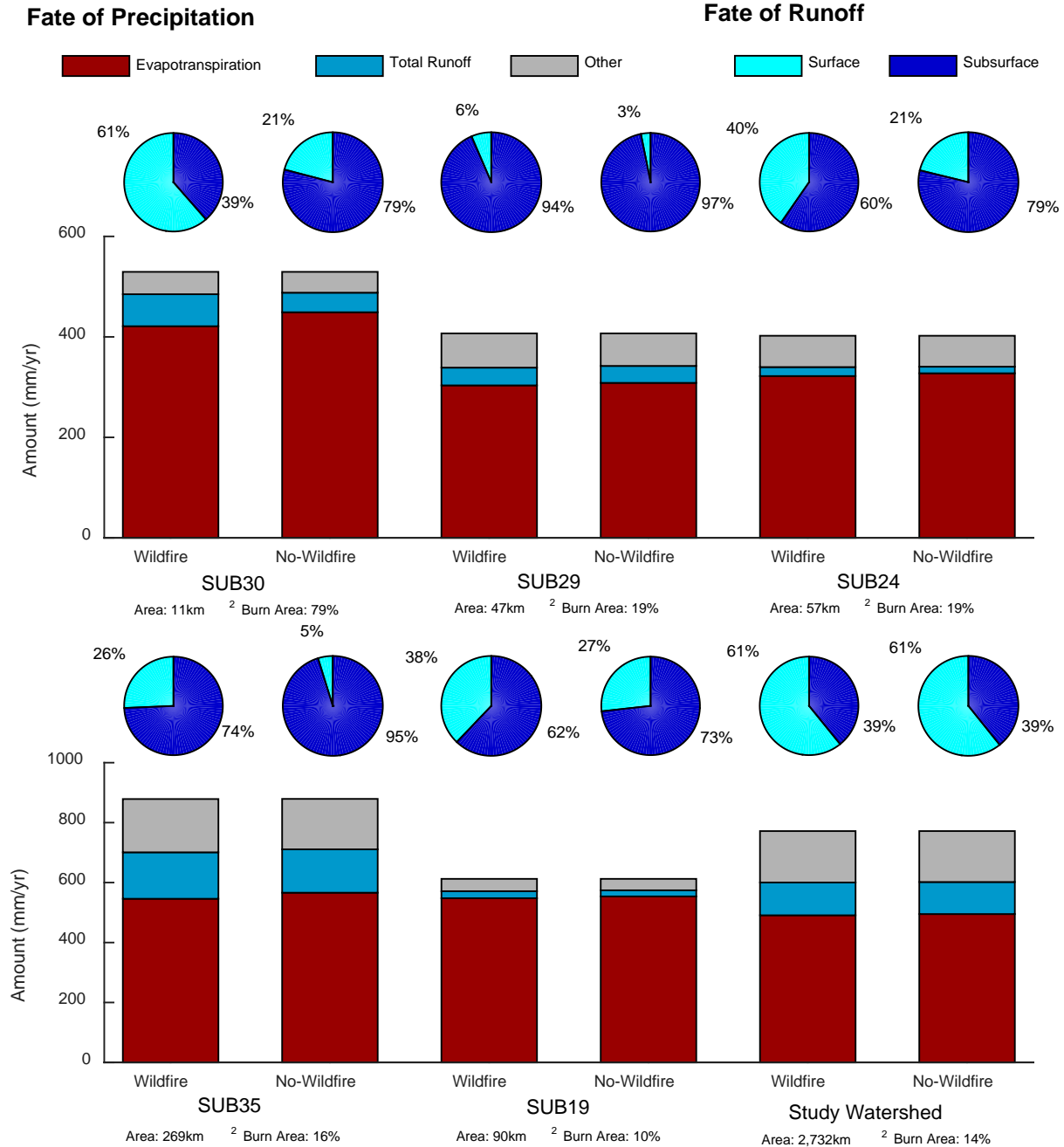
Figure 8. Hydrologic budgets showing the fate of average annual precipitation (i.e., evapotranspiration, total runoff, and other) with the fate of average annual total runoff (i.e., surface and subsurface) for select sub-basins and the entire study watershed.

It is evident that hydrologic budgets change on the sub-basin scale following wildfire; but little change is seen at the watershed scale. This is consistent with a claim made by Batelis and Nalbantis (2014) that wildfire effects are practically indiscernible on a regional scale. Generally, Figure 8 shows under the wildfire scenario an increase in surface runoff and a corresponding

decrease in subsurface runoff at the sub-basin scale. For example, the hydrologic budget for sub-basin 30 (a heavily burned area) shows a change in surface runoff from 21 to 61 percent under the no-wildfire and wildfire scenarios, respectively. This is consistent with previous studies, in which it seems to be generally accepted that infiltration rates decease after wildfires. For example, infiltration rates have been shown to decrease by a factor of two to seven after wildfires (Moody and Martin, 2001).

At the sub-basin scale under the wildfire scenario we also see less evapotranspiration. This connects well with the results from Section 2.3.2, where generally we see an increase in total runoff for the wildfire scenario. Increased water yields (i.e., total runoff) primarily due to reduced evapotranspiration has been a reported effect on post-wildfire hydrology (Neary et al., 2003; Townsend and Douglas, 2004).

2.3.4   Implications of Wildfire Effects

Lastly, the daily simulation outputs from both no-wildfire and wildfire scenarios were analyzed and compared in order to determine potential implications of wildfire effects during the simulation period of 15 years (2000 to 2014). Figure 9 shows flow-duration curves for select burned sub-basins as well as for the entire study watershed and Table 5 lists the ecosurplus and ecodeficit values associated with each computed flow-duration curve. The flow-duration curves represent the percentage of time that streamflow is likely to equal or exceed a given streamflow value for both scenarios. Flow-duration curves were generated using total runoff, which includes both surface and subsurface water fluxes leaving the sub-basin or watershed. The ecosurplus and ecodeficit metrics are a dimensionless measure which represent the overall loss (ecodeficit) and gain (ecosurplus) in streamflow (Vogel et al., 2007) between scenarios.
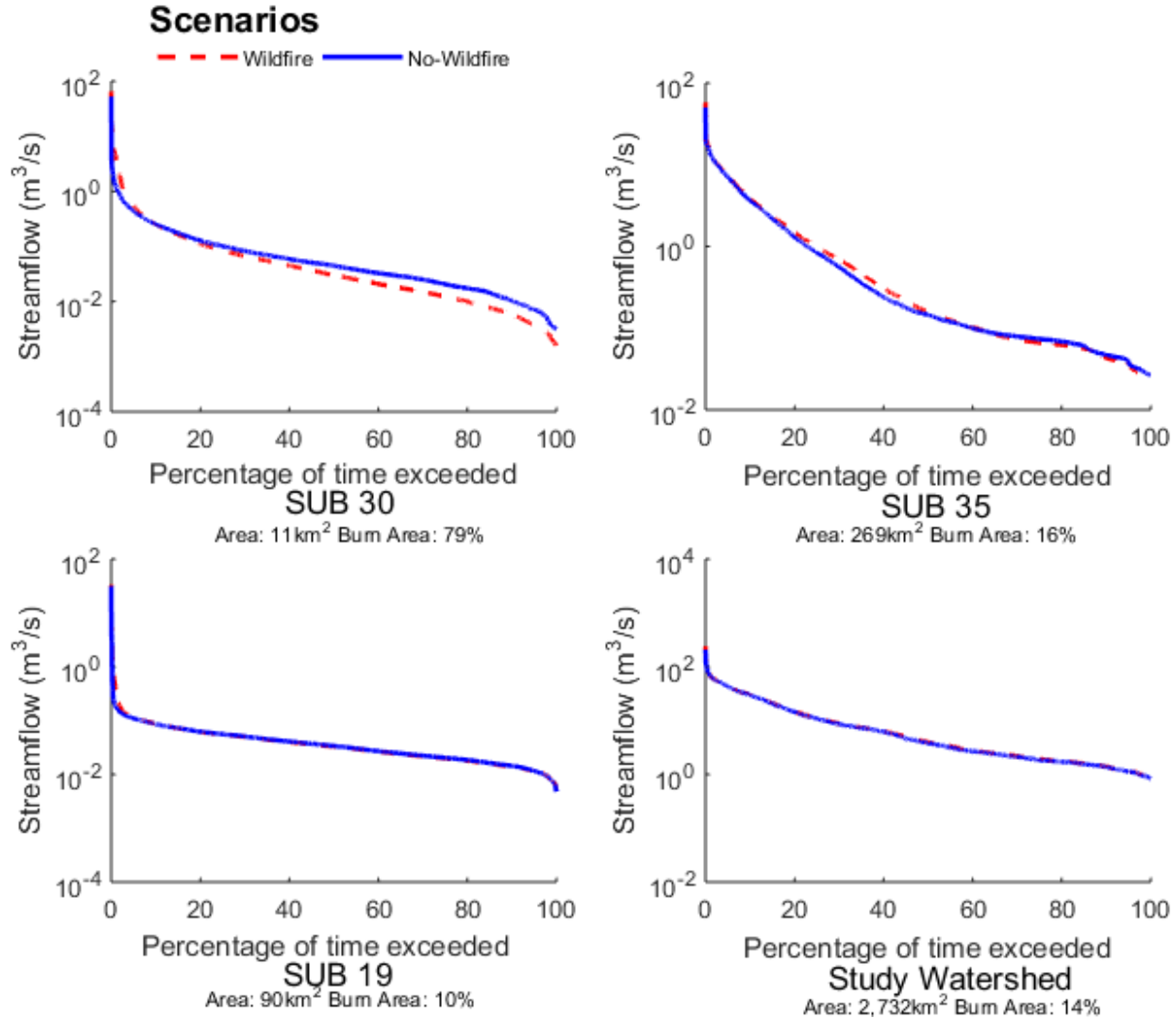
Figure 9. Flow-duration curves for select sub-basin as well as the entire study watershed.

Table 5. Ecosurplus and ecodeficit values for the burned sub-basins as well as for the entire study watershed.

Sub-basin	Ecosurplus	Ecodeficit
19	0.065	0.001
24	0.100	0.004
25	0.004	0.000
26	0.168	0.011
28	0.248	0.010
29	0.089	0.000
30	0.279	0.016
32	0.157	0.010
35	0.093	0.001
Study Watershed	0.093	0.001

Similar to findings from the hydrologic budgets, it is evident that flow-duration curves change under wildfire conditions on the sub-basin scale. Also, little change is seen at the watershed scale (Figure 9 and Table 5). This is perhaps the result of wildfire effects at the watershed scale being damped by non-burned portions of the contributing area. Again, this is consistent with the suggestion of Batelis and Nalbantis (2014) that wildfire effects are practically indiscernible on a regional scale.

Figure 9 also suggests that wildfire has little impact on flow-duration curves for areas with low total burn area percentages, but seems to impact flow-duration curves for area with higher total burn area percentages. For example, in sub-basins 30 we see that less frequent streamflows become greater in magnitude under the wildfire scenario (i.e. we see an ecosurplus). Whereas, in sub-basin 19 (a less burned area) we see little change in the flow-duration curve. Previous research efforts have involved a paired-catchment analysis to compare flow duration curves for pre and post-wildfire conditions (Liu et al., 2004; Newtson, 2013). Both Newtson (2013) and Liu et al. (2004) found a general increase in percentile streamflow as a result of wildfire. However, Liu et al. (2004) examined precipitation duration curves for the study areas and concluded that changes in precipitation between locations explained the difference in streamflow and not necessarily wildfire. For this study, the two scenario approach uses an identical precipitation record for both scenarios. Thus, the study eliminates limitations associated temporal and special variation in precipitation. Table 5 indicates the streamflows for the burned sub-basins appear to be ecosurplus versus ecodeficit when the wildfire scenario is compared with the no-wildfire scenario. The ecosurplus values range from 0.004 to 0.279. Kannan and Jeong (2011) indicate that for high streamflows a large ecosurplus is likely to have moderate to high impacts to stream health. In this case, the ecosurplus values assoacited with the heavily burned

sub-basins (i.e., sub-basins 28, 30, 26, and 32) are much greater in magnitude when compared to the other ecosuplus values. Thus, impacts to stream health are expected to be the greatest in heavily burned areas.

2.3.5   SWAT Model Limitations and Future Work

As with any modeling study, this study includes multiple sources of uncertainty. These may be broadly categorized as model uncertainty (i.e., hydrologic model structure and variability of observed model input and output values at smaller temporal and spatial scales) and measurement uncertainty (i.e., imprecision in measuring input values). While the importance and value of a detailed uncertainty analysis is recognized, such an analysis is outside the scope of this project. However, specific concerns with regard to hydrologic model uncertainty are highlighted below.

In general, rainfall-runoff prediction methods have been developed for unburned areas. For example, the CN method (used for this study) is commonly applied to unburned areas. However, this method has produced conflicting results for burned areas. Post-wildfire hydrologic response is still a topic under investigation, with few studies focused on this specific issue (Moody et al., 2013). It is generally assumed that peak discharge tends to increase as a result of wildfire. Nevertheless, one major unresolved issue is that currently there is no consistent, agreed-upon methodology to estimate post-wildfire CNs (Springer and Hawkins, 2005). Thus, uncertainty is introduced and it is recommended that future work be focused on further developing rainfall-runoff prediction methods for burned areas.

Figure 10 displays simulated versus observed monthly streamflows as well as average monthly simulated and observed streamflow for the Mouth of Canyon. This figure suggests the

model slightly overestimates larger monthly streamflows: specifically, those during the month of June when streamflows are elevated due to mountain snowpack melting. Also, the model appears to slightly underestimate streamflows during late summer into autumn. These systematic errors may be due to SWAT releasing snowmelt too quickly during spring runoff, thus, rising streamflows are simulated earlier than observations during the melting season. Further, perhaps the tendency of the model to simulate earlier snowmelt results in higher simulated streamflow during the latter part of summer and early autumn. This deficiency may be the result of SWAT misrepresenting snowmelt processes or perhaps faulty model parameterization. Thus, it is thought that hydrologic model uncertainty is introduced here and it is recommended that additional research be focused on better representing snowmelt processes in mountainous watersheds.
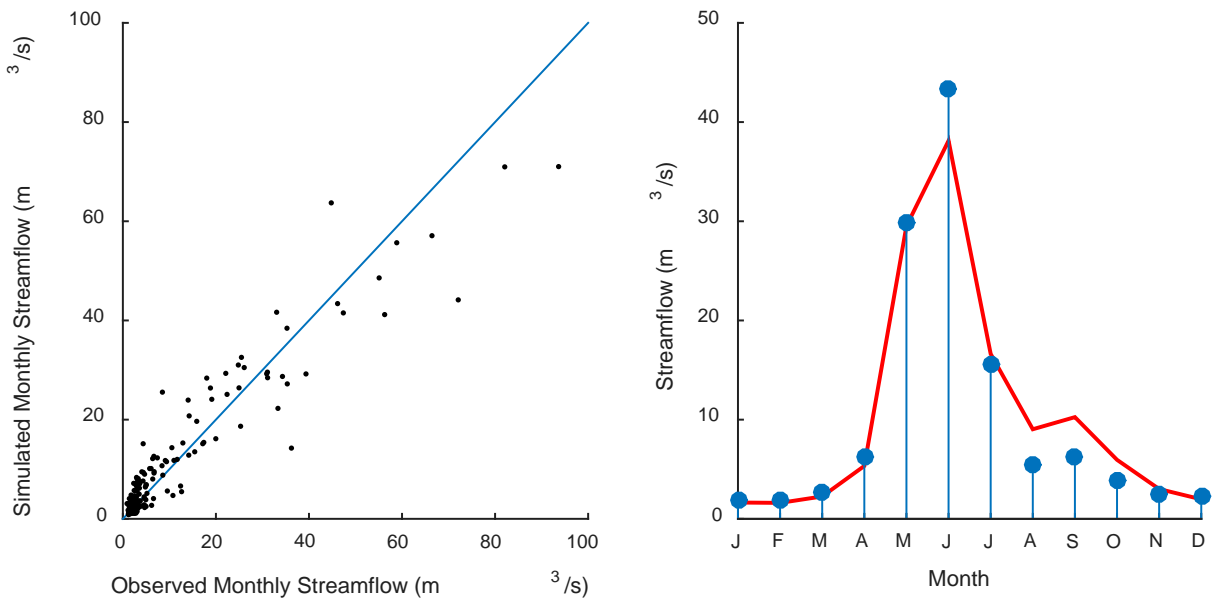
Figure 10. Plot of simulated versus observed monthly streamflows (left) and the observed versus simulated average monthly streamflows for the simulation period (right).

2.4   Conclusions

Long term simulation scenario analysis at the sub-basin and watershed scales was used to characterize hydrologic response to wildfires in mountainous regions. This was achieved by applying the hydrologic model SWAT to a watershed recently exposed to significant wildfire activity located in northern Colorado, USA. The model represents pre-wildfire and post-wildfire conditions by implementing the SWAT land use change module during simulations to represent burned area as a result of wildfire. Geospatial data representing LULC, soil, terrain, and climate attributes of the study watershed was used to develop the model. An optimal parameter set was obtained for pre-wildfire and post-wildfire conditions through the automated DDS optimization algorithm. Error statistics were calculated to evaluate model performance with regard to daily observed naturalized streamflows. Results indicate good model performance, with an E_{NS} of 0.82 during calibration as well as 0.71 and 0.88 for the no-wildfire and wildfire testing periods, respectively, for daily streamflows at the Mouth of Canyon. No-wildfire and wildfire scenarios representing a 15 year (2000 to 2014) simulation period were created from the optimal parameter set achieved during model calibration. These scenarios were used to characterize the hydrologic response to wildfires.

Specific objectives of this study were to investigate changes in average annual total runoff volume, average annual hydrologic budgets, and flow-duration curves across multiple scales. Results were generally comparable to the literature. At the watershed scale, wildfire conditions appear to have little effect on the hydrologic responses with the exception of total runoff volume. However, at the sub-basin scale, simulations suggest that wildfire effects trend with burn area upstream. A total runoff increase up to approximately 75 percent between scenarios was found. Generally, water budgets showed more surface runoff versus subsurface

41

runoff which suggests infiltration rates decrease under post-wildfire conditions. Flow-duration curves for burned sub-basins show that less frequent streamflows become greater in magnitude leading to ecosurplus values up to 0.279.

Results reported in this study show an overall acceptable performance of the SWAT model in simulating daily streamflows under pre and post-wildfire conditions to characterize the hydrologic response to wildfires. However, this method required comprehensive knowledge of the watershed, was time consuming, and was computationally intensive. Further, this study demonstrates the need for improvement in understanding the rainfall-runoff prediction relationship for burned areas.

CHAPTER. 3 CHARACTERIZING HYDRAULIC BEHAVIOR RESPONSE TO WILDFIRES USING THE HEC-RAS MODEL INFORMED BY SWAT MODEL HYDROLOGIC BOUNDARY CONDITIONS

3.1   Introduction

The HEC-RAS model requires hydrologic boundary conditions. To appropriately represent changing streamflow conditions it is important to apply unique boundary conditions to each segment with the study reach. Further, the SWAT model uses Manning's equation to define the rate and velocity of streamflow. This approach is based on using uniform channel geometry along reaches within the channel network. This is inadequate for investigating in-channel responses to wildfires because reaches within SWAT are generally quite long (i.e., on the order of 10^1 km). For these reasons, it is advantageous to use a HEC-RAS model informed by SWAT model hydrologic boundary conditions.

The primary goal for the research discussed in this chapter is to demonstrate the practical implementation of a modelling cascade to characterize channel hydraulic behavior response to wildfires at the channel scale in a major river downstream of wildfire activity. To accomplish this goal, the previously developed hydrologic model for a watershed recently exposed to significant wildfire activity located in northern Colorado, USA was used as boundary conditions for a newly developed HEC-RAS hydraulic model. The purpose of this model is to simulate streamflow for various floods associated with no-wildfire and wildfire scenarios. Specific objectives of this study are to: (1) quantify changes in streamflows for various floods between no-wildfire and wildfire scenarios; and (2) quantify response to wildfires in terms of hydraulic behavior including flood inundation area, velocity, and shear stress for reaches downstream of burned areas, all at the channel scale.

3.2   Methods

3.2.1   Hydraulic Model

This section is organized in the following manner:

- Section 3.2.1.1 – Describes the HEC-RAS software in detail.

- Section 2.2.1.2 – Describes the process domain concept used to partition the study reach.

- Section 3.2.1.3 – Reviews the HEC-RAS model data used for this study.

- Section 3.2.1.4 – Provides detailed information regarding the development of the cross sections for input to HEC-RAS.

- Section 3.2.1.5 – Shows in detail how the HEC-RAS model was developed.

- Section 3.2.1.6 – Describes how the HEC-RAS model was calibrated and tested.

3.2.1.1   HEC-RAS

The HEC-RAS Version 4.1 (U.S. Army Corps of Engineers, 2010), developed by the United States Army Corps of Engineers, was used for this study. This software was developed by Hydrologic Engineering Center (HEC), which is a division of the Institute for Water Resources within the United States Army Corps of Engineers (USACE) (Brunner, 2010a). The well-tested HEC-RAS model is available in the public domain and is widely used by many administrations, universities, and engineers worldwide (Kiesel et al., 2013). The model is well documented and capable of performing 1-D hydraulic calculations for a full network of natural and constructed channels (Brunner, 2010a).

The HEC-RAS software allows the user to produce water surface profiles for both steady gradually varied flow (GVF) and unsteady flow conditions. The program uses a common geometric data representation and common hydraulic computation routines to perform water surface profile calculations. The steady GVF module in HEC-RAS is specifically designed to evaluate floodway encroachments for application in floodplain management (Brunner, 2010a).

Therefore, the steady flow module was used for this analysis, using flows associated with particular events of interest.

Steady GVF is a non-uniform flow where the streamflow depth variation along the channel is gradual enough that the transverse pressure distribution may be considered hydrostatic. Thus, streamflow and other state variables such as velocity and streamflow depth may be treated as 1-D where the only transverse pressure gradients present are those created by gravity (Sturm, 2010). HEC-RAS uses the 1-D energy equation, which accounts for energy losses using the Manning's equation and contraction/expansion coefficients to perform steady GVF computations. Also, in situations where a water surface profile is rapidly varied, the momentum equation is utilized. This module allows modeling of subcritical, supercritical, and mixed flow regime water surface profiles (Brunner, 2010a). Additional details regarding the 1-D equations used by the program may be found in the HEC-RAS Hydraulic Reference Manual, Version 2010 (Brunner, 2010a).

3.2.1.2 *Process Domains*

The study reach was delineated into segments using a process domain concept. This approach allows areas to be spatially identified and characterized by unique suites of geomorphic processes. These unique areas contain community structure and dynamics that respond in distinctly different ways to any given disturbance regime (Montgomery, 1999). The process domain concept provides an organizational framework which may be applied to numerous aspects of river systems (Wohl, 2010). This conceptual model was applied to the study reach, a bedrock dominated system, to delineate segments with inherently unique hydraulic process from one another. This delineation was used to help select appropriate cross section spacing as well to define calibration segments, both of which are discussed in following sections.

Similar to Wohl (2010), which focused on applying the process domain concept in the context of sediment dynamics, channel and valley geometry was the most practical criterion for differentiating individual process domains. Channel and valley geometry in the form of gradient and confinement (valley width) were used to classify the study reach into two categories. The categories include confined and partially confined. Confined valleys were defined to be steeper, in the upstream to downstream direction, and have narrower valley bottoms relative to the partially confined valleys. An upstream to downstream direction slope threshold of 2 percent was selected based on Wohl (2010) for the gradient classification. A lateral slope threshold of 16 percent was selected based on Gallant (2003) and a trial and error processes. With these thresholds defined, the analysis detailed in APPENDIX D was performed in ArcMap to delineate the study reach into segments. The analysis resulted in the study reach being broken into three segments shown in Figure 11.
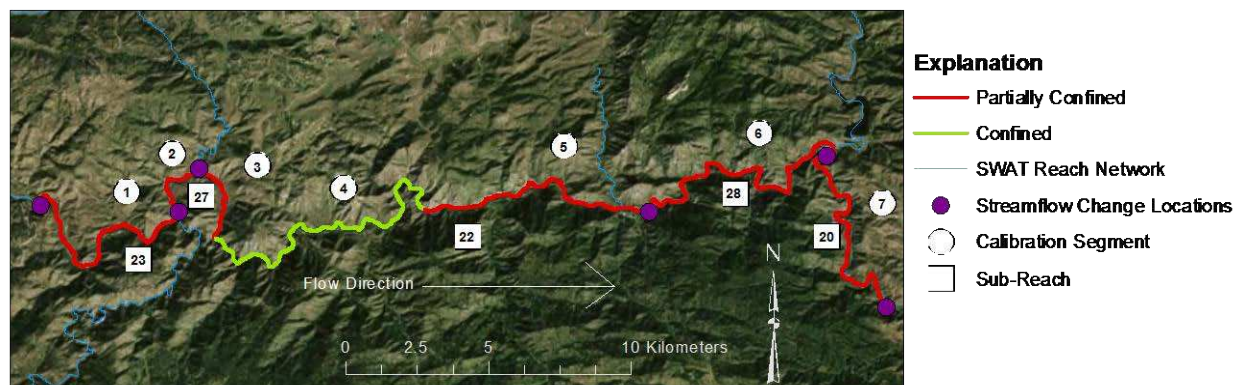
Figure 11. Study reach detail including the process domain classification, the SWAT reach network, streamflow change locations, calibration segments, sub-reaches, and imagery basemap (Esri, 2015b).

3.2.1.3 HEC-RAS Model Data

The hydraulic modeling process was initiated by collecting and preparing the necessary data, summarized in Table 6. The hydraulic model spatial datasets were converted, transformed,

46

clipped, and merged using ArcMap as described in Section 2.2.1 to produce consistent seamless

spatial datasets.

Table 6. HEC-RAS model input data.

Data type	Data used	Description
Floodplain Terrain	Digital Elevation Model	Federal Emergency Management Agency Light Detection and Ranging Dataset	3/4 m
Stream Centerline	Reach Network	From SWAT Model
Cross Sections	Survey Points	RTK-GPS Survey
Hydraulic Structures	As-built Drawings	City of Fort Collins, Colorado Division of Water Resources, and Northern Colorado Water Conservancy District
Hydraulic Roughness	Manning's n Values	From Chow (1959) and Model Calibration
Steady Flow Data	Flood Events	From SWAT Model
Boundary Condition	Discharge Rating Curve	Colorado Division of Water Resources
Stage-Streamflow	Digital Elevation Model and Simulated Streamflow	From Federal Emergency Management Agency Light Detection and Ranging Dataset	3/4 m and SWAT Model

Floodplain Terrain

Floodplain topography along the study reach was described using a 3/4 m resolution

DEM obtained from the Federal Emergency Management Agency (FEMA) (Federal Emergency

Management Agency, 2014). This DEM was derived from Light Detection and Ranging

(LiDAR) data collected by FEMA and the USGS during the latter part of 2013 after the

catastrophic floods in September 2013 throughout the Front Range of Colorado, USA.

Stream Centerline

The stream centerline for the study reach was described using the reach network

generated during the creation of the SWAT model discussed in CHAPTER. 2. Note that the

reach network generated in ArcSWAT was based on a 10 m DEM whereas the HEC-RAS model was based on the 3/4 m DEM. Thus, additional adjustments were required to the SWAT reach network prior to use in the HEC-RAS model because the alignment is pixelated at the channel scale. The SWAT generated reach network was smoothed using the AcrMap Generalize tool with a 10 m tolerance.

Cross Sections

Cross sections were developed from the combination of detailed cross section survey data as well as 3/4 m DEM data. The used on the 3/4 m DEM data is discussed in a subsequent section, but the detailed cross section survey data collection process is discussed here. In part, detailed cross sections were used to describe the channel geometry throughout the study reach. We surveyed detailed cross sections using Real Time Kinematic (RTK) United States Global Positioning System (GPS) survey equipment. Spacing was selected based on the overall length of the study reach, constraints associated with limited resources, and the process domain classification for the study reach. Spacing goals in partially confined and confined segments were set at 1,000 m and 500 m, respectively. Specific cross section locations were initially establish in ArcMap using the spacing goals and the 3/4 m DEM as a reference to ensure cross sections were perpendicular to the streamflow. Bathometric and floodplain elevation data for a total of 45 cross sections were obtained from 23 separate surveys performed during the spring and fall of 2014. Collected survey data were post-processed and converted to a data format compatible with ArcMap. Unwanted points for the HEC-RAS model were manually filtered out and the remaining points were corrected. These points included duplicate measurement points, survey control points, and points that were affected by the presents of ice. Corrections were determined using static data collected during each survey that were processed with the NOAA's

National Geodetic Survey (NGS) Online Positioning User Service (OPUS). A summary of the detailed cross section data is provided in APPENDIX E. When possible, the survey was checked using vertical and GPS control information obtained from the NOAA's NGS database. A summary of survey control errors for 16 of the 23 surveys may be found in APPENDIX B.

Hydraulic Structures

Elevations for two hydraulic structures within the study reach were provided by the City of Fort Collins in the form of as-built drawings. Northern Water provided as-build survey points for a third hydraulic structure. Also, CDWR provided survey information at the Mouth of Canyon surface water gauge station. In all cases, obtained data were georeferenced using a 3/4 m DEM because the necessary metadata were not available.

Hydraulic Roughness

Final Manning's n values were determined through the calibration process discussed in a subsequent section. However, values obtained from Chow (1959) were used as an initial starting point. A value of 0.05 was assigned to the entire model with the exception of the structures, where 0.011 was used. The 0.05 value is described by Chow (1959) as a minor mountain stream with: no vegetation in the channel; banks usually steep; trees and brush along banks submerged at high stages; and a cobble and large boulder bottom. The 0.011 value is described by Chow (1959) as a concrete, nonmetal, lined or built-up channel.

Steady Flow Data

Streamflow outputs from SWAT were preprocessed and then used as steady flow data input for the HEC-RAS model. This preprocessing was accomplished in several steps. First, the

SWAT output daily average naturalized streamflow was converted to daily maximum non-naturalized streamflow. Non-naturalized streamflow is the flow directly measured at a surface water gage station. Second, a flood frequency analysis was performed to obtain flood flows for various events of interest. Flood flows are of particular interest because in flood modeling, peak streamflow is required to predict the maximum flooding area and the associated velocities.

A two-step regression approach was used to (1) predict non-naturalized streamflows from naturalized streamflow (Figure 12), and (2) predict daily maximum streamflows from average daily streamflows (Figure 13). The regression analysis was based on naturalized streamflow used during the SWAT model calibration, along with daily and hourly streamflow data obtained from CDWR's Colorado Surface Water Conditions (CSWC) database (CO Division of Water Resources, 2014) for the Mouth of Canyon. Data for a period of 15-years (2000 to 2014) were collected. This period was selected based on the completeness of the available data. Using a trial and error procedure, a power function relationship was determined to be most appropriate. Once these relationships were established, they were used to convert streamflows outputs from SWAT at each streamflow change location.
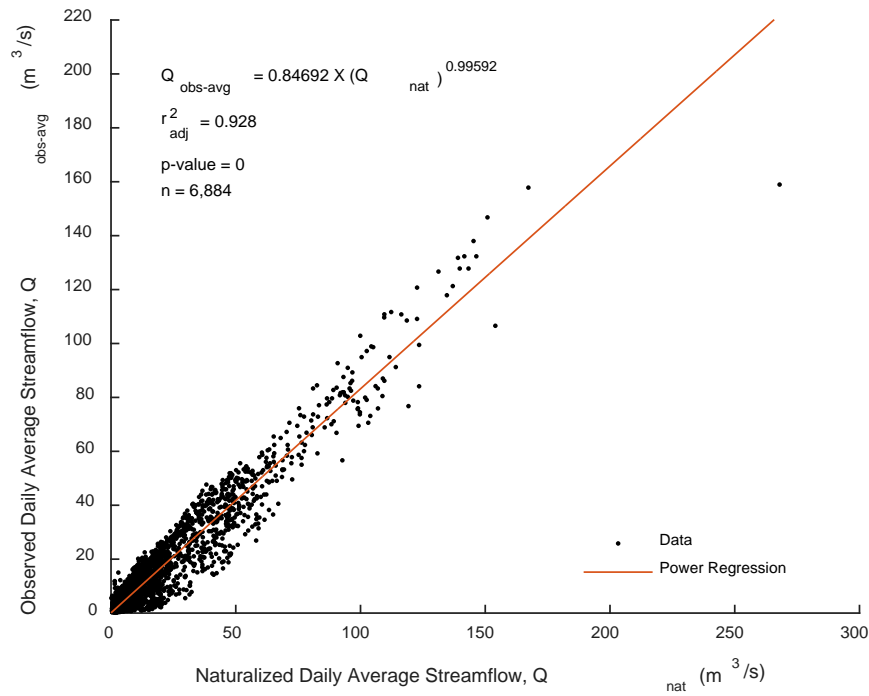
Figure 12. CDWR naturalized daily average streamflow versus observed daily average streamflow and corresponding power regression for the study reach at the Mouth of Canyon.
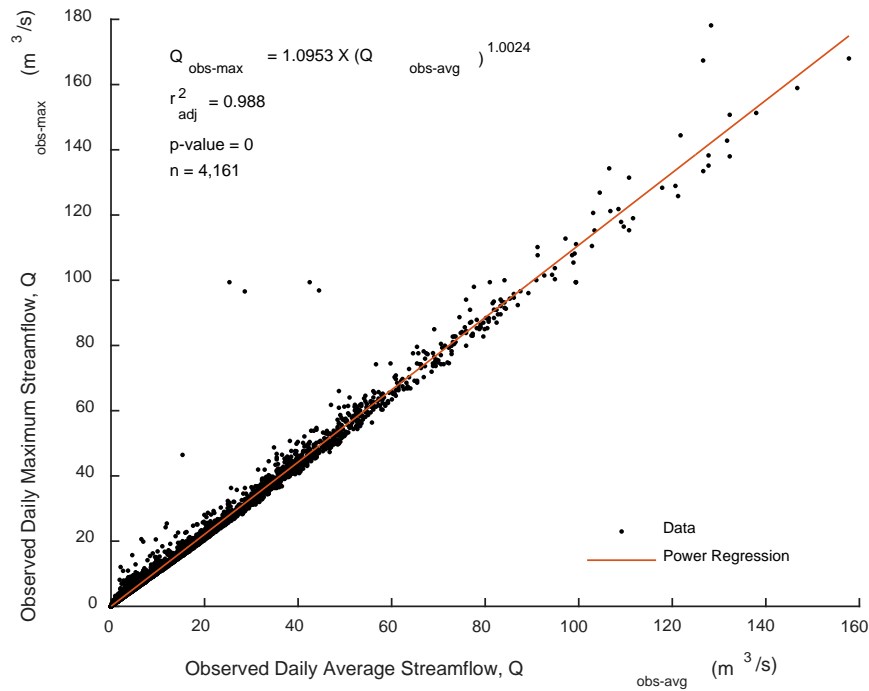
Figure 13. CDWR observed daily average streamflow versus observed daily maximum streamflow and corresponding power regression for the study reach at the Mouth of Canyon.

Next, a flood frequency analysis was performed using a technique outlined in Bulletin #17B (B17) of the Hydrology Subcommittee by the USGS. This statistical analysis is based on using a Pearson Type III distribution with log transformation of the data (log-Pearson Type III distribution). The general procedure involves determination of the frequency curve with an assessment of risk and uncertainty (Rallision et al., 1982). A Matlab code developed by Burkey (2009) was used to perform this analysis. A regional skewness coefficient is required for the analysis and a value of -0.15 was selected using the national regional skewness map found in the B17 documentation. This analysis provided 2, 10, 100, 200, and 500 year event flood flows for both the wildfire and no-wildfire scenarios.

Boundary Conditions

HEC-RAS requires the user to input an upstream and downstream boundary condition for simulations. The rating curve shown in APPENDIX A was obtained from CDWR's CSWC database (CO Division of Water Resources, 2014) and used as a downstream boundary condition for the study reach. For the upstream boundary condition, the normal depth option was selected and was based on a slope of 0.01 estimated from the 3/4 m DEM. These boundary conditions were selected based on the best available data for the study reach.

Stage-Streamflow

Observations of water surface elevations are required for HEC-RAS model calibration and validation. Stage-streamflow relationships were described by matching SWAT model streamflow output with a combination of water surface elevation sources including the detailed cross section survey and the 3/4 m DEM. This analysis was performed in ArcMap as described below.

The first set of stage-streamflow relationships involved first extracting the necessary information from the 3/4 m DEM, which included flight path lines and fly dates obtained from metadata as well as water surface elevations along the entire study reach. This is feasible because LiDAR technology does not penetrate water and thus provides a representation of the water surface at the time of data collection. Water surface elevations were assumed to be the minimum elevation according to the 3/4 m DEM within the channel boundary at any given cross section of interest along the study reach. The channel boundary was defined as a significant break in slope on each side of the stream centerline, and was determined by examining a slope raster generated from the 3/4 m DEM. Then streamflows from the SWAT model output were matched with the appropriate fly date and corresponding water surface elevations. The result is a water surface profile for the entire study reach with corresponding streamflows. Next, the regression discussed above used to predict non-naturalized streamflows from naturalized streamflow was used to convert the SWAT model streamflow output prior to the matching.

The second set of stage-streamflow relationships was described using information from the detailed cross sections. During the detailed cross section survey, water surface elevations were also obtained in addition to the cross section geometry. Similar to the methodology discussed above, streamflows from the SWAT model output were matched with the appropriate survey date and corresponding water surface elevations.

3.2.1.4 Cross Section Development

The detailed cross sections spacing was to coarse (i.e., the detailed cross sections surveyed with the GPS-RTK equipment were spaced too far apart) to provide acceptable results at the channel scale. Thus, the detailed cross section data were supplemented. This was accomplished by burning interpolated cross sections created from a tool developed by Venkatesh

Merwade of Purdue University into the 3/4 m DEM. This approach was selected to best represent both the in-stream and floodplain components of the channel geometry using the available data.

The interpolation tool, which is an add-in for ArcMap, was used to analyze the detailed cross sections in a channel-fitted coordinate system. Performing the analysis in a channel fitted coordinate system allows for data along and across the flow to be treated differently (Merwade et al., 2008). The tool requires several inputs, including: three-dimensional cross section lines, stream centerline, a bank lines layer, an average channel width, number of profiles, and cross section spacing. The bank lines layer was defined using the channel boundary (mentioned above) representing the edge of the water surface when the LiDAR data were collected. This tool lacks the ability to account for islands found within a river system. Thus, the channel boundary layer was adjusted to not include side channels. Next, the cross section lines and stream centerline described above were loaded and converted to the appropriate format. An average channel width of 20 m was approximated based on several random measurements along the study reach. The tool was then used to create 21 profile lines (the tools default) with a cross section spacing of 10 m. This spacing was established using Samuels' equation, as recommended by the HEC-RAS Hydraulic Reference Manual (Brunner, 2010b):

$$Cross\ Section\ Spacing \leq \frac{0.15D}{S_o}$$

where D is the average bank full depth of the main channel (m) and S_o is the average bed slope (m/m). This equation was used to calculate the maximum cross section for each detailed cross section. Equation parameters for each detailed cross section were approximated through inspection of the cross section geometry. The detailed cross section with the smallest calculated maximum spacing was applied as the interpolation spacing for the entire study reach. Using a

single spacing for the entire study reach simplifies the interpolation procedure and is anticipated to be conservative. This spacing analysis is summarized in APPENDIX B. The result of the interpolations was an additional 4,242 cross sections. The number of interpolated cross sections is much greater than the number of detail cross sections. The limitations associated with this are discussed in Section 3.3.5.

Next, the interpolated cross sections were "burned" into the surrounding topography. This was achieved by adjusting the entirety of each interpolated cross section by the difference of the mean of the bank elevations between the 3/4 m DEM and the interpolated cross sections, as depicted in Figure 14. This adjustment was applied to allow the model to capture variations in channel slope that were not captured in the interpolated cross sections. This resulted in a smooth transition between the floodplain (obtained from the 3/4 m DEM) and the main channel elevations (generated using interpolation).
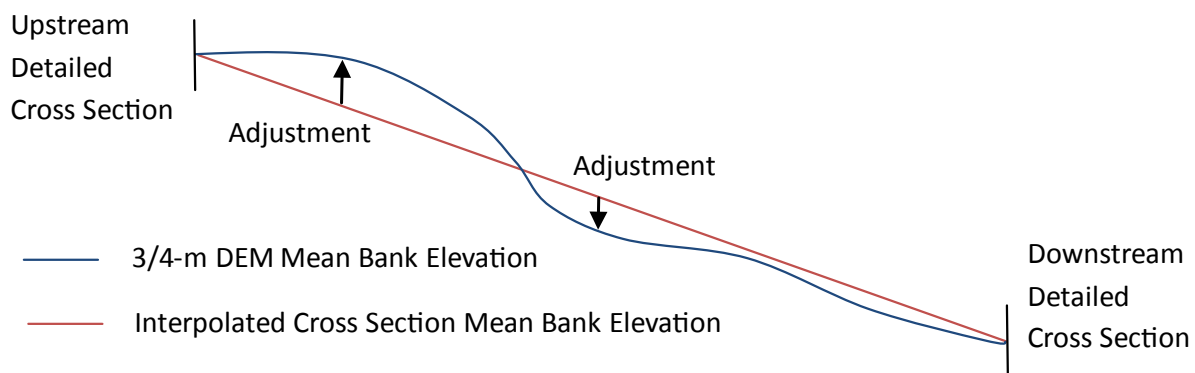
Figure 14. Depiction of adjustments made to interpolated cross sections.

3.2.1.5   *HEC-RAS Model Development*

The geometric data for the HEC-RAS model were prepared using HEC-GeoRAS 10.1 (U.S. Army Corps of Engineers, 2013). HEC-GeoRAS is an ArcMap extension that provides a graphical user input interface that aids with preparing HEC-RAS geometry input data. First, the

stream centerline and bank lines layers were loaded. Next, flow path centerlines were created by manually adjusting a 15 m offset of the stream centerline as needed. Then the XS Cutlines layer was generated using the detailed cross sections, geo-referenced hydraulic structures, and adjusted interpolated cross sections. The adjusted interpolated cross sections were extended from the edge of the 3/4 m DEM out onto the floodplain perpendicular to the streamflow. Lastly, ineffective flow areas were identified using a slope raster generated from the 3/4 m DEM. Figure 15 provides an example of each of these layers. With the layers created, the necessary attributes were assigned using the RAS Geometry tool within the HEC-GeoRAS extension. Table 7 provides a summary of the geometric data attributes generated. Finally, these geometric data were exported to HEC-RAS, where Manning's n values were manually assigned in the HEC-RAS geometric editor interface. All other model geometric parameters were left as default values.
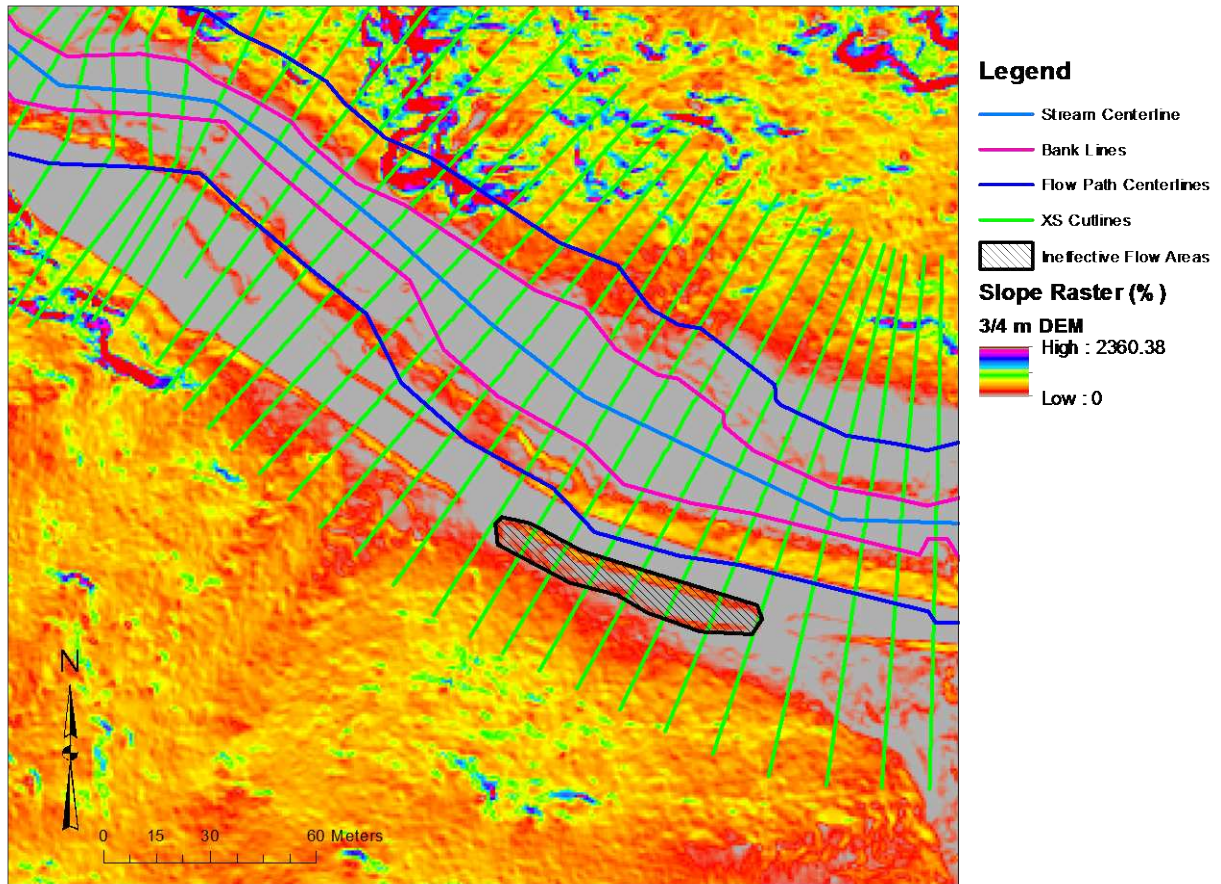
Figure 15. HEC-GeoRAS geometric data near station 29+636 with the slope raster background generated from the 3/4 m DEM.

Table 7. HEC-GeoRAS geometric data layers and attributes.

Layer	Attributes
Stream Centerline	River and Reach Code | Topology | Length/Stations
Bank Lines	-
Flow Path Centerlines	Line Type (i.e. left, right, or channel)
XS Cutlines	River and Reach Code | Stationing | Bank Stations | Downstream Lengths | Elevations
Ineffective Flow Areas	Positions

The steady flow data were entered into HEC-RAS using 5 streamflow change locations, thus breaking the study reach into 5 sub-reaches (Figure 11). The regressions discussed above were assumed to be appropriate for each sub-reach even though the regression analysis was based solely on data from the Mouth of Canyon. The streamflow change locations correspond to

outlet points manually added during the creation of the SWAT model. A steady flow analysis plan was developed using mixed flow regime. A mixed flow regime was selected because transitions between subcritical and supercritical flow are expected to occur, given the non-prismatic and steep nature of the study reach. All modeling options were left at default values with the exception of the maximum number of iterations. This was set to 40 (the maximum allowed by HEC-RAS) to give the program more chances to converge on a solution; although this number increases computation time.

3.2.1.6 *Model Calibration and Testing*

The HEC-RAS model was calibrated and tested to the stage-streamflow relationships. The Manning's n value was the only parameter adjusted during calibration. This is consistent with other studies using HEC-RAS (Beltaos et al., 2012; Md Ali et al., 2014; Saleh et al., 2013). The study reach was broken into 7 calibration segments based on flow change locations and the process domain segments (Figure 11). The Manning's n value was adjusted in each segment to best conform to the first set of stage-streamflow relationships. A trial and error procedure was used to minimize the average error between the stage measurements and the simulated water surface elevations. A Matlab code was developed to semi-automate the trial and error procedure. This code reads the cross section station and corresponding simulated water surface elevation from the HEC-RAS model output. For each calibration segment, the code then computes the error between the simulated and measured water surface elevations. For any given calibration segment, varying the Manning's n value within a plausible range resulted in little to no change in the average simulated water surface elevations of calibration segments upstream and/or downstream. Thus, the order in which the model was calibrated (i.e., what calibration segment was assigned a Manning's n value first, second, etc.) was determine to be irrelevant. If this was

not the case (which would be more likely if the calibration segments were much smaller), a sensitivity analysis would be required to determine whether each segment was downstream or upstream controlled. The model was then tested using the same code with the second set of stage-streamflow relationships obtained from the detailed cross section surveys.

3.2.2   Output Data Post-Processing

Matlab was used to analyze the HEC-RAS output by comparing average velocities and shear stress for each sub-reach. Further, HEC-GeoRAS was used to post-process model results using RAS Mapping tools found within the extension. This process was initiated by first importing the HEC-RAS output data into ArcMap using RAS Mapping tools. Next, flood inundation polygons for each event were generated using the water surface elevations in the HEC-RAS output and the 3/4 m DEM. This allows flood inundation areas to be calculated for each sub-reach.

3.3   Results and Discussion

3.3.1   Steady Flow Data

Table 8 shows the data used as steady flow input into the HEC-RAS model. These data are the result of the SWAT outputs preprocessing (i.e., the two power regressions and flood frequency analysis) for each sub-reach. Streamflows ranged between 34.75 m^3/s and 305.65 m^3/s throughout the study reach for the various floods.

Table 8. HEC-RAS steady flow input data with area upstream for reference.

Sub-reach	Area Upstream (km^2)	Scenario	Streamflows for various flood events (m3/s)					
			2-yr	10-yr	50-yr	100-yr	200-yr	500-yr
23	647.1	Wildfire	34.75	53.60	69.90	76.84	83.81	93.16
		No-Wildfire	34.75	53.60	69.90	76.84	83.81	93.16
27	963.3	Wildfire	42.52	69.33	93.74	104.40	115.28	130.09
		No-Wildfire	41.79	67.23	90.11	100.04	110.15	123.87
22	1059	Wildfire	43.07	72.13	99.44	111.59	124.10	141.32
		No-Wildfire	42.41	69.94	95.35	106.54	118.01	133.71
28	1238	Wildfire	44.09	81.73	121.66	140.66	160.98	190.13
		No-Wildfire	42.48	74.97	107.94	123.26	139.44	162.30
20	2718	Wildfire	50.22	109.51	185.30	225.43	271.04	340.96
		No-Wildfire	49.09	103.39	170.82	205.97	245.55	305.65
Study Watershed	2732	Wildfire	49.37	104.87	174.21	210.46	251.37	313.61
		No-Wildfire	48.28	98.20	158.22	188.94	223.19	274.62

3.3.2   HEC-RAS Model Performance

The optimal calibrated values for the Manning's n parameter yielded good results overall. Final Manning's n values for each calibration segment are shown in Table 9. Manning's n-values ranged from 0.025 to 0.135 throughout the study reach. Previous studies in this region have shown Manning's n values ranging from 0.028 to 0.159 (Jarrett, 1984). Thus, the calibrated values were considered appropriate. The model performed best during model calibration, but still performed well during model testing. Model performance was evaluated based on the RE between the observed and simulated water surface elevations as well as visual inspection of the graphical results.

Table 9. Final calibrated values for Manning's n.

Calibration Segment	Manning's n value
1	0.1
2	0.05
3	0.135
4	0.065
5	0.065
6	0.12
7	0.025

The best calibration achieved for the entire study reach is RE of 0.13. This calibration yielded a RE of -5.49 during model testing. Supplementary error statistics calculated for both the calibration and testing efforts are displayed in APPENDIX B. Figure 16 summarizes this effort by graphically representing the HEC-RAS model calibration and testing results. Generally, the average error between the calibration stage measurements and the simulated water surface elevations was minimized to nearly zero for each calibration segment. Also, in general, the testing stage measurements agreed with simulated water surface elevations. Figure 17 shows the errors associated with the calibration and testing efforts. Calibration errors ranged from -0.68 m to 0.74 m and testing errors ranged from -0.40 m to 0.32 m. These errors were considered acceptable given the uncertainties associated with the vertical accuracy of the 3/4 m DEM as well as varying topography. In several instances the calibration stage measurements were lower than the invert of the adjusted interpolated cross sections. This discrepancy is suspected to be an artifact of the modeling limitations discussed in Section 3.3.5. These measurements were omitted from the calibration procedure.
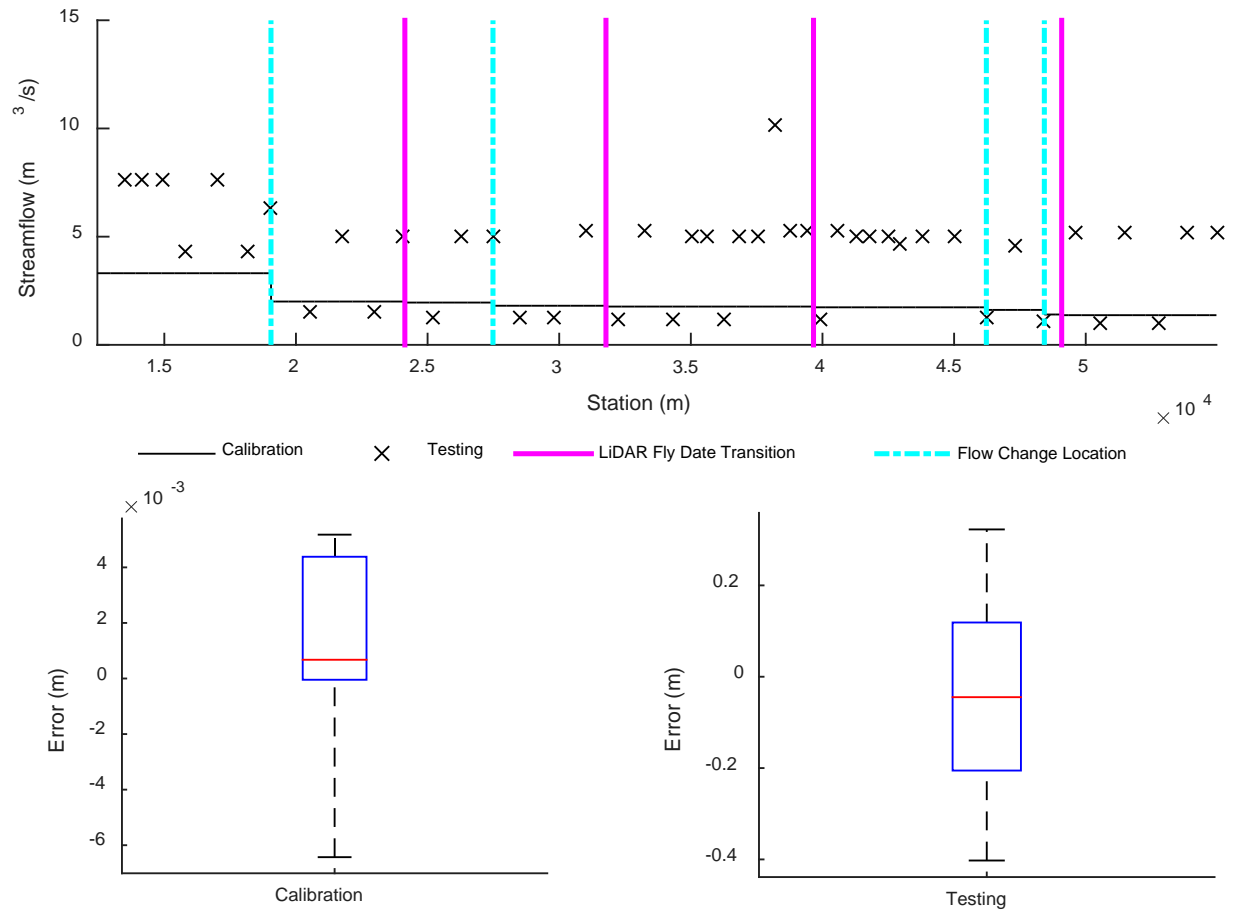
Figure 16. Steady flow data used during both model calibration and testing with LiDAR fly date transitions and flow change transitions (top); the average errors between the calibration stage measurements and the simulated water surface elevations (bottom left); and the errors between the testing stage measurements and the simulated water surface elevations (bottom right).
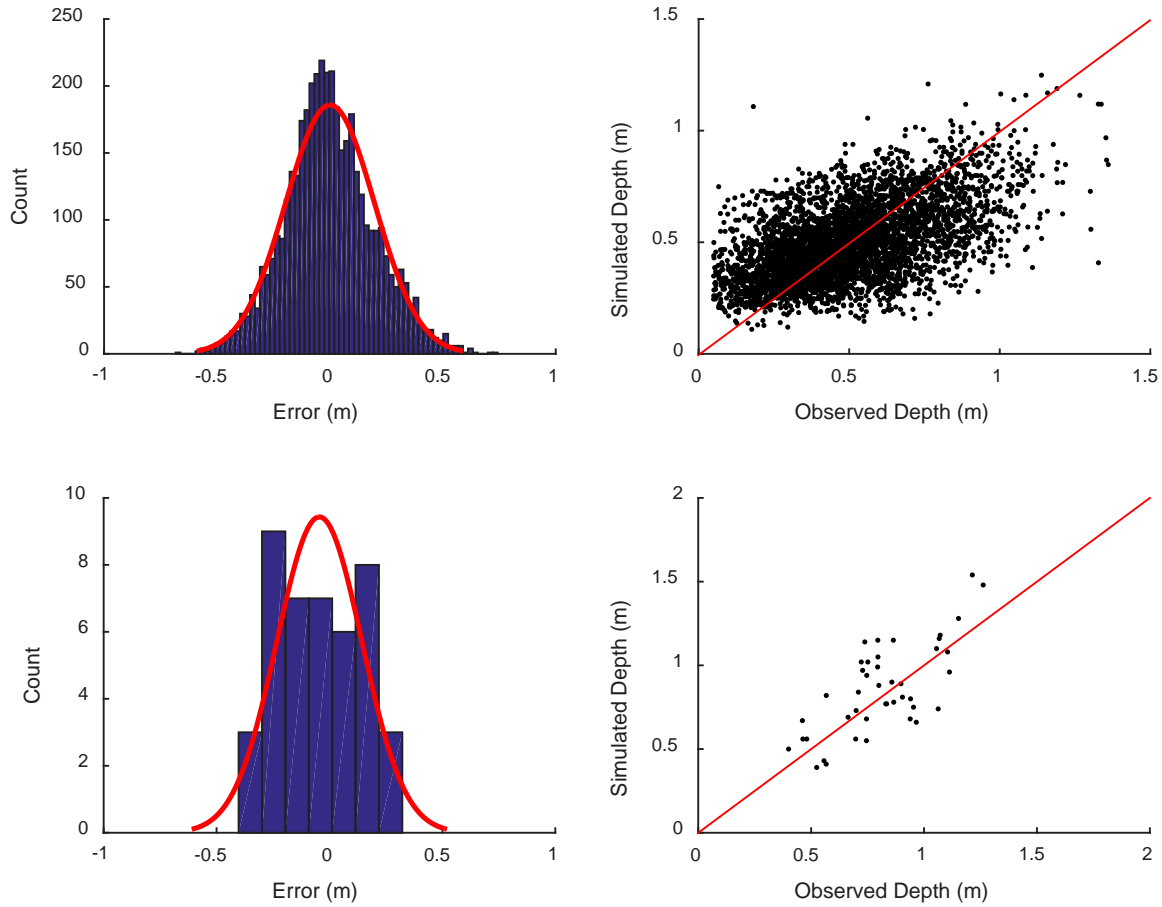
Figure 17. Histogram of overall HEC-RAS calibration (top left) and testing (bottom left) errors. Plot of simulated versus observed streamflow depths for each calibration (top right) and testing (bottom right) location.

The performance results above indicate that the comprehensive method based on integrating high resolution LiDAR throughout the modeling process was an effective technique to establish a HEC-RAS model. Previous studies have used LiDAR to provide additional floodplain topographic detail. In this study, though, LiDAR provided a surface to burn interpolated cross sections into as well as providing calibration information. Further, the SWAT and HEC-RAS model cascade and associated results presented in the chapter indicate this methodology may be successfully implemented for simulation of water fluxes from the watershed to the channel scale.

3.3.3   Wildfire Effects on Flood Streamflows

The steady flow input data for the HEC-RAS model were analyzed and compared in order to quantify changes in streamflows for various floods between the no-wildfire and wildfire scenarios. Figure 18 displays the burn severity distribution associated with the contributing area to each sub-reach for reference. Figure 19 displays the streamflow increase (m^3/s and percent) for each sub-reach impacted by wildfire as well as the entire study watershed based on the values presented in Table 8. Note sub-reach 23 was omitted from these figures as well as the remaining figures within this section because that particular segment is upstream of any wildfire influence.
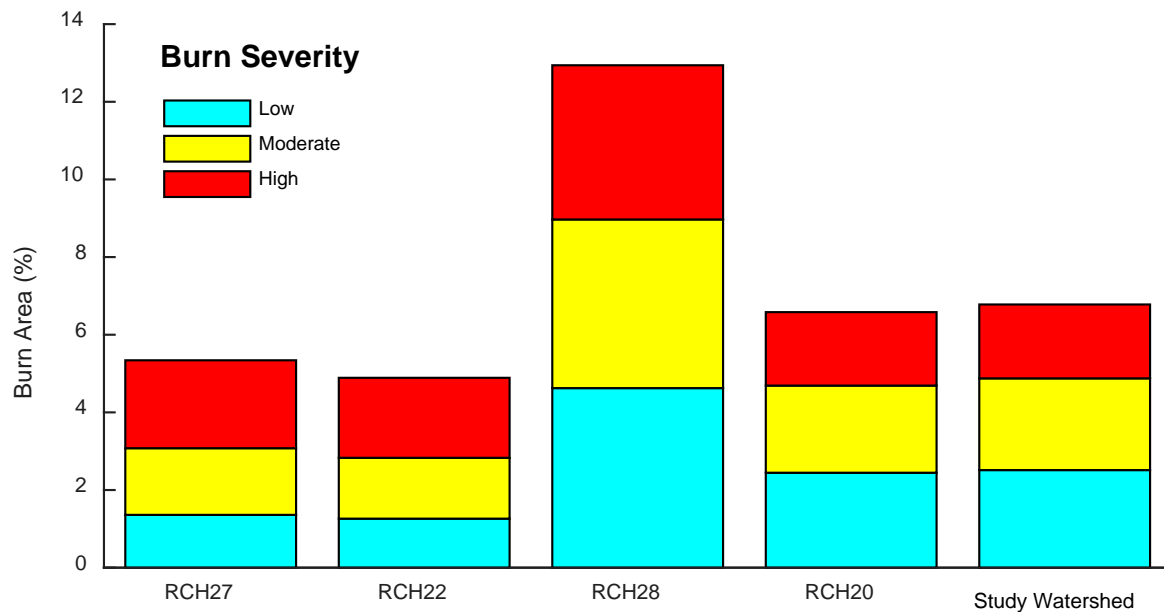
Figure 18. Burn severity distribution associated with the contributing area to each sub-reach, as well as for the entire study watershed presented in the direction from upstream (left) to downstream (right).
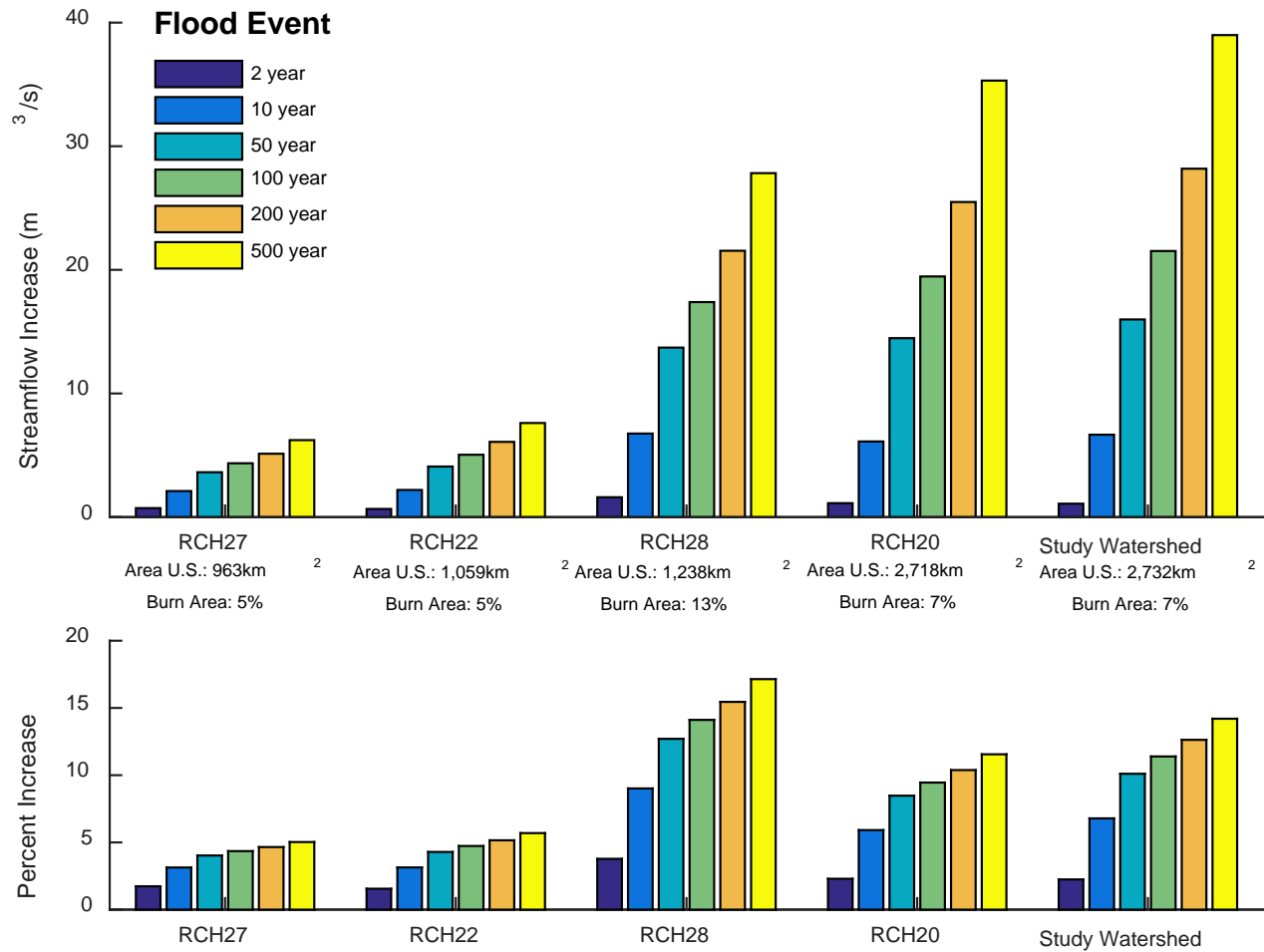
Figure 19. Streamflow increases in m^3/s (top) and percent (bottom) associated with various floods between no-wildfire and wildfire scenarios for sub-reaches 27, 22, 28, and 20, as well as the entire study reach.

The results shown in Figure 19 indicate that wildfires for the scenarios defined in this study can increase streamflows between 2 and 14 percent depending on the reaches proximity to the wildfire and the flood. Note that the impact to sediment transport (and related channel alteration) due to these increases in streamflow would be disproportionately higher due to the non-linear response of sediment capacity to changes in streamflow (Williams, 1989). Following substantial wildfire in northern New Mexico during 1997, peak streamflows were reported at 100 times greater than pre-wildfire levels (Bolin and Ward, 1987). Other reported responses have been even higher. For example, in north-central Arizona peak streamflows up to 2,350 times

previous flow records were found following the Rodeo-Chediski wildfire in 2002 (Gottfried et al., 2003). However, these evaluations were performed on smaller areas with a larger percentage of the contributing area burned (Bolin and Ward, 1987; Gottfried et al., 2003). It has been found that under the scenario of wildfires, streamflow increases are a function of the upstream area burned as well as the severity of the wildfire (Neary et al., 2008). Hence, we expect streamflow increases to be less in the case of this study due to the small upstream burn percentages.

In Figure 19 we also see that for sub-reach 20 and the entire study watershed the streamflow increase (percent) is slightly less for each flood when compared to sub-reach 28. This appears to correspond with a decrease in total burn area upstream for these segments as shown in Figure 18. The total burn area upstream decrease is suspected to stem from the fact that the North Fork (a large contributing area with little area burned) of the Poudre joins the main-stem directly downstream of sub-reach 28. Regardless, this trend is consistent with the cited literature above indicating that, under the scenario of wildfires, streamflow increases are a function of the upstream area burned.

3.3.4   Wildfire Effects on Hydraulic Behavior

The HEC-RAS model output data were analyzed and compared in order to quantify response to wildfires in terms of hydraulic behavior for reaches downstream of burned areas at the channel scale. Figure 20, Figure 21, and Figure 22 present flood area, average cross section velocity, and average cross section shear stress increases. These increases are associated with various floods between no-wildfire and wildfire scenarios for sub-reaches 27, 22, 28, and 20. Changes in flood area were extracted from the RAS mapping results and the average cross section velocity and shear stress increases were extracted directly from the HEC-RAS model output data.
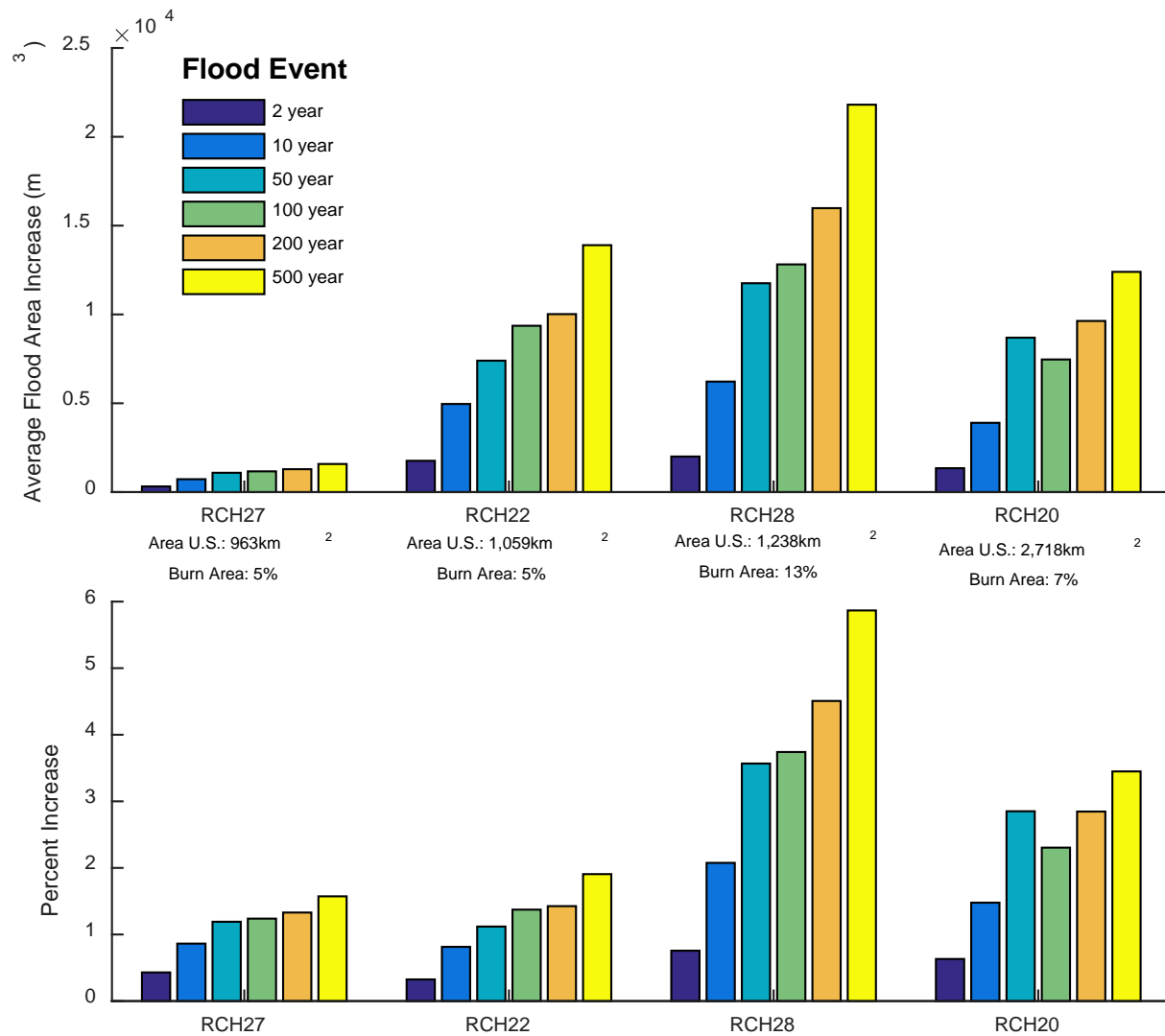
Figure 20. Flood area increases in m^3 (top) and percent (bottom) associated with various floods between no-wildfire and wildfire scenarios for sub-reaches 27, 22, 28, and 20.

Sub-reach 28 has the highest flood area percent increases; whereas, generally, sub-reach 22 has the lowest flood area percent increases. The exception to this trend occurs for larger floods (i.e., 100, 200, and 500 year) for sub-reach 22, which are found to be slightly larger than those of sub-reach 27. The cause of this may be the result of the streamflows being increased for these specific events. A flood area increases range from nearly zero to 6 percent for the various floods and sub-reaches.
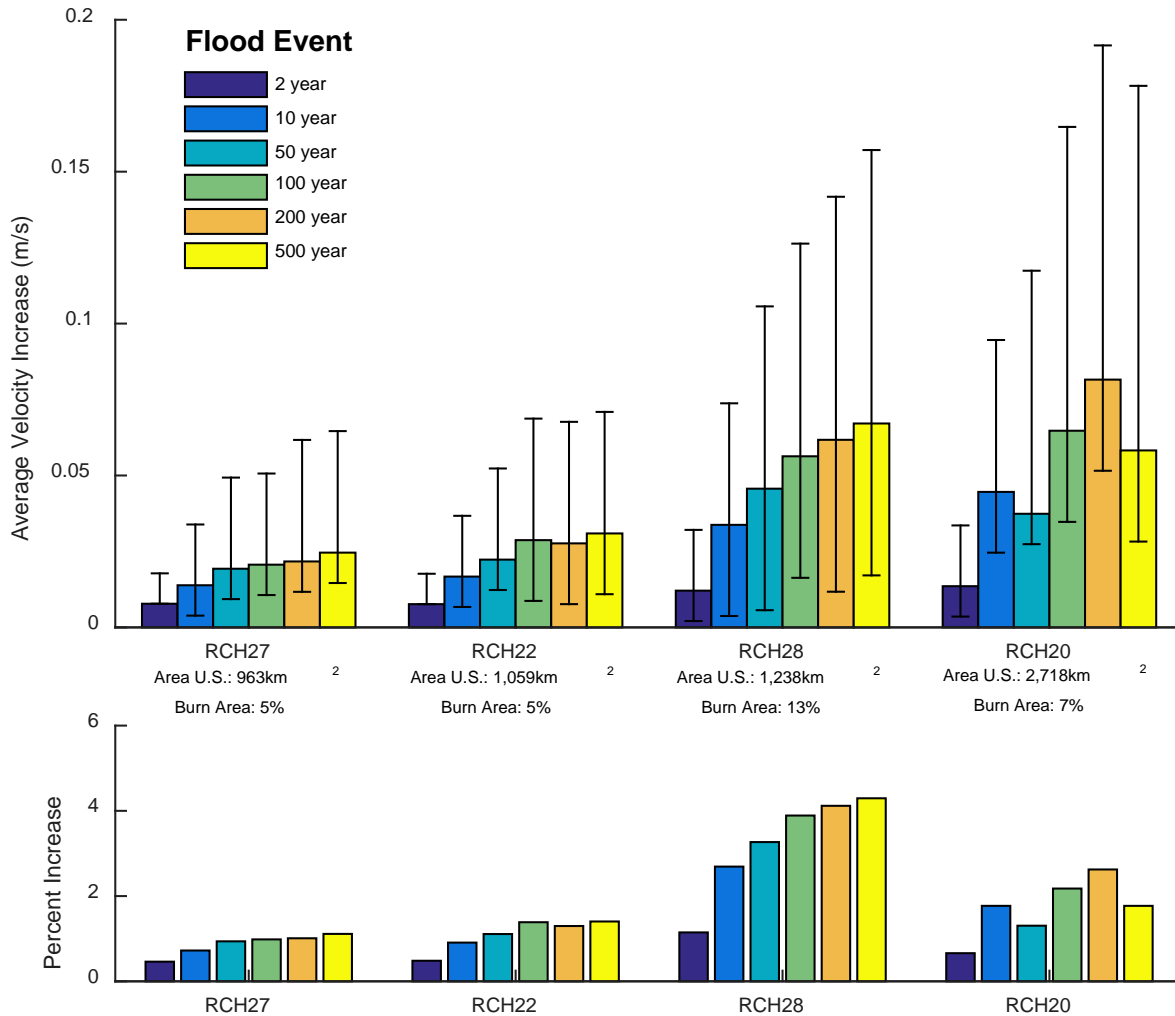
Figure 21. Average cross section velocity increases in m/s with the first and third quartiles plotted as whiskers (top) and percent (bottom) associated with various floods between no-wildfire and wildfire scenarios for sub-reaches 27, 22, 28, and 20.

On average over the simulation period, wildfire conditions have been impacted by increases in the average cross section velocity in each sub-reach. Sub-reach 28 experienced the greatest increases, although generally all of the increases were quite small, ranging from 0.0077 to 0.0816 m/s. The remaining sub-reaches experience even smaller increases. Overall, average cross section velocity increases ranged from nearly to 4 percent.
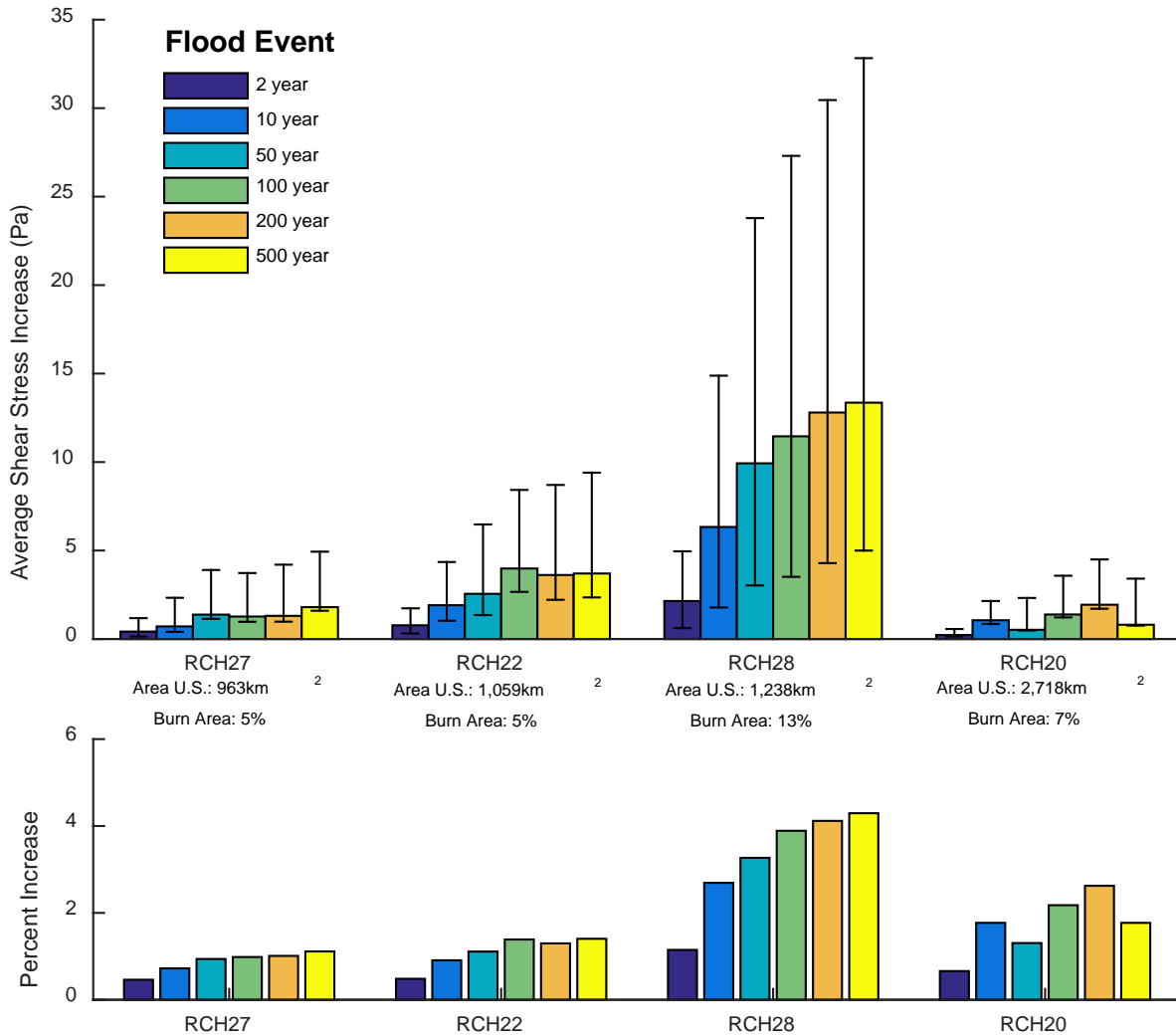
Figure 22. Average cross section shear stress increases in Pa with the first and third quartiles plotted as whiskers (top) and percent (bottom) associated with various floods between no-wildfire and wildfire scenarios for sub-reaches 27, 22, 28, and 20.

Similar to the other results reported above, cross section shear stress increases were greatest in sub-basin 28 with an increase of 13 Pa on average for the 500-year event. Flood area increases range from 1 to 6 percent for the various floods and sub-reaches. Average shear stresses are notably smaller in sub-reach 20. Shear stress is function of streamflow depth as well as slope in the upstream to downstream direction. Thus, the smaller values may be a direct result of the terrain along sub-reach 20 being less steep, as suggested by the slope calculation during the cross section spacing analysis (APPENDIX B).

The slight increases in flood area, average cross section velocity, and shear stress are not surprising, as these variables are related to streamflow. Streamflow is a function of the velocity and the cross sectional area of water. Generally, as the depth rises we would expect to see an increase in flood area as well as shear stress. In this case, it is believed that the average increase of all of these parameters is a result of the increase in streamflow. No specific study could be found that specifically examines how these variables respond to wildfire. However, as indicated previously, post-wildfire conditions have been documented to increase peak streamflows (Moody and Martin, 2001) and thus by extension we would expect to see an increase in these variables due to their inherent connection to one another.

3.3.5 HEC-RAS Model Assumptions, Limitations, and Future Work

Uncertainties associated with the 1-D streamflow modeling approach discussed in the literature include input/output uncertainty as well as parameter uncertainty. Various studies have identified the causes of these uncertainties, which include model structure, numerical scheme and topography variation. Despite these issues, the 1-D streamflow modeling approach is common practice. This may be explained by the fact that 1-D models are (in comparison to higher dimensional models) simpler to use and require a minimal amount of input data and computer power. Also, the basic 1-D concepts and programs have been around for many years. Further, higher dimensional models will have similar uncertainty problems to the simpler one, but on a larger scale because of the additional model parameters required (Pappenberger et al., 2005). Given the constraints associated with data ability as well as the fact that it is common practice, HEC-RAS with its 1-D modeling capabilities was used for this project. A detailed uncertainty analysis as it applies to this study is outside the scope of this project. However, specific concerns with regards to these uncertainties are acknowledged below.

Uncertainty is likely to propagate from the SWAT model to the HEC-RAS model due to the hierarchical nature of the modeling cascade. Model uncertainty associated with the hydrologic portion is discussed in Section 2.3.5. Building on that discussion, many assumptions were required to preprocess the SWAT model output data. First, it is assumed that the regression relationships developed in the steady flow data section represent the non-naturalized to naturalized streamflow relationship at not only the Mouth of Canyon (i.e., where the data used in the analysis were collected), but also flow change locations upstream. Streamflows in the Poudre are expected to fluctuate significantly, depending on the location of reservoirs and diversions (Richer, 2009). Thus, the established relationship may not appropriately represent streamflow conditions, but was implemented due to the lack of available streamflow surface water gauge data. Second, the flood frequency analysis was based on only 15 years of streamflow data. This limits the ability to account for climatic trends and watershed changes that are likely occurring over long periods of time (Rallision et al., 1982). Streamflows for these same floods were also obtained using the Environmental Risk Assessment & Management (eRAMs) platform for comparison purposes. The eRAMs platform contains a flow analysis tool that also uses the B17 methodology and the analysis was based on 125 observations at the Mouth of Canyon versus the 15 years of preprocessed SWAT model output. This comparison, shown in APPENDIX B, revealed that HEC-RAS steady flow input ranged from 74 to 79 percent smaller than those reported by the eRAMs tool. Despite these discrepancies, we integrated the preprocessed SWAT model output into the HEC-RAS model input because of our inability to develop a SWAT model for longer simulation periods at the daily timestep due to limited data availability and time constraints. A potential solution to both these issues may involve the development of a full unsteady flow HEC-RAS model. An unsteady flow model would allow for continuous

simulations to be performed in HEC-RAS that matches the SWAT simulation period. Historical diversions and reservoirs releases data could be integrated into the model as well. Thus, development of an unsteady flow HEC-RAS model for use in the model cascade is recommended as future work.

Appropriately representing the riverbed and the floodplain area topography is an important element of hydraulic modeling (Schäppi et al., 2010). Limitations and assumptions associated with the geometric data that represent this topography for this study include:

 - Much of the bathometric data used in the model were obtained through interpolation techniques versus actual measurements. Thus, portions of the model may not accurately reflect the river channel geometry. In part, this was addressed by burning the interpolated cross sections in the floodplain. Ultimately, given that cross section interpolation is a common approach (Merwade et al., 2008), this procedure was considered acceptable.

 - Upon visual inspection of the final cross section, a smooth transition between the interpolated cross sections and the 3/4 m DEM was generally found. However, in locations where the channel boundary was drawn slightly incorrectly, the "burning" procedure resulted in abrupt and/or rough transitions. Analysis of these transitions revealed these distances to be within a 1/2 m tolerance with a majority of cross sections close to zero. These errors were considered acceptable given the uncertainties associated with the vertical accuracy of the 3/4 m as well as varying topography. A histogram of these distances is shown in APPENDIX A.

 - The geometric input is based on data that were collected at various times during the latter part of 2013 and throughout 2014. Much of the upper Poudre watershed consists of bedrock (Wohl, 2010). Thus, the channel geometry was assumed to be constant throughout this period.

Channel geometry plays a significant role in how flood area, velocity, and shear stress respond to streamflow increases. For instance, velocity depends on the geometry of the channel. Under decreasing streamflow, the velocity does not necessarily increase in all cross sections. For example, consider streamflows passing through a narrower main channel with a wide floodplain. For the situation with lower flows (i.e. pre-fire conditions) where the streamflow is contained in the main channel, friction and area are significantly decreased, which causes an increase in velocity. Conversely, for the situation with high flows (e.g., post-fire conditions), where the streamflow is not contained in the main channel, velocities are potentially reduced due to the large flow area as well as high friction generally associated with the floodplain (Javaheri and Babbar-Sebens, 2014). Along with velocity, both flood area and shear stress may increase or decrease depending on the geometry of the channel and surrounding floodplains. Given this, it is difficult to extract a direct relationship between percent of contributing area burned and the hydraulic behavior without considering channel geometry. Thus, it is recommended that thresholds and classifications of the process domain procedure used in this study be adjusted to be more sensitive to changes in channel geometry. This may prove to be useful in establishing a relationship between the upstream burn area and downstream hydraulic behavior for a given river segment.

3.4 Conclusions

The practical implementation of a modelling cascade was demonstrated in this study to characterize streamflow and channel hydraulic behavior response to wildfires at the channel scale in a major river downstream of wildfire activity. This was achieved by applying a SWAT and HEC-RAS model cascade to a mountainous system recently exposed to significant wildfire activity located in northern Colorado, USA. Steady flow data input for the HEC-RAS model was

obtained from a previously developed SWAT model which simulated no-wildfire and wildfire scenarios for a 15 year (2000 to 2014) period. The HEC-RAS model was developed using detailed sets of data representing floodplain terrain, stream centerline, cross sections, hydraulic structures, boundary conditions, and stage-stream relationships. Then the model was calibrated using stage-streamflow relationships extracted for a 3/4–m DEM and was tested using stage-streamflow relationships obtained from detailed cross section surveys. Optimal Manning's n values were achieved during calibration and error statistics were calculated to rate model performance in regards to stage-streamflow relationships. Results indicate confidence in the model, with a RE of 0.13 during calibration and -5.49 during testing period over the study reach. HEC-RAS steady flow data input and simulation results were used to investigate changes occurring in response to wildfires.

Specific objectives of this study were to investigate changes in streamflows for floods, flood inundation area, flow velocity, and shear stress for reaches downstream of burned areas, all at the channel scale. Streamflow increases were less than those reported in literature, with increases between 2 and 14 percent depending on the reach's proximity to the wildfire and the flood. Slight increases in flood area, average cross section velocity, and shear stress are seen, which is consistent with the relationship to streamflow.

Results report in this study indicate an overall satisfactory performance of the model cascade in simulating the no-wildfire and wildfire scenarios and in quantifying response to wildfires in terms of hydraulic behavior. However, this method required comprehensive knowledge of the channel and was time consuming and computationally intensive. Further, this study demonstrates the potential benefits of using an unsteady flow model versus a steady flow

model when using a model cascade, as well as highlighting numerous issues associated with obtaining geometric data input for 1-D streamflow modeling.

CHAPTER. 4 CONCLUSIONS

The headwaters of many from mountainous regions are relied upon for freshwater resources. Inconveniently, wildfires worldwide in these same regions are becoming an increasing concern. However, limited work has involved the development, calibration, and testing of a numerical model to simulate hydrologic processes in a mountainous area accounting for land use change (i.e., wildfire) to investigate hydrologic response to wildfires. Moreover, the applicability of a modeling cascade where hydrologic and hydraulic models are linked in a hierarchical fashion for the specific purpose of investigating wildfire effects across multiple scales for a particular event is not well documented.

Thus, this research was undertaken to evaluate the effects of a significant wildfire event across multiple scales using simulation. We this study we (i) characterized the hydrologic response to wildfires at the sub-basin and watershed scales in mountainous regions using long term simulation scenario analysis; and (ii) demonstrated the practical implementation of a modelling cascade to characterize channel hydraulic behavior response to wildfires at the channel scale in a major river downstream of wildfire activity. SWAT was used to perform long term simulation of wildfire and no-wildfire scenarios. The unique situation of a significant wildfire occurring in a gauged watershed, along with the modeling capabilities of SWAT, allowed for the characterization of the hydrologic response to wildfires. HEC-RAS was used to perform event-based analysis using results from the SWAT model to evaluate wildfire effects on the hydraulic behavior of the system at the channel scale. Overall, the SWAT and HEC-RAS model cascade was useful for evaluating effects of wildfire at watershed, sub-basin, and channel scales.

REFERENCES

Alho, P., Roberts, M.J., Käyhkö, J., 2007. Estimating the inundation area of a massive, hypothetical jökulhlaup from northwest Vatnajökull, Iceland. Nat. Hazards 41, 21–42. doi:10.1007/s11069-006-9007-z

Batelis, S., Nalbantis, I., 2014. Potential effects of forest fires on streamflow in the Enipeas River Basin , Thessaly , Greece. Environ. Process. 1, 73–85. doi:10.1007/s40710-014-0004-z

Beltaos, S., Tang, P., Rowsell, R., 2012. Ice jam modelling and field data collection for flood forecasting in the Saint John River, Canada. Hydrol. Process. 26, 2535–2545. doi:10.1002/hyp.9293

Benavides-Solorio, J., MacDonald, L.H., 2001. Post-fire runoff and erosion from simulated rainfall on small plots, Colorado Front Range. Hydrol. Process. 15, 2931–2952. doi:10.1002/hyp.383

Bolin, S.B., Ward, T.J., 1987. Recovery of a New Mexico drainage basin from a forest fire, in: Proceedings of the Forest Hydrology and Watershed Management Vancouver Symposium, 1987. pp. 191–198.

Brunner, G., 2010a. HEC-RAS River Analysis System Hydraulic Reference Manual, United States Army Corps of Engineers, Hydrologic Engineering Center.

Brunner, G., 2010b. HEC-RAS River Analysis System User 's Manual, United States Army Corps of Engineers, Hydrologic Engineering Center.

Buhman, D.L., Gates, T.K., Watson, C.C., 2002. Stochastic variability of fluvial hydraulic

    geometry : Mississippi and Red Rivers. J. Hydraul. Eng. 128, 426–437.

    doi:10.1061/(ASCE)0733-9429(2002)128:4(426)

Burkey, J., 2009. Log-Pearson Flood Flow Frequency using USGS 17B. Available at

    http://www.mathworks.com/matlabcentral/fileexchange/

Canfield, E.H., Goodrich, D.C., Burns, S.I., 2005. Selection of parameters values to model post-

    fire runoff and sediment transport at the watershed scale in southwestern forests, in:

    Managing Watersheds for Human and Natural Impacts. doi:10.1061/40763(178)48

Chow, V., 1959. Open-Channel Hydraulics, New York.

CO Division of Water Resources, 2014. Colorado Surface Water Conditions database. Available

    at http://www.dwr.state.co.us/SurfaceWater/Default.aspx.

El-Khoury, A., Seidou, O., Lapen, D.R., Que, Z., Mohammadian, M., Sunohara, M., Bahram, D.,

    2015. Combined impacts of future climate and land use changes on discharge, nitrogen

    and phosphorus loads for a Canadian river basin. J. Environ. Manage. 151, 76–86.

    doi:10.1016/j.jenvman.2014.12.012

Esri (World Wildlife Fund, Inc., U.S. Geological Survey, and U.S. Environmental Protection

    Agency), 2015a. World Hydro Reference Overlay.

Esri (World Wildlife Fund, Inc., U.S. Geological Survey, and U.S. Environmental Protection

    Agency), 2015b. World Imagery.

Fan, C., Li, J., 2004. A modelling analysis of urban stormwater flow regimes and their

    implication for stream erosion. Water Qual. Res. J. Canada 39, 356–361.

Fan, M., Shibata, H., 2015. Simulation of watershed hydrology and stream water quality under

    land use and climate change scenarios in Teshio River watershed, northern Japan. Ecol.

    Indic. 50, 79–89. doi:10.1016/j.ecolind.2014.11.003

Federal Emergency Management Agency, 2014. Available at

    http://archive.femadata.com/lidar/CO_LIDAR/.

Finco, M., Quayle, B., Zhang, Y., Lecker, J., Megown, K. a., Brewer, C.K., 2012. Monitoring

    Trends and Burn Severity (MTBS): Monitoring wildfire activity for the past quarter

    century using LANDSAT data. Mov. from Status to Trends For. Invent. Anal. Symp.

    222–228.

Foltz, R.B., Robichaud, P.R., Rhee, H., 2009. A synthesis of post-fire road treatments for BAER

    teams: methods, treatment effectiveness, and decision making tools for rehabilitation.

    Gen. Tech. Rep. RMRS-228 152.

Foy, C., Arabi, M., Yen, H., Asce, A.M., Gironás, J., Bailey, R.T., 2009. Multisite assessment of

    hydrologic processes in snow-dominated mountainous river basins in Colorado using a

    watershed model. J. Hydrol. Eng. doi:10.1061/(ASCE)HE.1943-5584.0001130.

Gallant, J.C., Dowling, T.I., 2003. A multiresolution index of valley bottom flatness for mapping

    depositional areas. Water Resour. Res. 39. doi:10.1029/2002WR001426

Gesch, D., Oimoen, M., Greenlee, S., Nelson, C., Steuck, M., and Tyler, D., 2002. The National

    Elevation Dataset: Photogrammetric Engineering and Remote Sensing, v. 68, no. 1, p. 5-

    11.

Gesch, D.B., 2007. The National Elevation Dataset, in Maune, D., ed., Digital Elevation Model Technologies and Applications: The DEM Users Manual, 2nd Edition: Bethesda, Maryland, American Society for Photogrammetry and Remote Sensing, p. 99-118.

Goode, J.R., Wohl, E., 2010. Substrate controls on the longitudinal profile of bedrock channels: Implications for reach-scale roughness. J. Geophys. Res. 115. doi:10.1029/2008JF001188

Goodrich, D.C., Canfield, H.E., Burns, S.B., Semmens, D.J., Miller, S.N., Hernandez, M., Levick, L.R., Guertin, D.P., Kepner, W.G., 2005. Rapid post-fire hydrologic watershed assessment using the AGWA GIS-based hydrologic modeling tool, in: Managing Watersheds for Human and Natural Impacts. doi:10.1061/40763(178)44

Gottfried, G.J., Neary, D.G., Baker, M.B., Ffolliott, P.F., 2003. Impacts of wildfires on hydrologic processes in forest ecosystems : Two case studies, in: First Interagency Conference on Research in the Watersheds. Department of Agriculture, Agricultural Research Service. pp. 668–673.

Higginson, Brad; Jarnecke, Jeremy. 2007. Salt Creek BAER-2007 Burned Area Emergency Response. Provo, UT: Uinta National Forest. Hydrology Specialist Report.

Inbar, M., Tamir, M., Wittenberg, L., 1998. Runoff and erosion processes after a forest fire in Mount Carmel, a Mediterranean area. Geomorphology 24, 17–33. doi:10.1016/S0169-555X(97)00098-6

Jarrett, R.D., 1984. Hydraulics of high-gradient streams. J. Hydraul. Eng. 110, 1519–1539.

Javaheri, A., Babbar-Sebens, M., 2014. On comparison of peak fl ow reductions , flood inundation maps, and velocity maps in evaluating effects of restored wetlands on channel flooding. Ecol. Eng. 73, 132–145. doi:10.1016/j.ecoleng.2014.09.021

Jin, S., Yang, L., Danielson, P., Homer, C., Fry, J., Xian, G., 2013. A comprehensive change detection method for updating the National Land Cover Database to circa 2011. Remote Sens. Environ. 132, 159–175. doi:10.1016/j.rse.2013.01.012

Kannan, N., Jeong, J., 2011. An approach for estimating stream health using flow duration curves and indices of hydrologic alteration, United States Environmental Protection Agency.

Kiesel, J., Schmalz, B., Brown, G.L., Fohrer, N., 2013. Application of a hydrological-hydraulic modelling cascade in lowlands for investigating water and sediment fluxes in catchment, channel and reach. J. Hydrol. Hydromechanics 61, 334–346. doi:10.2478/johh-2013-0042

Lavabre, J., Torres, D.S., Cernesson, F., 1993. Changes in the hydrological response of a small Mediterranean basin a year after a wildfire. J. Hydrol. 142, 273–299. doi:10.1016/0022-1694(93)90014-Z

Li, Z., Shao, Q., Xu, Z., Cai, X., 2010. Analysis of parameter uncertainty in semi-distributed hydrological models using bootstrap method: A case study of SWAT model applied to Yingluoxia watershed in northwest China. J. Hydrol. 385, 76–83. doi:10.1016/j.jhydrol.2010.01.025

Liu, S., Leslie, L.M., Speer, M., Bunker, R., Mo, X., 2004. The effects of bushfires on hydrological processes using a paired-catchment analysis. Meteorol. Atmos. Phys. 86, 31–44. doi:10.1007/s00703-003-0614-x

Lu, Z., Zou, S., Xiao, H., Zheng, C., Yin, Z., Wang, W., 2015. Comprehensive hydrologic calibration of SWAT and water balance analysis in mountainous watersheds in northwest China. Phys. Chem. Earth. doi:10.1016/j.pce.2014.11.003

Mahat, V., Anderson, A., Silins, U., 2015. Modelling of wildfire impacts on catchment hydrology applied to two case studies. Hydrol. Process. doi:10.1002/hyp.10462

Maingi, J.K., Marsh, S.E., 2002. Quantifying hydrologic impacts following dam construction along the Tana River, Kenya. J. Arid Environ. 50, 53–79. doi:10.1006/jare.2000.0860

McLin, S.G., Springer, E.P., Lane, L.J., 2001. Predicting floodplain boundary changes following the Cerro Grande wildfire. Hydrol. Process. 15, 2967–2980. doi:10.1002/hyp.385

Md Ali, A., Di Baldassarre, G., Solomatine, D.P., 2014. Testing different cross-section spacing in 1D hydraulic modelling: a case study on Johor River, Malaysia. Hydrol. Sci. J. 60, 351–360. doi:10.1080/02626667.2014.889297

Menne, M.J., Durre, I., Vose, R.S., Gleason, B.E., Houston, T.G., 2012. An overview of the global historical climatology network-daily database. J. Atmos. Ocean. Technol. 29, 897–910. doi:10.1175/JTECH-D-11-00103.1

Merwade, V., Cook, A., Coonrod, J., 2008. GIS techniques for creating river terrain models for hydrodynamic modeling and flood inundation mapping. Environ. Model. Softw. 23, 1300–1311. doi:10.1016/j.envsoft.2008.03.005

Monitoring Trends in Burn Severity Project (U.S. Geological Survey and U.S. Forest Service), 2014. Monitoring Trends in Burn Severity Data Access: Fire Map Geospatial Data. Available at http://www.mtbs.gov/dataaccess.html.

Montgomery, D.R., 1999. Process domains and the river continuum. J. Am. Water Resour. Assoc. 35, 397–410.

Moody, J.A., Martin, D.A., 2001. Post-fire, rainfall intensity-peak discharge relations for three mountainous watersheds in the Western USA. Hydrol. Process. 15, 2981–2993. doi:10.1002/hyp.386

Moody, J.A., Shakesby, R.A., Robichaud, P.R., Cannon, S.H., Martin, D.A., 2013. Current research issues related to post-wildfire runoff and erosion processes. Earth-Science Rev. 122, 10–37. doi:10.1016/j.earscirev.2013.03.004

Moriasi, D.N., Arnold, J.G., Van Liew, M.W., Bingner, R.L., Harmel, R.D., Veith, T.L., 2007. Model evaluation guidelines for systematic quantification of accuracy in watershed simulations. Am. Soc. Agric. Biol. Eng. 50, 885–900. doi:10.13031/2013.23153

Mosquera-Machado, S., Ahmad, S., 2007. Flood hazard assessment of Atrato River in Colombia. Water Resour. Manag. 21, 591–609. doi:10.1007/s11269-006-9032-4

Motovilov, Y., Gottschalk, L., Engeland, K., Rodhe, A., 1999. Validation of a distributed hydrological model against spatial observations. Agric. For. Meteorol. 257–277. doi:10.1016/S0168-1923(99)00102-1

Nash, E., Sutcliffe, V., 1970. River Flow Forecasting Through Conceptual Models Part I - A Discussion of Principles. J. Hydrol. 10, 282–290.

Neary, D.G., Gottfried, G.J., Ffolliott, P.F., 2003. Post-Wildfire Watershed Flood Responses, Second International Fire Ecology and Fire Management Congress, Orlando, Florida, 16-20 November 2003, Paper 1B7.

Neary, D.G., Kevin, R.C., Leonard, D.F., 2008. Wildland fire in ecosystems, effects of fire on soil and water, United States Department of Agriculture, Forest Service. General Technical Report RMRS-GTR-42-vol. 4.

Neitsch, S., Arnold, J., Kiniry, J., Williams, J., 2011. Soil & Water Assessment Tool Theoretical Documentation Version 2009, United States Department of Agriculture, Agricultural Reseach Service, Texas Agricultural Experiment Station.

Neupane, R.P., White, J.D., Alexander, S.E., 2015. Projected hydrologic changes in monsoon-dominated Himalaya Mountain basins with changing climate and deforestation. J. Hydrol. 525, 216–230. doi:10.1016/j.jhydrol.2015.03.048

Newtson, J., 2013. The impact of fire on flow duration curves in Southern California shrubland watersheds.

Nicklow, J., Boulos, P., Muleta, M., 2006. Comprehensive Yrban Hydrologic Modeling Handbook for Engineers and Planners, California.

Northern Colorado Water Conservancy District, 2014. Cache la Poudre River Naturalized Streamflow data.

Oropeza, J., Heath, J., 2013. Five year summary report (2008- 2012) Upper Cache la Poudre River Collaborative Water Quality Monitoring Program, City of Fort Collins Utilities.

Pai, N., Saraswat, D., 2001. SWAT2009_LUC: A tool to activate the land use change module in SWAT 2009. Trans. ASABE 54, 1649–1658.

Pappenberger, F., Beven, K., Horritt, M., Blazkova, S., 2005. Uncertainty in the calibration of effective roughness parameters in HEC-RAS using inundation and downstream level observations. J. Hydrol. 302, 46–69. doi:10.1016/j.jhydrol.2004.06.036

Parkyn, R., 2010. Duration (CDF) Plot. Available at http://www.mathworks.com/matlabcentral/fileexchange/.

Rallision, R.E. et al., 1982. Guidelines for determining flood flow frequency, United States Geological Survey, Hydrology Subcommittee. Bulletin 17B.

Records, R., 2013. Water quality benefits of wetlands under historic and potential future climate in the Sprague River Watershed, Oregon.

Richer, E., 2009. Snowmelt runoff analysis and modeling for the Upper Cache la Poudre River Basin, Colorado.

Robichaud, P.R., Beyers, J.L., Neary, D.G., 2000. Evaluating the effectiveness of postfire rehabilitation treatments, United States Department of Agriculture, Forest Service. General Technical Report RMRS-GTR-63.

Ryan, S.E., Dwire, K. a., Dixon, M.K., 2011. Impacts of wildfire on runoff and sediment loads at Little Granite Creek, western Wyoming. Geomorphology 129, 113–130. doi:10.1016/j.geomorph.2011.01.017

Saleh, F., Ducharne, a., Flipo, N., Oudin, L., Ledoux, E., 2013. Impact of river bed morphology on discharge and water levels simulated by a 1D Saint–Venant hydraulic model at regional scale. J. Hydrol. 476, 169–177. doi:10.1016/j.jhydrol.2012.10.027

Sanadhya, P., Gironas, J., Arabi, M., 2014. Global sensitivity analysis of hydrologic processes in major snow-dominated mountainous river basins in Colorado. Hydrol. Process. 28, 3404–3418. doi:10.1002/hyp.9896

Schäppi, B., Perona, P., Schneider, P., Burlando, P., 2010. Integrating river cross section measurements with digital terrain models for improved flow modelling applications. Comput. Geosci. 36, 707–716. doi:10.1016/j.cageo.2009.12.004

Scott, D.F., 1993. The hydrological effects of fire in South African mountain catchments. J. Hydrol. 150, 409–432. doi:10.1016/0022-1694(93)90119-T

Soil Survey Staff, 2015a. The Gridded Soil Survey Geographic (SSURGO) Database for Colorado. U.S. Department of Agriculture, Natural Resources Conservation Service. Available at http://datagateway.nrcs.usda.gov/.

Soil Survey Staff, 2015b. The Gridded Soil Survey Geographic (SSURGO) Database for Wyoming. U.S. Department of Agriculture, Natural Resources Conservation Service. Available at http://datagateway.nrcs.usda.gov/.

Spencer, D.F., Colby, L., Norris, G.R., 2013. An evaluation of flooding risks associated with giant reed (Arundo donax). J. Freshw. Ecol. 28, 397–409. doi:10.1080/02705060.2013.769467

Springer, E.P., Hawkins, R.H., 2005. Curve number and peakflow responses following the Cerro Grande fire on a small watershed, in: American Society of Civil Engineers Watershed Management 2005 Symposium Williamsburg, VA. doi:10.1061/40763(178)40

Strum, T., 2010. Open Channel Hydraulics. New York.

Tolson, B. a., Shoemaker, C. a., 2007. Dynamically dimensioned search algorithm for computationally efficient watershed model calibration. Water Resour. Res. 43. doi:10.1029/2005WR004723

Townsend, S. a., Douglas, M.M., 2004. The effect of a wildfire on stream water quality and catchment water yield in a tropical savanna excluded from fire for 10 years (Kakadu National Park, North Australia). Water Res. 38, 3051–3058. doi:10.1016/j.watres.2004.04.009

U.S. Army Corps of Engineers, 2010. HEC-RAS Version 4.1. Available at http://www.hec.usace.army.mil/software/.

U.S. Army Corps of Engineers, 2013. HEC-GeoRAS 10.1. Available at http://www.hec.usace.army.mil/software/.

U.S. Department of Agriculture Agricultural Research Service, 2012. SWAT 2012 Revision 591. Available at http://swat.tamu.edu/.

U.S. Department of Agriculture Agricultural Research Service. 2012. SWAT US SSURGO database. Available at http://swat.tamu.edu/.

U.S. Department of Agriculture Agricultural Research Service. 2014. ArcSWAT 2012.10_1.13. Available at http://swat.tamu.edu/.

Vogel, R.M., Sieber, J., Archfield, S.A., Smith, M.P., Apse, C.D., Huber-Lee, A., 2007. Relations among storage, yield, and instream flow. Water Resour. Res. 43, 1–12. doi:10.1029/2006WR005226

Williams, G.P., 1989. Sediment concentration versus water discharge during single hydrologic events in rivers. J. Hydrol. 111, 89–106. doi:10.1016/0022-1694(89)90254-0

Winchell, M., Srinivasan, R., Di Luzio, M., Arnold, J., 2013. ArcSWAT Interface For SWAT2012, Texas Agrilife Research, United States Department of Agriculture, Agricultural Reseach Service.

Wohl, E., 2010. A brief review of the process domain concept and its application to quantifying sediment dynamics in bedrock canyons. Terra Nov. 22, 411–416. doi:10.1111/j.1365-3121.2010.00950.x

Zhu, C., Li, Y., 2011. Land use/land cover change and its hydrological impacts from 1984 to 2010 in the Little River Watershed, Tennessee. Int. Soil Water Conserv. Res. 2, 11–21. doi:10.1016/S2095-6339(15)30002-2

APPENDIX A. SUPPLEMENTARY FIGURES
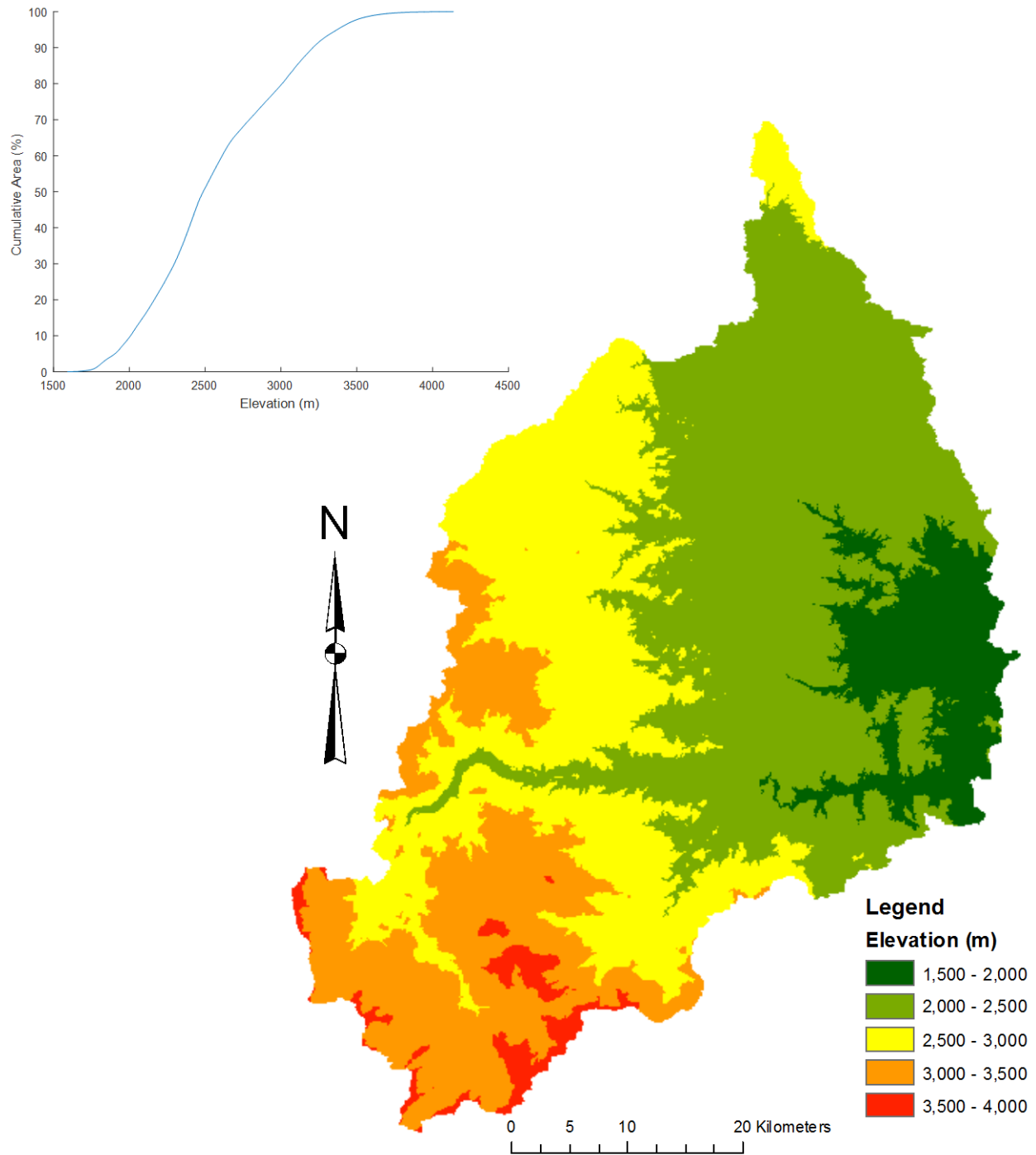
Figure 23. Distribution of elevation within the study watershed based on the 10 m DEM.
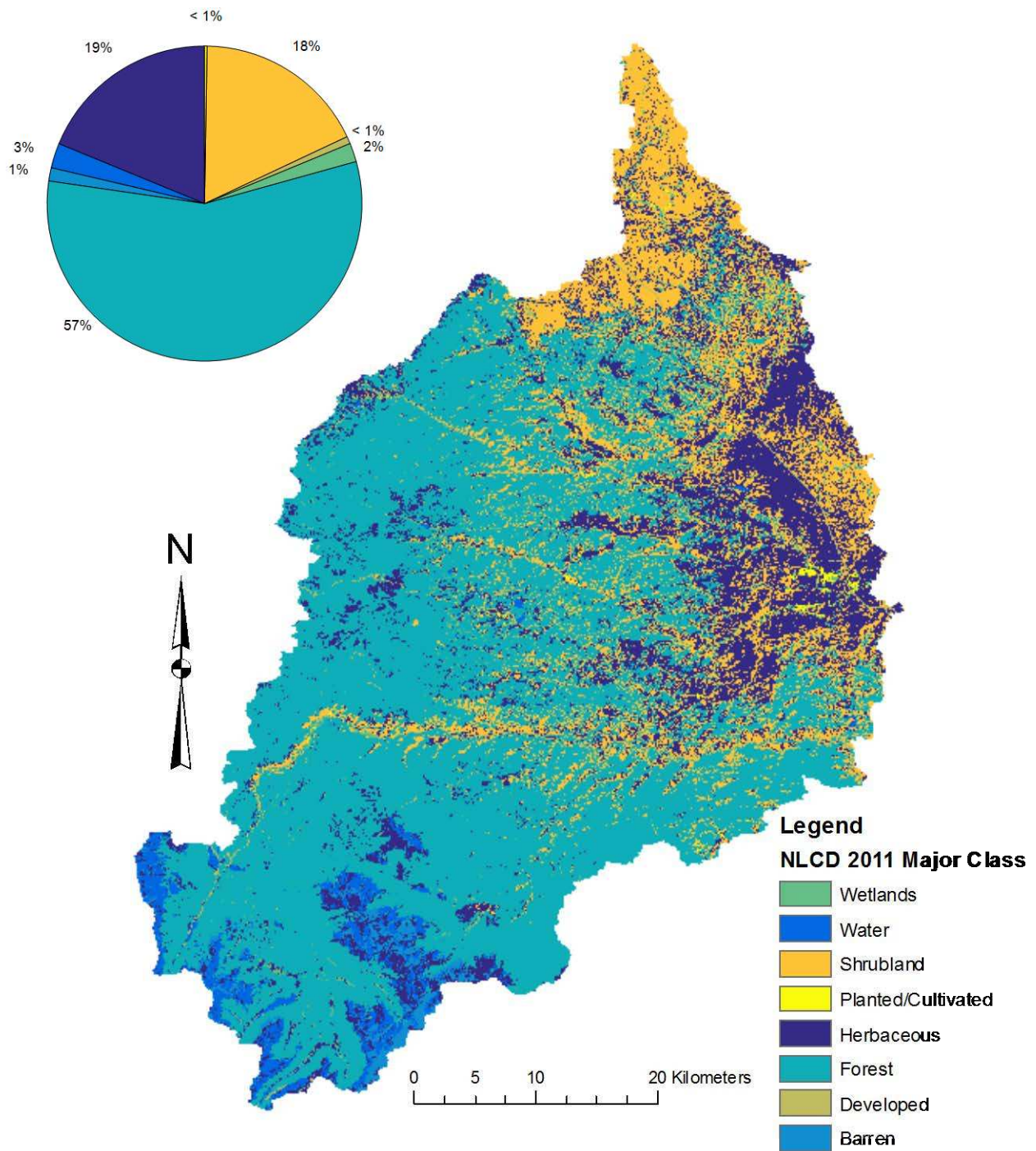
Figure 24. Distribution of major LULC types in study watershed based on MRLC's NLCD 2011 Land Cover dataset.
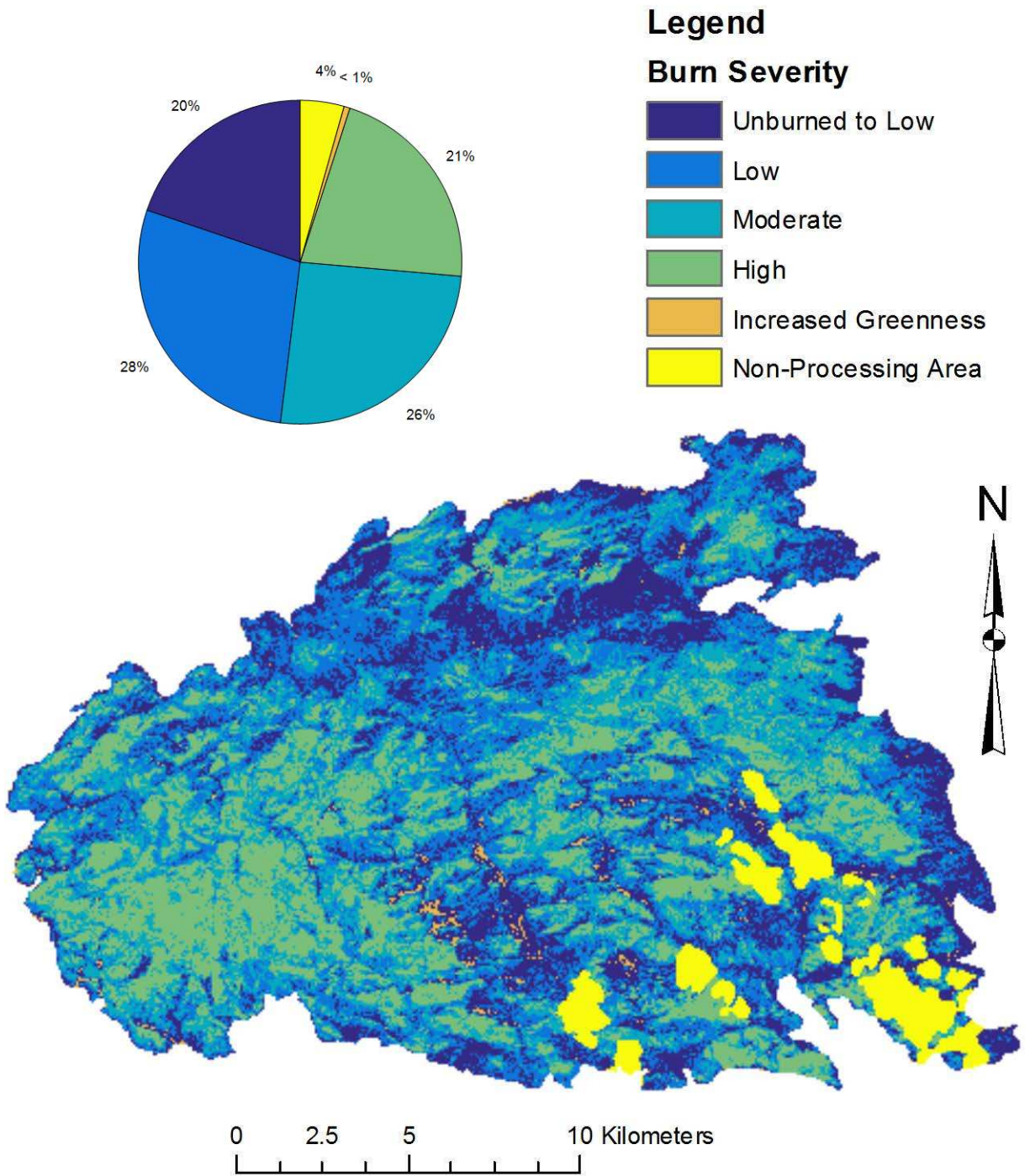
Figure 25. Distribution of burn severity of the Hewlett and High Park wildfires within the study watershed based on MTSB's High Park Fire Assessment.
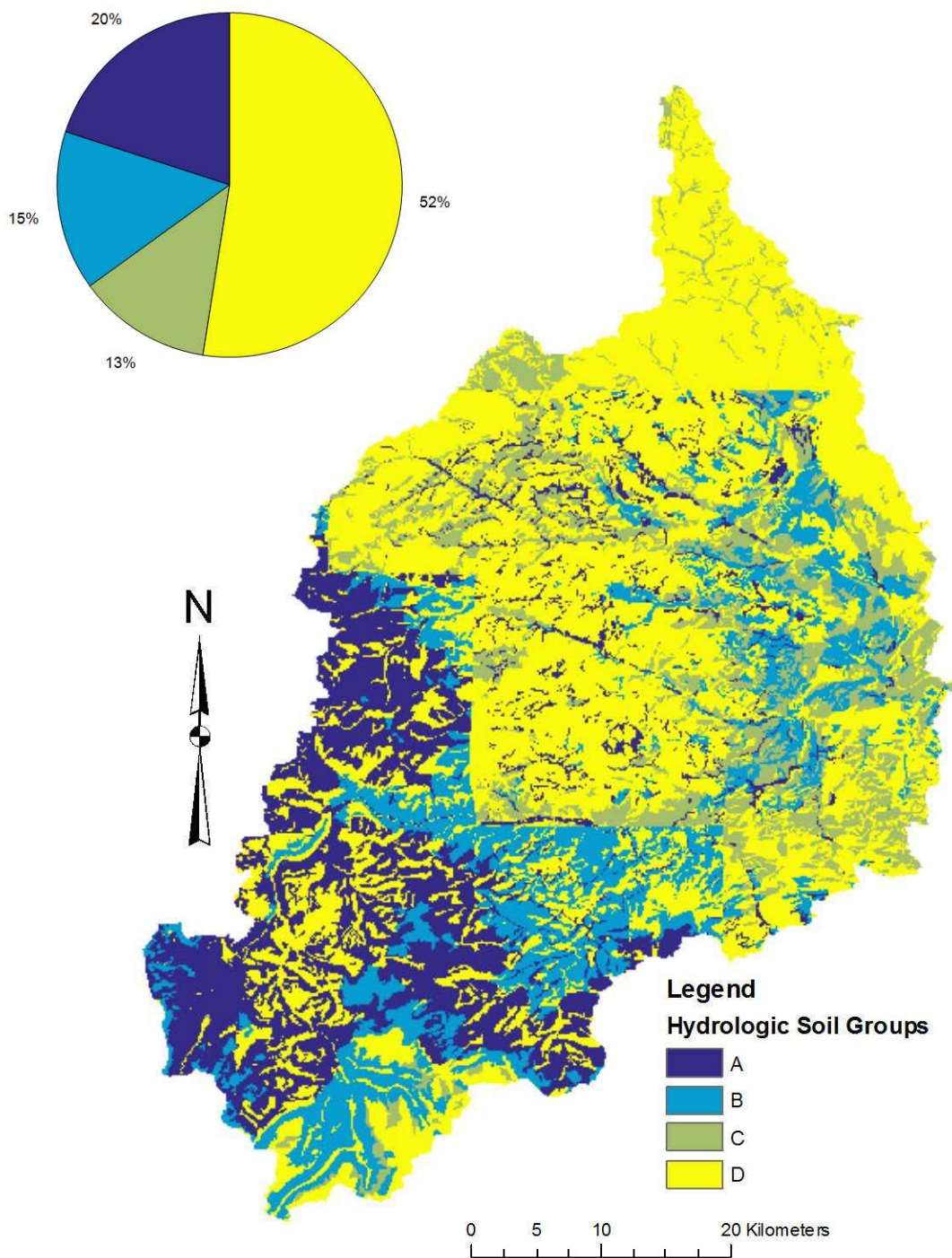
Figure 26. Distribution of soil as represented by Hydrologic Soil Groups A-D within the study watershed based on the USDA's gSSURGO database.
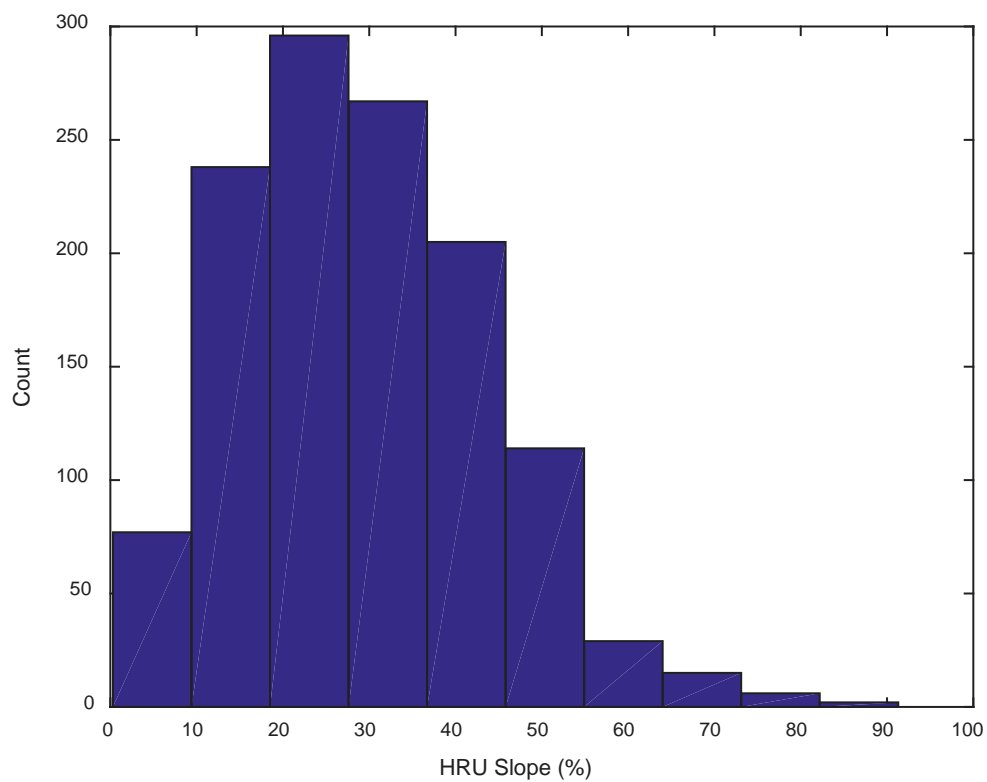
Figure 27. HRU slope histogram for the study watershed.
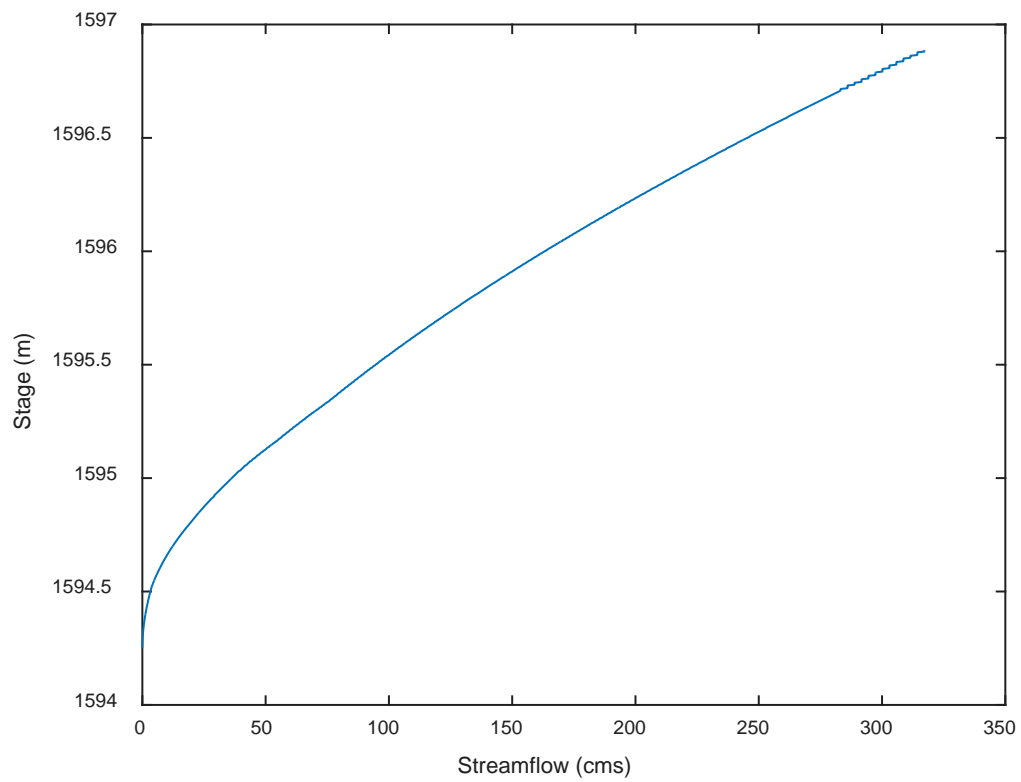
Figure 28. Rating curve for CLAFTCCO18 surface water gauge station at the Mouth of Canyon used for the HEC-RAS downstream boundary condition.
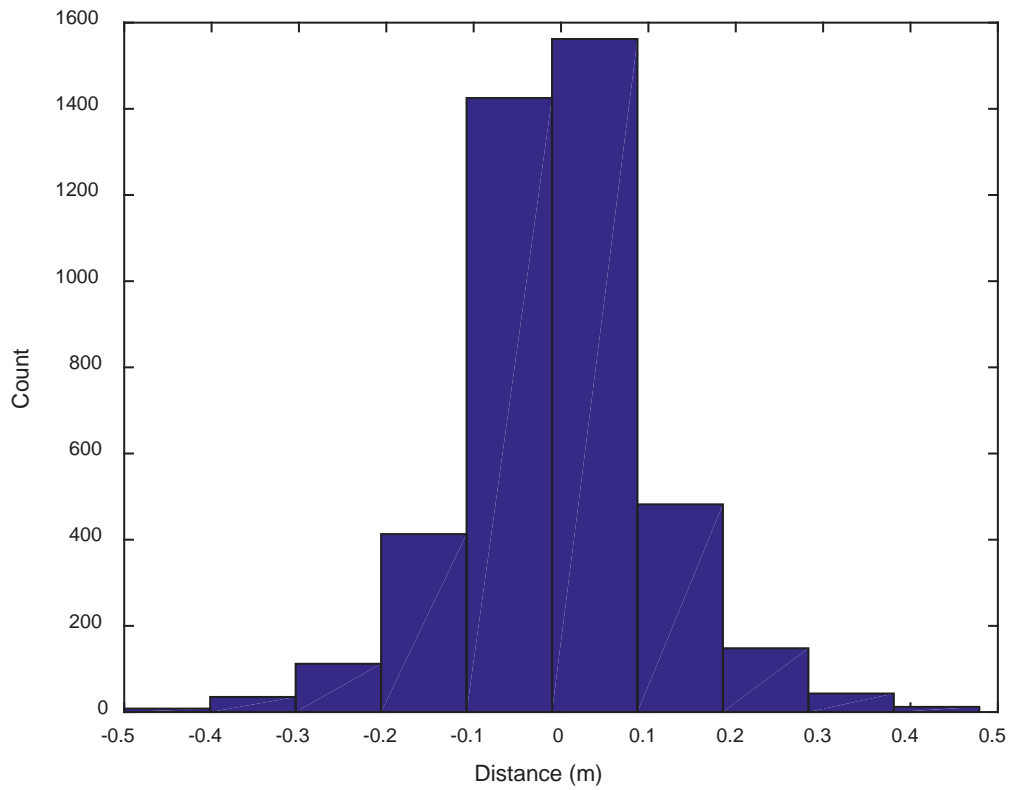
Figure 29. Histogram of distance between the interpolated cross sections and the 3/4 m DEM.

APPENDIX B. SUPPLEMENTARY TABLES

Table 10. Comprehensive distribution of LULC in study watershed based on NLCD 2001, 2006, and 2011.

Class	Description	Portion of study watershed (%)		
		2001	2006	2011
Water	Open Water	0.30	0.28	0.29
Water	Perennial Ice/Snow	2.27	2.27	2.27
Developed	Developed, Open Space	0.57	0.57	0.57
Developed	Developed, Low Intensity	0.17	0.17	0.17
Developed	Developed, Medium Intensity	0.01	0.01	0.01
Developed	Developed, High Intensity	0.00	0.00	0.00
Barren	Barren Land (Rock/Sand/Clay)	1.36	1.36	1.36
Forest	Deciduous Forest	0.58	0.58	0.57
Forest	Evergreen Forest	56.17	56.07	56.00
Forest	Mixed Forest	0.04	0.04	0.04
Shrubland	Shrub/Scrub	17.59	17.69	17.76
Herbaceous	Grassland/Herbaceous	18.76	18.79	18.79
Planted/Cultivated	Pasture/Hay	0.24	0.24	0.24
Planted/Cultivated	Cultivated Crops	0.01	0.01	0.01
Wetlands	Woody Wetlands	1.49	1.50	1.50
Wetlands	Emergent Herbaceous Wetlands	0.44	0.43	0.43

Table 11. Original SWAT database land use / land cover lookup table.

NLCD code	NLCD description	SWAT code	SWAT LULC description
11	Open Water	WATR	Water
12	Perennial Ice/Snow	WATR	Water
21	Developed, Open Space	URLD	Residential-Low Density
22	Developed, Low Intensity	URMD	Residential-Medium Density
23	Developed, Medium Intensity	URHD	Residential-High Density
24	Developed, High Intensity	UIDU	Industrial
31	Barren Land (Rock/Sand/Clay)	SWRN	Southwestern US (Arid) Range
32	Unconsolidated Shore	SWRN	Southwestern US (Arid) Range
41	Deciduous Forest	FRSD	Forest-Deciduous
42	Evergreen Forest	FRSE	Forest-Evergreen
43	Mixed Forest	FRST	Forest-Mixed
51	Dwarf Scrub	RNGB	Range-Brush
52	Shrub/Scrub	RNGB	Range-Brush
71	Grassland/Herbaceous	RNGE	Range-Grasses
72	Sedge/Herbaceous	RNGE	Range-Grasses
73	Lichens	RNGE	Range-Grasses
74	Moss	RNGE	Range-Grasses
81	Pasture/Hay	HAY	Hay
82	Cultivated Crops	AGRR	Agricultural Land-Row Crops
90	Woody Wetlands	WETF	Wetlands-Forested
91	Palustrine Forested Wetland	WETF	Wetlands-Forested
92	Palustrine Scrub/Shrub Wetland	WETL	Wetlands-Mixed
93	Estuarine Forested Wetland	WETF	Wetlands-Forested
94	Estuarine Scrub/Shrub Wetland	WETL	Wetlands-Mixed
95	Emergent Herbaceous Wetlands	WETN	Wetlands-Non-Forested
96	Palustrine Emergent Wetland (Persistent)	WETN	Wetlands-Non-Forested
97	Estuarine Emergent Wetland*	WETN	Wetlands-Non-Forested
98	Palustrine Aquatic Bed	WATR	Water
99	Estuarine Aquatic Bed	WATR	Water

Table 12. Pre-wildfire editied lookup table and corresponding curve numbers.

Code	NLCD description	SWAT code	SWAT LULC description	CN2A	CN2B	CN2C	CN2D
111	Open Water	WATR	Water	-	-	-	-
121	Developed, Open Space	PFLA	Pre-Fire Residential-Low Density Low Burn	31	59	72	79
122	Developed, Low Intensity	PFLB	Pre-Fire Residential-Medium Density Low Burn	31	59	72	79
123	Developed, Medium Intensity	PFLC	Pre-Fire Residential-High Density Low Burn	31	59	72	79
141	Deciduous Forest	PFLD	Pre-Fire Forest-Deciduous Low Burn	45	66	77	83
142	Evergreen Forest	PFLE	Pre-Fire Forest-Evergreen Low Burn	25	55	70	77
143	Mixed Forest	PFLF	Pre-Fire Forest-Mixed Low Burn	36	60	73	79
152	Shrub/Scrub	PFLG	Pre-Fire Range-Brush Low Burn	39	61	74	80
171	Grassland/Herbaceous	PFLH	Range-Grasses Low Burn	49	69	79	84
181	Pasture/Hay	PFLI	Pre-Fire Hay Low Burn	31	59	72	79
190	Woody Wetlands	PFLJ	Pre-Fire Wetlands-Forested Low Burn	45	66	77	83
195	Emergent Herbaceous Wetlands	PFLK	Pre-Fire Wetlands-Non-Forested Low Burn	49	69	79	84
211	Open Water	WATR	Water	-	-	-	-
221	Developed, Open Space	PFML	Pre-Fire Residential-Low Density Moderate Burn	31	59	72	79
241	Deciduous Forest	PFMM	Pre-Fire Forest-Deciduous Moderate Burn	45	66	77	83
242	Evergreen Forest	PFMN	Pre-Fire Forest-Evergreen Moderate Burn	25	55	70	77
243	Mixed Forest	PFMO	Pre-Fire Forest-Mixed Moderate Burn	36	60	73	79
252	Shrub/Scrub	PFMP	Pre-Fire Range-Brush Moderate Burn	39	61	74	80
271	Grassland/Herbaceous	PFMQ	Pre-Fire Range-Grasses Moderate Burn	49	69	79	84
290	Woody Wetlands	PFMR	Pre-Fire Wetlands-Forested Moderate Burn	45	66	77	83
295	Emergent Herbaceous Wetlands	PFMS	Pre-Fire Wetlands-Non-Forested Moderate Burn	49	69	79	84
321	Developed, Open Space	PFHT	Pre-Fire Residential-Low Density High Burn	31	59	72	79
341	Deciduous Forest	PFHU	Pre-Fire Forest-Deciduous High Burn	45	66	77	83
342	Evergreen Forest	PFHV	Pre-Fire Forest-Evergreen High Burn	25	55	70	77
343	Mixed Forest	PFHW	Pre-Fire Forest-Mixed High Burn	36	60	73	79
352	Shrub/Scrub	PFHX	Pre-Fire Range-Brush High Burn	39	61	74	80
371	Grassland/Herbaceous	PFHY	Pre-Fire Range-Grasses High Burn	49	69	79	84
390	Woody Wetlands	PFHZ	Pre-Fire Wetlands-Forested High Burn	45	66	77	83

Table 13. Post-wildfire editied lookup table and corresponding curve numbers.

Code	NLCD description	SWAT code	SWAT LULC description	CN2A	CN2B	CN2C	CN2D
111	Open Water	WATR	Water	-	-	-	-
121	Developed, Open Space	FRLA	Post-Fire Residential-Low Density Low Burn	36	64	77	84
122	Developed, Low Intensity	FRLB	Post-Fire Residential-Medium Density Low Burn	36	64	77	84
123	Developed, Medium Intensity	FRLC	Post-Fire Residential-High Density Low Burn	36	64	77	84
141	Deciduous Forest	FRLD	Post-Fire Forest-Deciduous Low Burn	50	71	82	88
142	Evergreen Forest	FRLE	Post-Fire Forest-Evergreen Low Burn	30	60	75	82
143	Mixed Forest	FRLF	Post-Fire Forest-Mixed Low Burn	41	65	78	84
152	Shrub/Scrub	FRLG	Post-Fire Range-Brush Low Burn	44	66	79	85
171	Grassland/Herbaceous	FRLH	Post-Fire Range-Grasses Low Burn	54	74	84	89
181	Pasture/Hay	FRLI	Post-Fire Hay Low Burn	36	64	77	84
190	Woody Wetlands	FRLJ	Post-Fire Wetlands-Forested Low Burn	50	71	82	88
195	Emergent Herbaceous Wetlands	FRLK	Post-Fire Wetlands-Non-Forested Low Burn	54	74	84	89
211	Open Water	WATR	Water	-	-	-	-
221	Developed, Open Space	FRML	Post-Fire Residential-Low Density Moderate Burn	41	69	82	89
241	Deciduous Forest	FRMM	Post-Fire Forest-Deciduous Moderate Burn	55	76	87	93
242	Evergreen Forest	FRMN	Post-Fire Forest-Evergreen Moderate Burn	35	65	80	87
243	Mixed Forest	FRMO	Post-Fire Forest-Mixed Moderate Burn	46	70	83	89
252	Shrub/Scrub	FRMP	Post-Fire Range-Brush Moderate Burn	49	71	84	90
271	Grassland/Herbaceous	FRMQ	Post-Fire Range-Grasses Moderate Burn	59	79	89	94
290	Woody Wetlands	FRMR	Post-Fire Wetlands-Forested Moderate Burn	55	76	87	93
295	Emergent Herbaceous Wetlands	FRMS	Post-Fire Wetlands-Non-Forested Moderate Burn	59	79	89	94
321	Developed, Open Space	FRHT	Post-Fire Residential-Low Density High Burn	46	74	87	94
341	Deciduous Forest	FRHU	Post-Fire Forest-Deciduous High Burn	60	81	92	98
342	Evergreen Forest	FRHV	Post-Fire Forest-Evergreen High Burn	40	70	85	92
343	Mixed Forest	FRHW	Post-Fire Forest-Mixed High Burn	51	75	88	94
352	Shrub/Scrub	FRHX	Post-Fire Range-Brush High Burn	54	76	89	95
371	Grassland/Herbaceous	FRHY	Post-Fire Range-Grasses High Burn	64	84	94	99
390	Woody Wetlands	FRHZ	Post-Fire Wetlands-Forested High Burn	60	81	92	98

Table 14. Meteorological stations used for this study.

Station name	Latitude	Longitude	Elevation (m)	Notes
STOVE PRAIRIE 2 WNW CO US	40.6263	-105.391	2357.9	Precip. only
RED FEATHER 5.9 NE CO US	40.86	-105.509	2414.9	Precip. only
BLV 4.0 NW CO US	40.6754	-105.215	1631.9	Precip. only
BUCKHORN MOUNTAIN 1 E CO US	40.6167	-105.283	2255.5	
HOURGLASS RESERVOIR CO US	40.5831	-105.632	2901.7	
RUSTIC 9 WSW CO US	40.7167	-105.717	2347	
VIRGINIA DALE 7 ENE CO US	40.9656	-105.219	2138.2	
RED FEATHER COLORADO CO US	40.7981	-105.572	2499.4	Temp. only
DEADMAN HILL CO US	40.8	-105.767	3115.1	
JOE WRIGHT CO US	40.5333	-105.883	3084.6	
WILLOW PARK CO US	40.4333	-105.733	3261.4	

Table 15. SWAT calibration parameters.

| Parameter | Description | File | Unit | Calibration inputs | | | Calibrated value |
				Initial value	Lower bound	Upper bound	
DEPIMP_BSN	Depth to impervious layer for modeling perched water tables.	.bsn	mm	3000	0	6000	1356
EPCO	Plant uptake compensation factor.	.bsn	-	0.5	0.01	1	0.2306
SFTMP	Snowfall temperature.	.bsn	°C	0	-5	5	1.381
SMFMN	Minimum melt rate for snow during year.	.bsn	mm/°C-day	5	0	10	2.078
SMFMX	Maximum melt rate for snow during year.	.bsn	mm/°C-day	5	0	10	2.078
SMTMP	Snow melt base temperature.	.bsn	°C	0	-5	5	-0.9346
SNO50COV	Snow water content that corresponds to 50% snow cover.	.bsn	mm	0.5	0.01	0.99	0.3092
SNOCOVMX	Minimum snow water content that corresponds to 100% snow cover.	.bsn	mm	1	1	650	152.1
SURLAG	Surface runoff lag time.	.bsn	day	4	1	24	12.5
TIMP	Snow pack temperature lag factor.	.bsn	-	0.5	0.01	1	0.5362
ADJ_PKR	Peak rate adjustment factor for sediment routing in the sub-basin.	.bsn	-	1.25	0.5	2	1.052
PRF	Peak rate adjustment factor for sediment routing in the channel.	.bsn	-	1	0	2	1.803
ALPHA_BF	Baseflow alpha factor.	.gw	days	0.048	0	1	0.6387
GW_DELAY	Groundwater delay.	.gw	day	250	0	500	472.1
GW_REVAP	Groundwater "revap" coefficient.	.gw	-	0.1	0.02	0.2	0.04354
GW_SPYLD	Specific yield of the shallow aquifer.*	.gw	m^3/m^3	0.25	-0.5	1	-0.08856
GWHT	Initial groundwater height.	.gw	m	12.5	0	25	1.101
GWQMN	Threshold depth of water in the shallow aquifer for return flow to occur.	.gw	mm	2500	0	5000	4442
RCHRG_DP	Deep aquifer percolation fraction.	.gw	-	0.05	0	1	0.2275
REVEP_MN	Threshold depth of water in the shallow aquifer for "revap" to occur.	.gw	mm	250	0	500	472.9
CANMX	Maximum canopy storage.	.hru	mm	0	0	10	3.057
ESCO	Soil evaporation compensation factor.	.hru	-	0.05	0.01	1	0.3678
OV_N	Manning's "n" value for overland flow.	.hru	-	0.15	0.01	0.3	0.2764
SLOPE	The mean slope within the HRU.*	.hru	m/m	0	-0.1	0.1	-0.09433
DEP_IMP	Depth to impervious layer in soil profile.	.hru	mm	2000	1500	2500	2304
SLSUBBSN	Average slope length.	.hru	m	50	10	150	90.45
DDRAIN	Depth to subsurface drain.	.mgt	mm	1000	500	1500	1173
TDRAIN	Time to drain soil to field capacity.	.mgt	hr	36	0	72	55.54
CH_KII	Effective hydraulic conductivity in main channel alluvium.	.rte	mm/hr	256	-0.01	500	401.2

Table 15. Continued.

Parameter	Description	File	Unit	Calibration inputs			Calibrated value
				Initial value	Lower bound	Upper bound	
CH_NII	Manning's "n" value for the main channel.	.rte	-	0.15	0.01	0.3	0.0255
CH_SII	Average slope of main channel*	.rte	m/m	0	-0.05	0.05	0.02677
SOL_AWC	Available water capacity.*	.sol	mm/mm	1	-0.1	2	0.9813
SOL_K	Saturated hydraulic conductivity.*	.sol	mm/hr	2	-0.5	5	-0.4585
SOL_ALB	Moist soil albedo.*	.sol	-	0.25	-0.5	1	-0.3694
SOL_Z	Depth from soil surface to bottom layer.*	.sol	mm	0.25	-0.5	1	-0.1593
CH_KI	Effective hydraulic conductivity in tributary channel alluvium.	.sub	mm/hr	150	0	300	244.2
CH_NI	Manning's "n" value for the tributary channels.	.sub	-	0.15	0.008	0.3	0.2437
CH_SI	Average slope of tributary channels.*	.sub	m/m	0	-0.05	0.05	-0.02402

* These parameters were varied as a percentage of to maintain spatial variability.

Table 16. Supplementary error statistics for SWAT model.

Simulation	Simulation period	Timestep	Bias	Root mean squared error	Coefficient of correlation
Pre-wildfire testing	2000-2004	Daily	-1.49	6.51	0.86
Calibration	2005-2013	Daily	0.18	7.78	0.91
Post-wildfire testing	2014	Daily	2.12	11.34	0.96
All	2000-2014	Daily	-0.29	7.63	0.91
Pre-wildfire testing	2000-2004	Monthly	-1.48	4.77	0.91
Calibration	2005-2013	Monthly	0.19	5.59	0.94
Post-wildfire testing	2014	Monthly	2.14	5.20	0.99
All	2000-2014	Monthly	-0.27	5.30	0.95

Table 17. RTK-GPS survey errors.

| Survey | NGS control | | | | | Error coordinates | | |
| | Name | Type | Coordinates | | | | | |
			Northing (m)	Easting (m)	Orthometric height (m)	Northing (m)	Easting (m)	Orthometric height (m)
XS1-03172014-A	Dailey	GPS	454905.9531	936595.173	1622.1	0.0903	-0.0193	-0.0448
XS18-03182014-A	E135	Vertical	455312.8498	915035.7917	2077.098	20.3977	-14.7762	-0.0819
XS15-03182014-B	HIPP	GPS	456174.3238	919096.2049	1990.6	0.0306	-0.0272	-0.0431
XS4-03192014-A	R135	Vertical	455740.9589	934570.1336	1662.997	-4.7061	13.7569	-0.3642
XS7-03192014-B	P135	GPS	455112.2391	930658.9574	1731.121	0.0802	-0.0072	-0.1776
XS10-03202014-C	L135	GPS	454758.303	924534.6487	1833.548	0.0544	0.0409	-0.1438
XS-S1-A-10-14-14	E135	Vertical	455312.8498	915035.7917	2077.098	20.3607	-14.7699	-0.0733
XS-S2-A-10-14-14	G135	Vertical	455036.5071	918816.2514	2005.012	-37.8996	20.4308	-0.1085
XS-S4-A-10-18-14	P135	GPS	455112.2391	930658.9574	1731.121	0.0484	0.0909	-0.2028
XS-S5-C-10-18-14	Dailey	GPS	454905.9531	936595.173	1622.1	0.2038	-0.7975	-0.1539
XS-S6-C-10-18-14	L135	GPS	454758.303	924534.6487	1833.548	0.0563	0.1078	-0.1015
XS-S7-A-10-19-14	HIPP	GPS	456174.3238	919096.2049	1990.6	0.0408	-0.0574	-0.0629
XS-S8-A-10-19-14	L135	GPS	454758.303	924534.6487	1833.548	-0.0216	0.0887	-0.1297
XS-S9-A-11-01-14	E61	Vertical	456763.6215	936257.6352	1639.016	26.6714	20.4362	-0.0596
XS-S10-A-11-01-14	R135	Vertical	455740.9589	934570.1336	1662.997	-4.7572	13.8575	-0.1048

Table 18. Cross section spacing analysis summary.

Station (m)	Cross section invert (m)	Slope between cross sections (m/m)	Cross section spacing (m)	Estimated bank full elevation (m)	Estimated bank full depth (m)	Calculated minimum cross section spacing (m)
54964.59	2067.84	0.0095	1107.08	2070.82	2.98	47
53857.51	2057.31	0.0082	1076.67	2059.14	1.83	34
52780.84	2048.51	0.0138	1313.08	2051.48	2.97	32
51467.76	2030.4	0.0088	915.36	2032.23	1.83	31
50552.4	2022.34	0.0126	959.61	2024.80	2.46	29
49592.79	2010.24	0.0119	1227.86	2011.51	1.27	16
48364.93	1995.68	0.0091	1046.30	1997.45	1.77	29
47318.63	1986.12	0.0121	1093.61	1987.86	1.74	22
46225.02	1972.94	0.0100	1229.95	1975.29	2.35	35
44995.07	1960.63	0.0141	1208.71	1965.11	4.48	48
43786.36	1943.6	0.0243	860.95	1945.27	1.67	10
42925.41	1922.7	0.0313	411.31	1927.30	4.60	22
42514.1	1909.83	0.0161	755.53	1911.86	2.03	19
41758.57	1897.64	0.0244	462.62	1899.41	1.77	11
41295.95	1886.33	0.0284	727.40	1888.41	2.08	11
40568.55	1865.69	0.0123	626.62	1869.07	3.38	41
39941.93	1857.98	0.0106	550.74	1859.04	1.06	15
39391.19	1852.15	0.0085	625.40	1853.24	1.09	19
38765.79	1846.85	0.0094	601.40	1848.34	1.49	24
38164.39	1841.17	0.0117	623.43	1844.16	2.99	38
37540.96	1833.86	0.0149	672.11	1835.89	2.03	20
36868.85	1823.84	0.0100	613.08	1825.79	1.95	29
36255.77	1817.73	0.0134	612.69	1822.10	4.37	49
35643.08	1809.54	0.0145	639.26	1814.32	4.78	49
35003.82	1800.28	0.0145	696.86	1801.28	1.00	10
34306.96	1790.21	0.0127	1029.36	1791.48	1.27	15
33277.6	1777.1	0.0094	1042.67	1778.17	1.07	17
32234.93	1767.34	0.0142	1228.76	1768.87	1.53	16
31006.17	1749.87	0.0091	1239.86	1751.96	2.09	34
29766.31	1738.54	0.0068	1245.32	1743.43	4.89	107
28520.99	1730.04	0.0102	1036.53	1731.46	1.42	21
27484.46	1719.5	0.0167	1178.12	1721.69	2.19	20

Table 18. Continoued.

Station (m)	Cross section invert (m)	Slope between cross sections (m/m)	Cross section spacing (m)	Estimated bank full elevation (m)	Estimated bank full depth (m)	Calculated minimum cross section spacing (m)
26306.34	1699.85	0.0103	1068.09	1701.28	1.43	21
25238.25	1688.85	0.0113	1149.51	1691.27	2.42	32
24088.74	1675.91	0.0081	1091.45	1677.89	1.98	37
22997.29	1667.04	0.0100	1217.02	1670.65	3.61	54
21780.27	1654.92	0.0086	1226.90	1656.44	1.52	26
20553.37	1644.35	0.0082	1501.71	1649.22	4.87	90
19051.66	1632.11	0.0054	878.58	1633.92	1.81	50
18173.08	1627.36	0.0067	1172.01	1628.85	1.49	33
17001.07	1619.52	0.0060	1224.00	1621.77	2.25	56
15777.07	1612.19	0.0049	820.36	1616.12	3.93	119
14956.71	1608.14	0.0067	847.26	1611.87	3.73	84
14109.45	1602.48	0.0050	590.81	1603.81	1.33	40
13518.64	1599.5	-	-	1601.23	1.73	-

Table 19. Supplementary error statistics for HEC-RAS model.

Simulation	Bias	Root mean squared error	Nash-Sutcliffe efficiency
Calibration	0.0006	0.20	0.25
Testing	-0.0429	0.19	0.17

Table 20. Flood streamflows comparison between SWAT no-wildfire scenario output and eRAMS flood analysis tool results.

Event (year)	Flood flow (m^3/s)		Difference (%)
	eRAMS*	No-wildfire scenario steady flow data	
200	389.05	223.19	74.31
100	328.62	188.94	73.93
50	274.86	158.22	73.72
10	171.14	98.20	74.27
2	86.30	48.28	78.75

* Based on 125 observations at the Mouth of Canyon from 1882 to 2007.

APPENDIX C. STATISTICS

Nash-Sutcliffe Efficiency (N_{SE})

The Nash-Sutcliffe efficiency (E_{NS}) is a normalized statics that indicates how well observed versus simulated plot fits a 1:1 line. N_{SE} is computed as:

$$E_{NS} = 1 - \left[\frac{\sum_{i=1}^{n}(Y_i^{obs} - Y_i^{sim})^2}{\sum_{i=1}^{n}(Y_i^{obs} - Y_i^{mean})^2} \right]$$

where for this study Y^{obs} is the observed streamflow, Y^{sim} is the simulated streamflow, and Y^{mean} is the mean of observed streamflows (Nash and Sutcliffe, 1970). The optimal value for NSE is 1 although can range between $-\infty$ and 1.0, with values between 0.0 and 1.0 generally regarded as satisfactory levels of performance. Values ≤ 0.0 indicate the mean simulated value is a worse predictor than the observed value (Moriasi et al., 2007).

Relative Error

The Relative Error (RE) gives an indication of how good simulated values are relative to the magnitude of corresponding observed values. RE as a percentage is computed as:

$$RE = \frac{\sum_{i=1}^{n}(Y_i^{obs} - Y_i^{sim})}{\sum_{i=1}^{n} Y_i^{obs}} * 100$$

where for this study Y^{obs} is the observed streamflow and Y^{sim} is the simulated streamflow.

Bias

The Bais is a measure of the tendency of simulated values to be larger or smaller then corresponding simulated values. Bais is computed as:

$$Bias = \frac{1}{n}\sum\nolimits_{i=1}^{n} Y_i^{obs} - Y_i^{sim}$$

where for this study Y^{obs} is the observed streamflow and Y^{sim} is the simulated streamflow. The optimal value for bias is 0. Positive values indicate simulated streamflows tend to underestimate the observed streamflows values on average whereas negative values indicate simulated streamflows tend to overestimate the observed streamflow values on average (Moriasi et al., 2007).

Root Mean Square Error

The Root Mean Square Error (RMSE) is a measure of the diffidence between simulated and observed values with respect to magnitude and timing. RMSE is computed as:

$$RMSE = \sqrt{\frac{1}{n}\sum\nolimits_{i=1}^{n} Y_i^{obs} - Y_i^{sim}}$$

where for this study Y^{obs} is the observed streamflow and Y^{sim} is the simulated streamflow.

Coefficient of Correlation

The Coefficient of Correlation (R^2) is a measure of the correlation between observed and simulated values. R^2 is computed as:

$$R^2 = \frac{1}{n-1} \sum_{i-1}^{n} \left(\frac{Y_i^{obs} - Y_i^{sim}}{s_{Y_i^{obs}}} \right) \left(\frac{Y_i^{obs} - Y_i^{sim}}{s_{Y_i^{sim}}} \right)$$

where for this study Y^{obs} is the observed streamflow, Y^{sim} is the simulated streamflow, $s_{Y_i^{obs}}$ is the standard deviation of the observed streamflows and $s_{Y_i^{sim}}$ is the standard deviation of the simulated streamflows.

APPENDIX D. PROCESS DOMAIN CLASSIFICATION WORKFLOW

ArcMap was used to classify the study reach using the procedure outlined below.

1. The 10 m DEM and 3/4 m DEM were loaded.

2. The reach layer representing the stream network generated during the creation of the SWAT model was loaded and modified as follows to create a layer that represents the river centerline:

   a. The SWAT reach layer was clipped and merged to create a continuous line within the reach study area.

   b. Generalization was applied with a 10 m tolerance to smooth the line.

   c. The line was adjusted manually to insure line adequately represent the river centerline using a slope raster of the 3/4 m DEM.

   d. Line was arbitrarily delineated into 500 m sections.

3. The average upstream to downstream direction slope of each section was calculated using each sections length and elevations extracted from the 10 m DEM.

4. A buffer using a distance of 25 m was created around the newly river centerline.

5. The average slope within each area buffer section of the 10 m DEM was calculated with the zonal statistics tool. This average slope was calculated to represent the lateral slope.

6. Sections where the average upstream to downstream direction slope was greater than 2 percent and the average lateral slope was greater than 16 percent were defined as confined sections. All remain sections were defined as partially confined.

7. To simplify the results, sections were generalized so that the minimum length of a confined section was an arbitrary 1500 m.

APPENDIX E. DETAILED CROSS SECTION DATA SUMMARY

The relationship between streamflow depth (h) and streamflow area (A) and hydraulic radius (R) for each detailed cross section was described through hydraulic geometry using the following equations:

$$A = a_1 h^{a_2} + \epsilon_A$$

$$R = r_1 h^{r_2} + \epsilon_R$$

where a_1 and r_1 a scale factors and a_2 and r_2 are shape factors. ϵ_A and ϵ_R are at a station residuals that represent uncertainty (Buhman et al., 2002). Theses parameters at a given cross section were determined using a least-squares nonlinear regression. Examples of the power functions displayed above obtained through this regression are shown in Figure 30 for a selected detailed cross section. A complete list of parameters for each detailed cross section is shown in Table 21. Also, these values were also plotted as shown in Figure 31 and Figure 32.
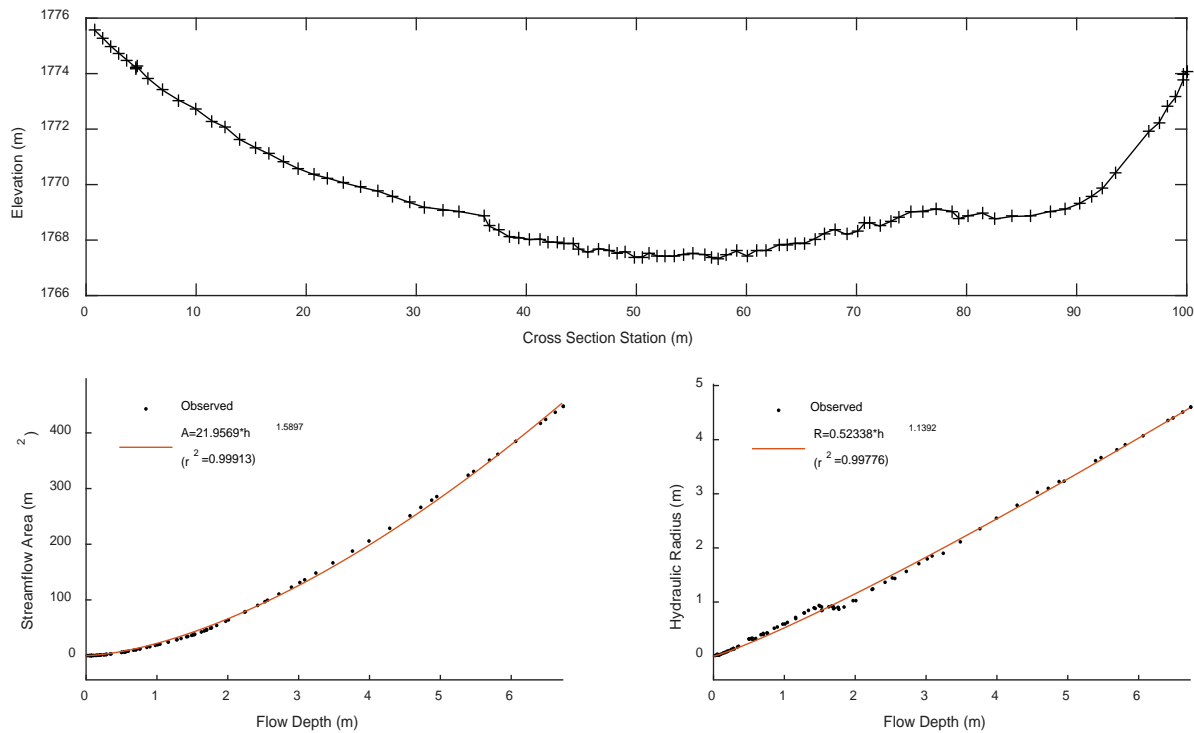

Figure 30. Select detailed cross section (above), observed data, and fitted power functio for streamflow area (lower left) and hydraulic radius (lower right) for cross section 32+162.

Table 21. Summary of hydraulic geometry parameters for the study reach.

| Station	a_1	a_2	mean(ε_A)	variance(ε_A)	r_1	r_2	mean(ε_R)	variance(ε_R)
13506.4	13.18	1.62	-0.0859	0.0360	0.59	1.05	-0.0051	0.0012
14097.2	17.97	1.39	-0.0468	0.4902	0.80	0.77	-0.0282	0.0208
14945.6	22.11	1.44	0.3029	10.3684	0.77	0.87	-0.0321	0.0180
15767.4	29.62	1.33	-0.4018	2.5748	0.76	0.96	-0.0212	0.0085
16982.3	14.80	1.56	-0.4385	2.5156	0.63	0.97	-0.0262	0.0163
18155.9	12.15	1.60	0.5803	8.0636	0.82	0.79	-0.0155	0.0144
19034.5	11.03	1.59	-0.2597	0.6249	0.60	0.96	-0.0114	0.0240
20539.6	10.22	1.67	0.2718	14.6741	0.59	0.98	-0.0133	0.0518
21748.9	5.28	1.87	-0.0059	20.9395	0.45	1.06	0.0231	0.0500
22963.2	10.10	1.70	-0.1161	0.4576	0.55	0.96	-0.0046	0.0148
24059.8	3.05	2.21	0.5268	4.8713	0.69	0.66	-0.0139	0.0282
25205.8	10.96	1.61	-0.3998	4.0645	0.53	1.03	-0.0051	0.0172
26275.3	6.27	1.68	0.0618	15.0941	0.59	0.95	0.0010	0.0363
27454.8	16.08	1.72	0.5850	13.3179	0.71	0.80	-0.0219	0.0259
28492.2	16.39	1.47	-0.1219	0.0618	0.64	1.01	-0.0056	0.0013
29738.2	10.67	1.58	-0.1872	1.7788	0.61	0.97	-0.0109	0.0271
30948.1	11.05	1.68	0.0364	1.3574	0.59	0.99	-0.0035	0.0094
32161.9	21.96	1.59	-1.0730	12.9554	0.52	1.14	0.0093	0.0037
33205.3	11.57	1.74	0.1722	2.8193	0.60	0.93	-0.0084	0.0109
34224.9	10.89	1.57	-0.1008	8.8258	0.68	0.93	-0.0211	0.0384
34921.1	13.07	1.56	-1.1331	19.9589	0.51	1.08	-0.0003	0.0201
35559.6	11.01	1.60	-2.5035	100.5938	0.45	1.08	0.0119	0.0261
36172.2	12.57	1.51	-0.5758	20.9106	0.64	0.97	0.0013	0.0304
36786.5	11.35	1.55	-2.9417	85.7037	0.51	1.05	-0.0106	0.0257
37458.6	15.18	1.61	-0.5171	2.4772	0.57	1.02	-0.0127	0.0049
38078.9	12.87	1.59	-1.0120	9.3746	0.52	1.08	0.0054	0.0075
38657	18.99	2.01	-0.3962	1.5382	0.46	1.42	-0.0001	0.0015
39282.1	15.22	1.68	0.0943	0.7293	0.64	0.89	-0.0085	0.0038
39828.8	17.58	1.69	-0.4666	2.6843	0.52	1.16	0.0030	0.0049
40455.9	30.14	1.39	-2.0638	17.8163	0.67	1.01	-0.0493	0.0248
41183.7	13.06	1.61	0.2562	2.3588	0.67	0.91	-0.0069	0.0114
41647.9	22.16	1.37	-0.6585	2.3609	0.66	1.05	-0.0086	0.0025
42393.3	8.99	1.69	0.2339	11.8052	0.65	0.86	-0.0282	0.0560
42804.7	12.68	1.39	-2.2682	53.5351	0.79	0.84	-0.0681	0.1135
43654.5	16.24	1.38	-1.3694	6.7385	0.66	0.99	-0.0346	0.0148
44859.7	6.72	1.81	0.3726	6.8375	0.74	0.69	-0.0176	0.0537
46088	15.12	1.52	-0.9502	7.0741	0.55	1.10	-0.0164	0.0237
47156	11.12	1.80	0.5220	9.9023	0.73	0.76	-0.0210	0.0179
48147.7	9.34	1.83	-1.9721	38.7297	0.39	1.20	-0.0072	0.0508
49363.2	16.20	1.50	-0.2966	0.8985	0.62	1.01	-0.0034	0.0032
50316.7	15.41	1.84	-0.1979	1.0847	0.49	1.13	0.0053	0.0030
51225	7.28	1.83	-0.4028	7.9626	0.46	1.10	-0.0074	0.0256
52539.9	6.07	2.17	-0.5350	5.1486	0.26	1.52	0.0228	0.0115
53616.5	11.74	1.82	-0.3071	1.5392	0.47	1.14	0.0024	0.0035
54697.4	8.27	1.98	0.0499	0.3779	0.51	0.88	-0.0057	0.0043
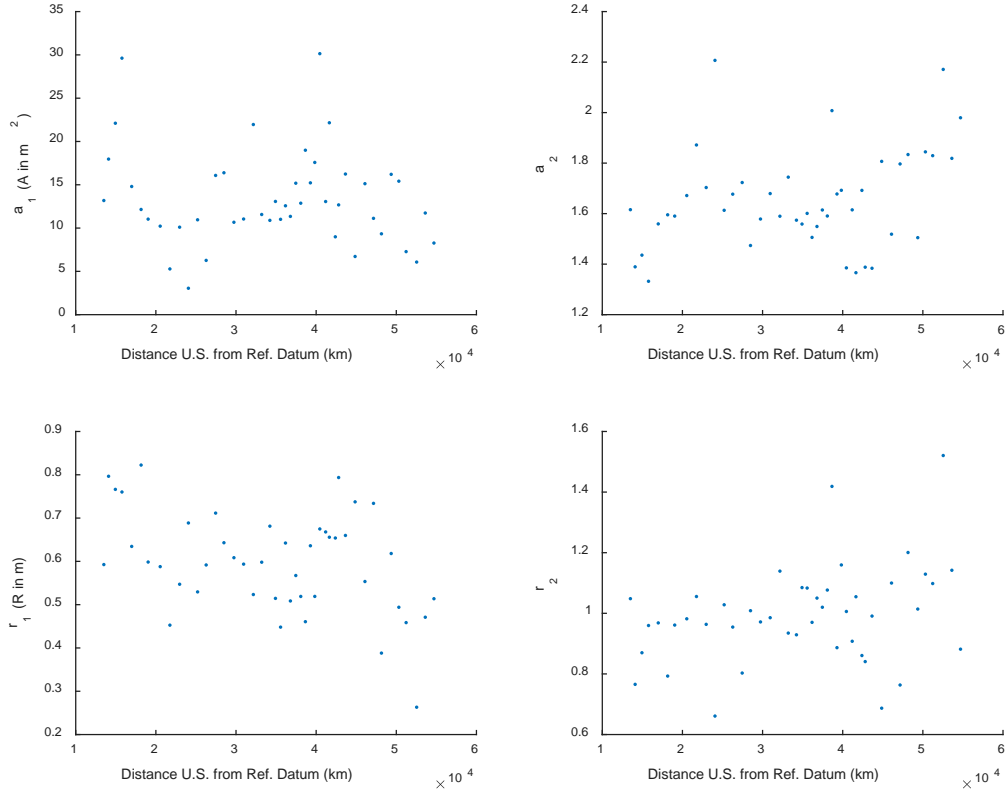
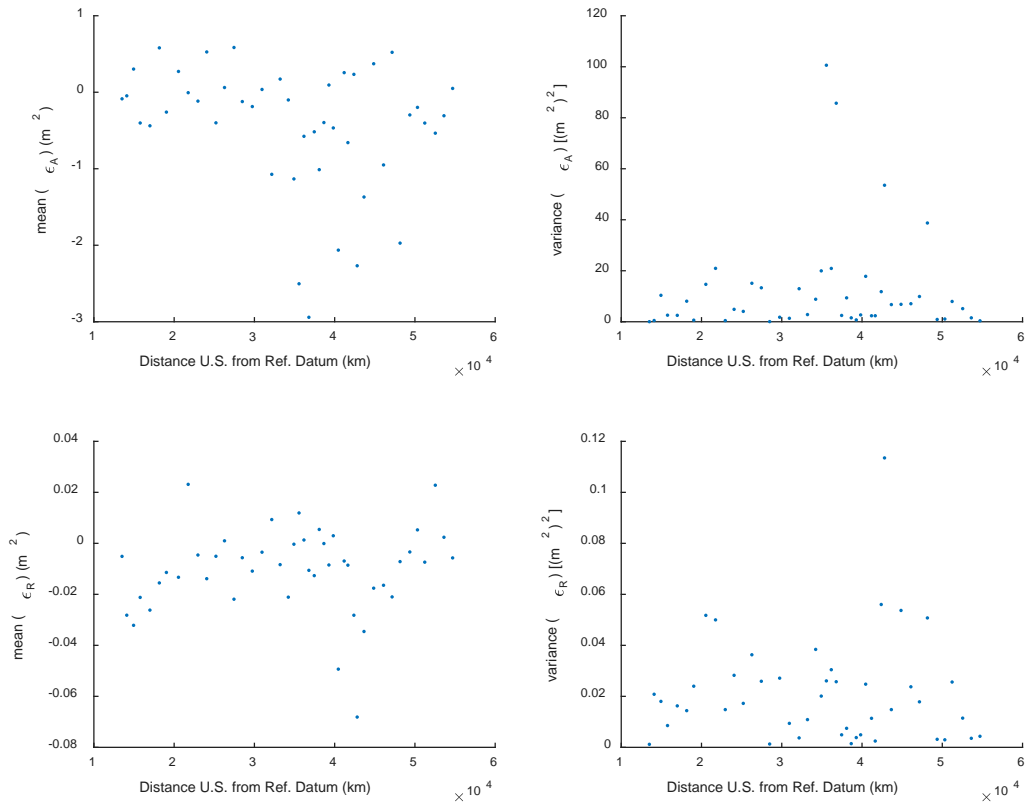Figure 31. Hydrualic geometry shape and scale parameters for the study reach.

Figure 32. Hydrulic geometry error statistics for the study reach.